[redacted]

Russian Original Vol. 35, No. 3, September, 1973

March, 1974

SATEAZ 35(3) 791-882 (1973)

SOVIET ATOMIC ENERGY

АТОМНАЯ ЭНЕРГИЯ
(ATOMNAYA ÉNERGIYA)

TRANSLATED FROM RUSSIAN

CONSULTANTS BUREAU, NEW YORK

SOVIET ATOMIC ENERGY

Soviet Atomic Energy is a cover-to-cover translation of *Atomnaya Énergiya*, a publication of the Academy of Sciences of the USSR.

An arrangement with Mezhdunarodnaya Kniga, the Soviet book export agency, makes available both advance copies of the Russian journal and original glossy photographs and artwork. This serves to decrease the necessary time lag between publication of the original and publication of the translation and helps to improve the quality of the latter. The translation began with the first issue of the Russian journal.

Consultants Bureau journals appear about six months after the publication of the original Russian issue. For bibliographic accuracy, the English issue published by Consultants Bureau carries the same number and date as the original Russian from which it was translated. For example, a Russian issue published in December will appear in a Consultants Bureau English translation about the following June, but the translation issue will carry the December date. When ordering any volume or particular issue of a Consultants Bureau journal, please specify the date and, where applicable, the volume and issue numbers of the original Russian. The material you will receive will be a translation of that Russian volume or issue.

Subscription
$80 per volume (6 Issues)
2 volumes per year
(Add $5 for orders outside the United States and Canada.)

Single Issue: $30
Single Article: $15

CONSULTANTS BUREAU, NEW YORK AND LONDON

227 West 17th Street
New York, New York 10011

Davis House
8 Scrubs Lane
Harlesden, NW10 6SE
England

Published monthly. Second-class postage paid at Jamaica, New York 11431.

Soviet Atomic Energy is abstracted or indexed in *Applied Mechanics Reviews, Chemical Abstracts, Engineering Index, INSPEC—Physics Abstracts and Electrical and Electronics Abstracts, Current Contents,* and *Nuclear Science Abstracts.*

SOVIET ATOMIC ENERGY

A translation of *Atomnaya Énergiya*

March, 1974

Volume 35, Number 3 September, 1973

CONTENTS

CONTENTS

(continued)

The Russian press date (podpisano k pechati) of this issue was 8/27/1973. Publication therefore did not occur prior to this date, but must be assumed to have taken place reasonably soon thereafter.

DYNAMICS OF THE CHANGES TAKING PLACE IN THE CONTENT OF RADIOACTIVE EMANATIONS IN THE AIR OF MINING INSTALLATIONS

N. P. Kartashov and G. F. Shumkov

UDC 621.039.8:614.8

The concentrations of radioactive aerosols constituting the decay products of emanations are of particular interest from the point of view of radiation safety [1]; in order to calculate them it is first essential to know the concentration of the emanation itself.

Many theoretical and experimental papers have been devoted to the determination of radon in mine atmospheres [2-5]. Information relating to two other emanations – thoron and actinon – with much shorter lives are considerably less in evidence. We thought that it would be logical to remedy this omission, since, in the course of their decay, these emanations form the relatively long-lived radioactive elements ThB and AcB, which may make a considerable contribution to the total dose entering the lung tissue, in relation to the so-called "latent energy" [6].

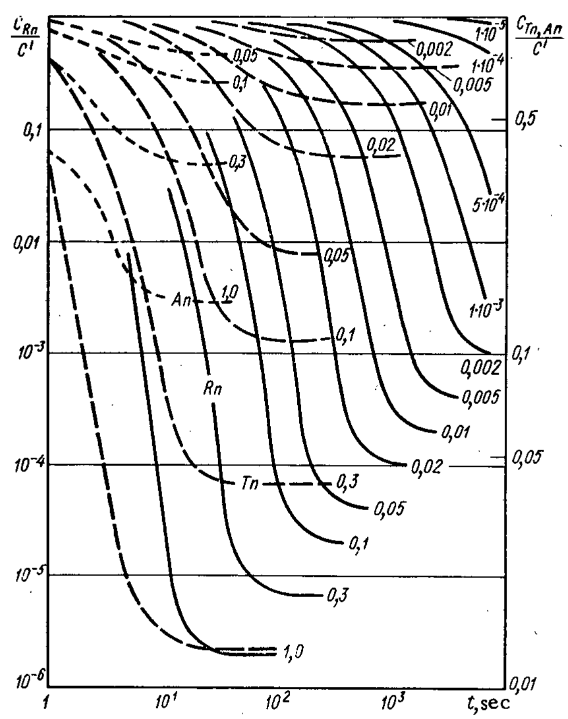

Fig. 1. Period required to establish dynamic equilibrium in relation to the multiplicity of air exchange L. The horizontal axis gives the time t, the vertical axis gives the concentration C of the emanation in units of the maximum content.

In this paper we shall attempt a theoretical estimation of the content of all three emanations (radon isotopes) in a mining atmosphere under various draught conditions (and also without ventilation) and also the rate at which the concentration changes after switching the fans on.

Content of Emanations in the Air of a Draughtless (Dead-End) Working. If a mine working is free from ventilation, the maximum concentration C' of the emanation for which its subsequent access from the surrounding rocks and ores, equal to jNS, will be balanced by the radioactive decay of the emanation in the whole volume of the working $\lambda C'V$ may be found from the expression

$$C' = jN\frac{1}{\lambda}\cdot\frac{S}{V}, \tag{1}$$

where N_i is the content of the i-th radioactive element in the rock, j is the specific flow of the emanation, λ is the decay constant of the emanation, V, S are the volume of the mine working and the area of its surface respectively.

For extended, one-dimensional regions (through-type workings), the ratio S/V depends solely on the shape of their cross section, and not on the length, being equal to 2ρ where ρ is the radius of the circular cross section of equivalent area.

The specific (normalized with respect to the content of the radioactive element) flow of emanation into the atmosphere of the mine working may, according to [7], be expressed thus:

Translated from Atomnaya Énergiya, Vol. 35, No. 3, pp. 155-158, September, 1973. Original article submitted July 21, 1972.

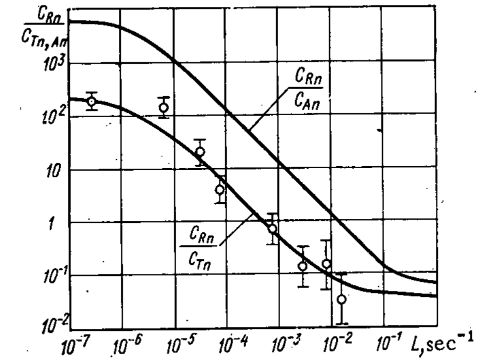

Fig. 2. Ratios of the equilibrium concentrations of the emanations for various air-exchange multiplicities and the same uranium and thorium contents in the rock: (○) results of the measurements.

TABLE 1. Maximum Concentrations of the Emanations in an Unventilated Working*

Emanation	K	l, cm	C, eman
Rn	$3{,}36\cdot10^{-6}$ *	51,2	18 600
Tn	$1{,}11\cdot10^{-6}$	0,66	79
An	$1{,}54\cdot10^{-7}$	0,173	2,9

* The coefficient of radioactive equilibrium between the uranium and radium is taken as unity.

$$j = Ka\sigma\sqrt{\lambda D}, \tag{2}$$

where σ is the density of the rock or ore, α is the emanation coefficient, K is the constant for transforming from the U or Th content to the concentration of the emanation, D is the diffusion coefficient of the emanation in the rock.

Since all three natural radioactive emanations, Rn, Tn, and An, are isotopes of the same element and have similar atomic weights, we may assume that $D_{Rn} = D_{Tn} = D_{An}$ [7]. Using Eqs. (1) and (2), we then obtain an expression suitable for calculating the maximum concentration of any of the three emanations:

$$C' = KN\alpha\sigma l\frac{2}{\rho}, \tag{3}$$

where $l = \sqrt{D/\lambda}$ is the diffusion length.

Taking the numerical value of the apparent diffusion coefficient of radon D^*_{Rn} in the rock as $0.52\cdot10^{-2}$ cm^2/sec [8], we may use Eq. (3) to calculate the maximum concentrations corresponding to the case of the purely diffusive evolution of the emanations from the saturated layer into the unventilated mine working. Table 1 shows these values for the conditions $N_U = N_{Th} = 1\%$, $\alpha = 0.2$ and $\sigma = 2.7$ in a mine working with a cross-sectional radius of $\rho = 100$ cm and $D^* = 0.52\cdot10^{-2}$ cm^2/sec.

We see from the table that the maximum Rn concentration is much greater than the other two. Hence in the absence of ventilation the Tn and An content may be neglected. However, we shall subsequently show that in ventilated workings the relative contribution of these contents increases substantially.

Dynamics of the Change Taking Place in the Emanation Content when the Fans are Switched On. If a ventilation (fan) system is set in action in a mine working with an initial emanation content of C', the change which takes place in the volume content of the emanation as time proceeds may be described by the transient equation

$$\frac{\partial C}{\partial t} = C_0L + jN\frac{S}{V} - CL - C\lambda, \tag{4}$$

where $L = \omega/V$ is the multiplicity of air exchange, ω is the volumetric velocity of the air flow, C_0 is the concentration of the emanation in the incoming air jet. The solution to this equation for initial conditions $t = 0$ and $C = C'$ may be written

$$C(t) = \frac{C_0\omega + jNS}{\omega + \lambda V}\left[1 - e^{-(L+\lambda)t}\right] + C'e^{-(L+\lambda)t}. \tag{5}$$

We see from an analysis of Eq. (5) that, as $\omega \to 0$, this transforms into the equation with which we are already acquainted, Eq. (1), while the concentration of the emanation tends toward the maximum $C(t) \to C'$. On the other hand, for a high multiplicity of air exchange, $\omega \to \infty$ and $C(t) \to C_0$. Taking $C_0 = 0$ for simplicity and dividing Eq. (5) by (1), we obtain an expression which may be used for calculating the relative content of the emanations (in units of the maximum C') at any instant of time after the fans have been switched on:

$$\frac{C(t)}{C'} = \frac{\lambda}{L+\lambda}\left[1 - e^{-(L+\lambda)t}\right] + e^{-(L+\lambda)t}. \tag{6}$$

Figure 1 shows the variation in the emanation content over periods of from 1 sec to 160 min after ventilation has started; the curves relate to a wide range of values of the parameter L, between 1 and 10^{-5} sec^{-1}. It follows from the graphs that, in the forced ventilation mode characterized by an air-exchange multiplicity of 10^{-2}-10^{-3} sec^{-1}, the change in the thoron (Tn) concentration is effected in 2.5-3.5 min and that of the actinon (An) in 10-15 sec, while the radon (Rn) concentration continues varying for 1.5 h after the fan has been switched on. The radon concentration falls by about a factor of 2000 and the thoron by only 30%. Ventilation of the kind in question ($L = 5 \cdot 10^{-3}$) has no marked effect on the actinon content at all.

After using Eq. (3) to calculate the maximum concentrations, we may use the graphs of Fig. 1 to determine the absolute contents of any of the three emanations at any instant of time after ventilation has started.† Thus if, as initial maximum concentrations, we take the concentrations indicated in Table 1 ($C'_{Rn} = 18{,}600$, $C'_{Tn} = 79$, and $C'_{An} = 2.9$ eman) then for $L = 10^{-2}$ sec^{-1} we obtain, for example, after 17 min $C_{Rn} = 5.6$, $C_{Tn} = 47.4$, and $C_{An} = 2.9$ eman. We see that the Tn content is now more than eight times as much as the Rn.

Under steady dynamic equilibrium, characterized by the condition $(L + \lambda_{Rn})t \gg 1$, Eq. (6) simplifies:

$$\frac{C(L)}{C'} = \frac{\lambda}{L+\lambda}. \tag{7}$$

In this case the concentration of the emanation will clearly depend solely on the multiplicity of air exchange L.

<u>Relation between the Rn, Tn, and An Concentrations in a Mine Atmosphere.</u> If the radioactive equilibrium is not infringed in the uranium–radium series, and, as before, the diffusion coefficients of Rn, Tn, and An are taken as identical, from Eqs. (1) and (3) we may easily derive expressions for the ratios of the maximum concentrations:

$$\frac{C'_{Rn}}{C'_{Tn}} = 2.36 \cdot 10^2 \frac{N_U}{N_{Th}} \cdot \frac{\alpha_{Rn}}{\alpha_{Tn}};$$
$$\frac{C'_{Rn}}{C'_{An}} = 6.45 \cdot 10^3 \frac{\alpha_{Rn}}{\alpha_{An}}. \tag{8}$$

For steady-state dynamic equilibrium we have the following from (6)

$$\frac{C_{Rn}(L)}{C_{Tn}(L)} = 3.9 \cdot 10^{-2} \frac{L+\lambda_{Tn}}{L+\lambda_{Rn}} \cdot \frac{N_U}{N_{Th}} \cdot \frac{\alpha_{Rn}}{\alpha_{Tn}};$$
$$\frac{C_{Rn}(L)}{C_{Ac}(L)} = 7.66 \cdot 10^{-2} \frac{L+\lambda_{An}}{L+\lambda_{Rn}} \cdot \frac{\alpha_{Rn}}{\alpha_{An}}. \tag{9}$$

It is not difficult to see that, in the absence of ventilation, when L = 0, Eqs. (9) transform into (8), which are valid for the ratios of the maximum concentrations. Curves calculated from Eqs. (9) under the conditions $N_U = N_{Th}$ and $\alpha_{Rn} = \alpha_{An}$ are presented in Fig. 2; we see from these curves, in particular, that for an air-exchange multiplicity of $L = 5 \cdot 10^{-3}$ sec^{-1} there should be the following relationship between the concentrations of the natural radioactive emanations: $C_{Rn} = 1$, $C_{Tn} = 8$, $C_{An} = 0.5$. This is confirmed by the results of simultaneous measurements of Tn and Rn carried out in one of the mines with a variable intensity of ventilation.

The calculations showed that, in weakly-ventilated mine workings ($L \le 10^{-4}$ sec^{-1}), passing through poor uranium–thorium ore or "empty" rock, the presence of Tn and An in the mine atmosphere could be neglected, since in this case the condition $C_{Rn} \gg C_{Tn} \gg C_{An}$ was always satisfied.

On the other hand, in workings with strong forced ventilation ($L \ge 10^{-3}$ sec^{-1}) passing into rich, mixed ore, the Tn and An concentrations increased considerably relative to the Rn, and even the condition $C_{Tn} > C_{Rn}$ was infringed. Hence in this case allowance must always be made for the daughter products of Tn in the "latent energy."

In addition to this, the time required to establish equilibrium concentration after starting the ventilation depends not only on the multiplicity of the air exchange, i.e., the intensity of the

† By virtue of the convection of the emanation from microcracks in the ventilated working, a correction factor $\psi = \sqrt{D/D^*}$ should be introduced into Eqs. (6) and (7), where D is the effective diffusion coefficient. Allowing for experimental data, the empirical expression for this correction valid for $0 \le L \le 10^{-2}$ sec^{-1} will take the form $\psi = 1 + aLe^{bL}$, where $a = b = 123$.

ventilation system, but also on the form of the emanation, being a maximum for Rn and a minimum for An.

LITERATURE CITED

1. D. I. Holliday et al., Problem of Radon in Uranium Mines [Russian translation], Gosatomizdat, Moscow (1961).
2. A. V. Vykhovskii, Hygienic Problems in the Underground Processing of Uranium Ores [in Russian], Medgiz, Moscow (1963).
3. A. V. Vykhovskii, N. N. Chesnokov, and I. D. Shalaev, At. Énerg., 19, No. 2, 161 (1965).
4. V. I. Baranov and L. V. Gorbushina, Questions of Safety in Uranium Mines [in Russian], Gosatomizdat, Moscow (1962).
5. Yu. P. Bulashevich and N. P. Kartashov, At. Énerg., 6, No. 5, 584 (1958).
6. L. S. Ruzer, Radioactive Aerosols [in Russian], Izd. Komiteta Standartov, Moscow (1968).
7. G. F. Novikov and Yu. N. Kapkov, Radioactive Methods of Prospecting [in Russian], Nedra, Leningrad (1965).
8. A. S. Serdyukova, Yu. T. Kapitanov, and M. P. Zavodskaya, Fizika Zemli, 7, 123 (1965).

A LOCAL HETEROGENEOUS CALCULATION OF A REACTOR

V. Lelek

UDC 621.039.521

In reactor calculations one often encounters problems in which one need find the neutron flux and other characteristics in only a limited region of the reactor. Ordinarily in order to find such quantities one must solve the entire problem. If, for example, one requires the ratio of the neutron fluxes on absorbing rods in the vicinity of a regulator, one must solve the entire system of heterogeneous equations; for a reactor with a large number of rods this can prove to be a rather difficult task [1]. A method of local calculation of a heterogeneous reactor in the approximation of axially independent pseudosources is described below.

We write the heterogeneous equations of a critical reactor symbolically as

$$\sum_l H_{kl}\Phi_l = \Phi_k, \tag{1}$$

where Φ_l is the neutron flux at the rods, and H_{kl} is the influence function. We are interested in the solution of equation (1) only inside some region (for concreteness we take a circle). Let us call this region a supercell. If we denote by the subscript $\bar{k}$ the rods inside the supercell and by k^* the rods outside it, then (1) can be formally written in the form

$$\sum_{\bar{l}} H_{\bar{k}\bar{l}}\Phi_{\bar{l}} + \sum_{l^*} H_{k\text{-}l^*}\Phi_{l^*} = \Phi_{\bar{k}}; \tag{2}$$

$$\sum_{\bar{l}} H_{k^*\bar{l}}\Phi_{\bar{l}} + \sum_{l^*} H_{k^*l^*}\Phi_{l^*} = \Phi_{k^*}. \tag{3}$$

If Φ_{l^*} is known, the second sum in Eq. (2) can be interpreted as an external neutron source in the supercell. With the determination of the magnitude of these sources by some means Eq. (3) becomes superfluous and the problem is significantly simplified.

We note that for such calculations one should always consider a critical reactor. (We assume that criticality is attained by control rods situated outside the supercell.)

Equations (2) and (3) yield another important piece of information: the fluxes Φ_{l^*} may be considered as linear functions of the $\Phi_{\bar{l}}$.

We introduce a model representation. Let the fictitious neutron sources which approximate the second sum of Eq. (2) be distributed on the radius $r^* > R_b$, where R_b is the radius of the supercell; its center coincides with the origin of coordinates.

The corresponding two group equations have the form

$$\begin{aligned}
&-d\,\Delta\Psi + \frac{d}{\tau}\Psi + \sum_k \omega_k \delta(\mathbf{x}-\mathbf{x}_k)\Psi_k \\
&+ \frac{1}{2\pi r^*}\delta(r-r^*)\,\Omega\sum_k \omega_k\Psi_k = \frac{1}{\nu}\sum_k \eta_k\gamma_k\delta(\mathbf{x}-\mathbf{x}_k) \\
&\times \varphi_k + \frac{1}{2\pi r^*}\delta(r-r^*)\frac{\Gamma_f}{\nu}\sum_k \eta_l\gamma_k\varphi_k; \\
&\qquad -D\Delta\varphi + \frac{D}{L^2}\varphi + \sum_k \gamma_k\delta(\mathbf{x}-\mathbf{x}_k)\varphi_k \\
&+ \frac{1}{2\pi r^*}\delta(r-r^*)\Gamma_s\sum_k \gamma_k\varphi_k = S\Psi + \sum_k \sigma_k\delta(\mathbf{x}-\mathbf{x}_k)\Psi_k
\end{aligned} \tag{4}$$

Translated from Atomnaya Énergiya, Vol. 35, No. 3, pp. 159-161, September, 1973. Original article submitted August 29, 1972.

TABLE 1. Ratio of the Thermal Neutron Fluxes in Rods, as Calculated by an Exact and by the Proposed Method.

Model	N	Number of the radius on which the rods are located (counting from the center of the reactor)							
		1	2	3	4	5	6	7	8
1 $\Gamma_s=0$	5	1,0000	0,9521	—	—	—	—	—	—
	13	1,0000	0,9890	0,9630	0,9292	—	—	—	—
	21	1,0000	0,9984	0,9933	0,9721	0,9564	—	—	—
	37	1,0000	0,9999	0,9998	0,9963	0,9945	0,9720	0,9716	0,9603
2 $\Gamma_f=0$	5	1,0000	0,9519	—	—	—	—	—	—
	13	1,0000	0,9888	0,9628	0,9283	—	—	—	—
	21	1,0000	0,9983	0,9932	0,9713	0,9551	—	—	—
	37	1,0000	1,0000	0,9998	0,9959	0,9938	0,9685	0,9650	0,9524
3 $\Gamma_s=\Gamma_f=\Gamma$	5	1,0000	0,9511	—	—	—	—	—	—
	13	1,0000	0,9962	0,9849	1,0158	—	—	—	—
	21	1,0000	0,9995	0,9967	0,9873	0,9832	—	—	—
	37	1,0000	1,0004	1,0010	1,0018	1,0047	1,0228	1,0498	1,0840
4 $J_b=0$	5	1,0000	1,0099	—	—	—	—	—	—
	13	1,0000	1,0001	0,9970	1,0687	—	—	—	—
	21	1,0000	1,0004	0,9995	0,9998	1,0057	—	—	—
	37	1,0000	1,0002	1,0003	0,9990	0,9994	0,9963	1,0078	1,0173
Exact flux, relative units		4,7409	7,4217	7,9959	8,4054	8,4672	8,4209	8,3600	8,2845

$$+\frac{1}{2\pi r^*}\delta(r-r^*)\Omega\sum_k \sigma_k\Psi_k, \tag{5}$$

where φ and Ψ are the fluxes of thermal and fast neutrons, D and d are the diffusion coefficients for thermal and fast neutrons, L and τ are the diffusion length and neutron age, S is the transfer cross section from the fast to the thermal group, x_k is the radius vector of the k-th rod, r^* is the radius on which the unknown neutron sources are distributed, γ_k and ω_k are the absorption cross sections for thermal and fast neutrons in the rod, σ_k is the cross section for transfer of fast neutrons to the thermal group (in the rod), ν is the eigenvalue for the problem, and Ω, Γ_f, and Γ_s are the relative magnitudes of the sources outside the supercell. The sum runs over all elements in the supercell. We write the solutions of Eqs. (4) and (5) in the form

$$\sum_k \left\{\delta_{lk}+\frac{\omega_k}{2\pi d}\left[K_0\left(\frac{r_{lk}}{\sqrt{\tau}}\right)+\Omega K_0\left(\frac{r^*}{\sqrt{\tau}}\right) I_0\left(\frac{r_l}{\sqrt{\tau}}\right)\right]\right\}\Psi_k$$
$$=\frac{1}{\nu}\frac{1}{2\pi d}\sum_k \eta_k\gamma_k\left[K_0\left(\frac{r_{lk}}{\sqrt{\tau}}\right)+\Gamma_f K_0\left(\frac{r^*}{\sqrt{\tau}}\right) I_0\left(\frac{r_l}{\sqrt{\tau}}\right)\right]\varphi_k; \tag{6}$$

$$\sum_k \left\{\delta_{lk}+\frac{\gamma_k}{2\pi D}\left[K_0\left(\frac{r_{lk}}{L}\right)+\Gamma_s K_0\left(\frac{r^*}{L}\right) I_0\left(\frac{r_l}{L}\right)\right]\right\}\varphi_k$$
$$=\frac{1}{2\pi D}\sum_k \left(\sigma_k\left[K_0\left(\frac{r_{lk}}{L}\right)+\Omega K_0\left(\frac{r^*}{L}\right) I_0\left(\frac{r_l}{L}\right)\right]\right.$$
$$-\frac{S\tau}{d}\frac{L^2}{L^2-\tau}\omega_k\left\{\left[K_0\left(\frac{r_{lk}}{L}\right)+\Omega K_0\left(\frac{r^*}{L}\right) I_0\left(\frac{r_l}{L}\right)\right]\right.$$
$$\left.\left.-\left[K_0\left(\frac{r_{lk}}{\sqrt{\tau}}\right)+\Omega K_0\left(\frac{r^*}{\sqrt{\tau}}\right) I_0\left(\frac{r_l}{\sqrt{\tau}}\right)\right]\right\}\right)\Psi_k$$
$$+\frac{1}{\nu}\frac{1}{2\pi D}\frac{S\tau}{d}\frac{L^2}{L^2-\tau}\sum_k \eta_k\gamma_k\left\{\left[K_0\left(\frac{r_{lk}}{L}\right)+\Gamma_f K_0\left(\frac{r^*}{L}\right) I_0\left(\frac{r_l}{L}\right)\right]\right.$$
$$\left.-\left[K_0\left(\frac{r_{lk}}{\sqrt{\tau}}\right)+\Gamma_f K_0\left(\frac{r^*}{\sqrt{\tau}}\right) I_0\left(\frac{r_l}{\sqrt{\tau}}\right)\right]\right\}\varphi_k, \tag{7}$$

where $r_l = |\mathbf{x}_l|$, $r_{lk} = |\mathbf{x}_l - x_k|$, and K_0 and I_0 are Bessel functions.

The system of homogeneous equations (6) and (7) depend on the magnitudes of the pseudosources. A relationship between these sources is given by the condition of existence of a solution of the system, i.e., by the vanishing of the determinant of the system,

$$det(\Omega,\ \Gamma_f,\ \Gamma_s)=0. \tag{8}$$

From the physical point of view this represents the condition that the supercell together with the pseudosources be critical.

Inasmuch as the matrix elements contain only first and second powers one can show that

$$det(\Omega, \Gamma_f, \Gamma_s) = d_0 + d_f\Gamma_f + d_s\Gamma_s + d_{fs} + d_{fs}\Gamma_f\Gamma_s, \tag{9}$$

where $d_\xi = d_{0\xi} + d_{\Omega\xi}\Omega + d_{\Omega\Omega\xi}\Omega^2$; $\xi = 0$, f, s, f_s.

Of course, Eq. (8) does not determine Γ_f, Γ_s and Ω uniquely; however, in practical calculations it turns out that the neutron fluxes in the rods in the supercell depend on the various solutions of Eq. (8) only in some not very large neighborhood of the boundary. This fact has a simple physical interpretation: at distances larger than the slowing down length it makes no difference whether a neutron was initially a fast or thermal neutron.

Since matrix elements of high degree are contained in the equation, it is possible to obtain solutions which when substituted into Eqs. (6) and (7) yield solutions of these equations which are not everywhere positive. In such a case ν represents the eigenvalue of some other reactor.

Equations (6), (7) and (8) were programmed (program MATTHAEUS [2]), and the results of the calculations compared to an accurate solution of the entire reactor obtained by the program HECATE [3]. Because of limitations of the program HECATE only thermal neutron fluxes were compared.

Four solutions of Eq. (8) with $\Omega = 0$ were considered:

$$\left.\begin{array}{ll} \Gamma_s = 0, & \Gamma_f \\ \Gamma_f = 0, & \Gamma_s \\ \Gamma_f = \Gamma_s = \Gamma, & \Gamma \end{array}\right\} \text{determined by Eq. (8),}$$

and a fourth solution found by the simultaneous solution of Eqs (8) and (10) with

$$J_b = R_b d \int_0^{2\pi} \frac{\partial\Psi}{\partial r}\Big|_{r=R_b} d\varphi = 0,$$

where $R_b = a\sqrt{N/\pi}$; N is the number of rods in the supercell and a is the pitch of the square lattice.

In this fourth case it is assumed that the flow of fast neutrons into the supercell is zero. The supercell consists of a highly effective central control rod surrounded by N−1 fuel rods.

The following data was used in the calculation: a = 25 cm; r^* = 100 cm; L = 100 cm; τ = 100 cm^2; D = 1 cm; d = 0.5 cm; S = 0.005 cm^{-1}; ρ is the rod radius, equal to 5 cm; $\omega_k = \sigma_k = 0$; $\nu = 1.21653$.

For the control rod $\eta = 0$ and $\gamma = 4$; for the fuel rods these parameters are 1.34 and 2 respectively. The reactor radius is 222 cm, and the total number of rods is 233.

Because of symmetry it is sufficient to calculate the neutron fluxes for only one eighth of the rods. The results of the calculation are presented in Table 1.

Models 1 and 2 give almost identical errors; these errors are somewhat larger than with the other models. The model which had zero current of fast neutrons into the supercell gave results which were closest to the exact results. This approximation is based on the constancy of the slowing down density in a thermal reactor. The relative error of 1% occurs only for the edge rods; for the interior rods the error is within the limits of accuracy of the calculations.

In conclusion, the proposed method of local calculation of a heterogeneous reactor is sufficiently accurate and quite efficient, if the behaviour of the flux is considered only in some part of the reactor, provided this part is relatively large compared to the slowing down length and the diffusion length in the lattice.

LITERATURE CITED

1. V. Lelek, Dissertation, Institute for Nuclear Research, Rzhezh, Czechoslovakia (1968).
2. V. Lelek, Preprint UJV 2705. R., (1971).
3. J. Rosek and A. Miasinikov, Program HECATE, UJV 2196 R. P. (1969).

NEUTRON FLUXES GENERATED BY HIGH ENERGY PROTONS IN THICK BLOCKS OF URANIUM

V. S. Barashenkov and V. D. Toneev

UDC 539.12.17

In recent years, in connection with discussions of the prospects of the electronuclear method of producing energy and generating isotopes of rare elements [1-3], there has been increasing interest in processes caused by beams of high energy particles in fissionable materials.

The present work presents some results of theoretical studies of these processed performed at the Joint Institute for Nuclear Research during the years 1964 to 1968. These results were obtained by the Monte Carlo method by means of direct modelling of the life history of each particle in the block of matter up to the radiative capture of the particle or its escape from the block.

Those characteristics of the interaction of the particles with nuclei which were required for the calculation were also computed by the Monte Carlo method on the basis of the cascade–evaporation model in conjunction with the statistical theory of fission; the results obtained by this procedure agree well with the

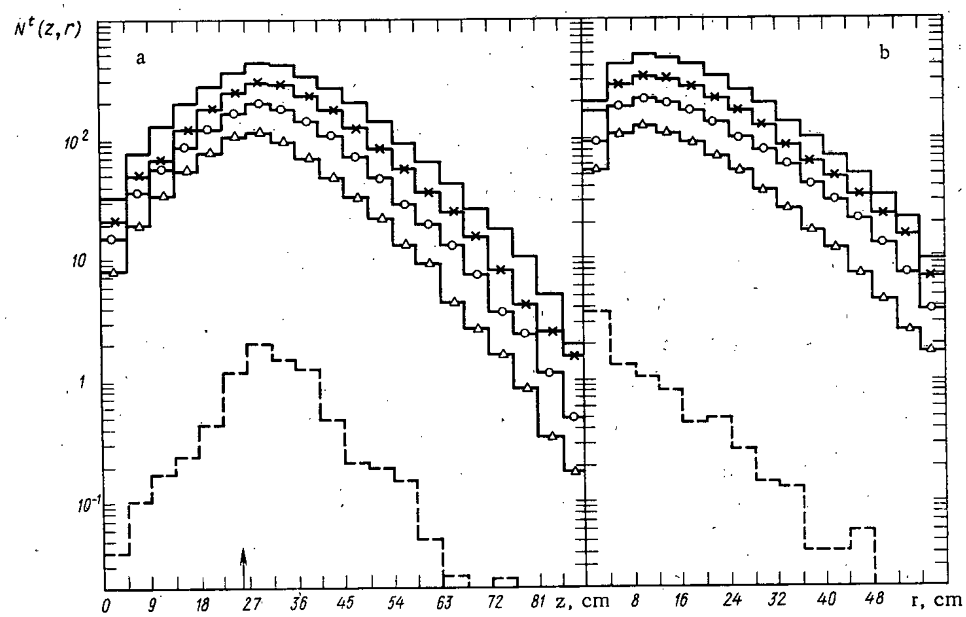

Fig. 1. The distribution of the total number of elastic and inelastic collisions of nucleons with nuclei in the longitudinal (a) and transverse (b) directions for a block of a natural mixture of uranium isotopes, irradiated by protons with energy T (normalized to one primary proton): (—) 660 MeV; (– × –) 500 MeV; (– ○ –) 400 MeV; (– Δ –) 300 MeV. The dashed line gives the distribution of the number of collisions of nucleons with E > 10.5 MeV for the case T = 660 MeV. In this figure, and in the succeeding figures, the arrow gives the location of the proton source.

Translated from Atomnaya Énergiya, Vol. 35, No. 3, pp. 163-168, September, 1973. Original article submitted August 28, 1972.

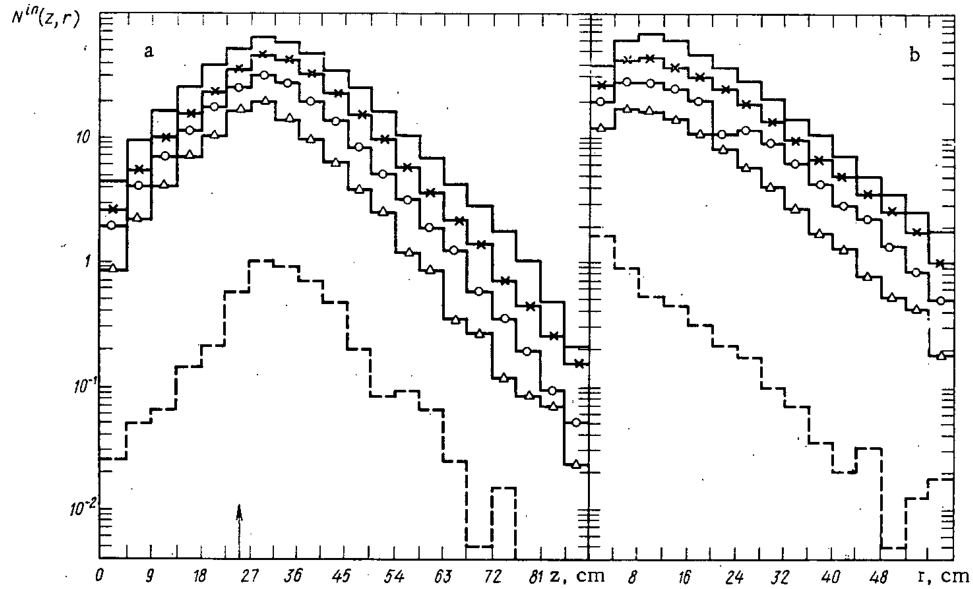

Fig. 2. The distribution of inelastic collisions of nucleons with nuclei in the longitudinal (a) and transverse (b) directions for a block of a natural mixture of uranium isotopes, irradiated by protons with energy T (normalized to one primary proton). The symbols are the same as in Fig. 1.

TABLE 1. The Mean Energy of Nucleons at Different Distances from the Axis of a Beam of Primary Protons with Energy T*

r, cm	T, MeV			
	300	400	500	660
5,6	0,63	0,86	0,95	1,16
8,4	0,57	0,70	0,72	0,85
12,2	0,34	0,53	0,52	0,67
14,0	0,38	0,57	0,46	0,61
16,8	0,32	0,48	0,45	0,50
30,0	0,29	0,30	0,30	0,34
33,6	0,21	0,28	0,32	0,35
39,2	0,22	0,27	0,35	0,40

*The energy of the nucleons is expressed in million electron volts; the statistical error of the calculation is ±5 to 7%.

known experimental data. Since the energy of the primary particles was not too high (T < 700 MeV), we neglected meson-production processes. Charged particles were tracked to an energy of 30 MeV, taking into account their ionization loss. The behavior of neutrons in the energy range less than 10.5 MeV was described with the help of a 25-group system of reactor constants [4].

The program which we used allowed the calculation to be performed for practically any geometry and for different compositions of the irradiated material; however, the data presented below relate only to a block of pure uranium U^{238} and to a natural mixture of the isotopes U^{238} and U^{235}, with a ratio of the number of nuclei of U^{235} and U^{238} of $\eta \equiv N_n^5/N_n^8 = 0.72\%$. For simplicity the calculation assumed the block was a cylinder of radius R = 60 cm and length L = 90 cm. A point source emitting protons along the central axis of the cylinder was placed inside the block at a distance z_0, equal to 26 cm, from its front face.†

Figure 1 presents the distribution in the block, as a function of the radius r and depth z, of the number of nuclear interactions of the nucleons in a cascade shower generated by one primary proton,

$$N_{\parallel}^{t}(z) = 2\pi \int_0^R N^t(z, r)\, r\, dr;\quad N_{\perp}^{t}(r) = \int_0^L N^t(z, r)\, dz.$$

Figure 2 presents the corresponding distributions of inelastic nuclear interactions $N_{\parallel}^{in}(r)$ and $N_{\perp}^{in}(r)$. For comparison Fig. 1 shows separately the distribution of the number of interactions associated only with the

†Experimentally this corresponds to a well collimated beam of primary protons directed in a narrow channel along the central axis of the cylinder from a depth z_0. Since, for the energy of the primary protons of the order of several hundred million electron volts, their ionization mean free path λ_{ioniz} and their nuclear mean free path for inelastic interactions $\lambda_{n.i.}$ is significantly smaller than the dimensions of the block being considered (for example, for T = 660 MeV, λ_{ioniz} = 19 cm and $\lambda_{n.i.}$ = 10 cm), the results of the calculation should be close to the data for the case of protons travelling in an infinite medium.

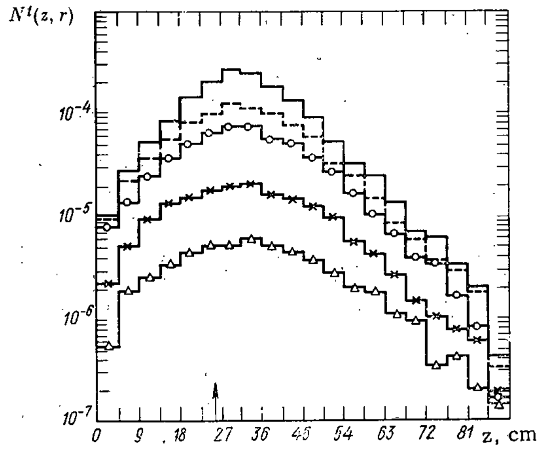

Fig. 3. The distribution in the longitudinal direction of the total number $\{2\pi r N^t(r)\}$ of elastic and inelastic collisions of nucleons with nuclei at various distances r from the axis of the block (normalized to one primary proton whose energy is T = 660 MeV). (—) 5.6 cm; (– – –) 12.2 cm; (– ○ –) 16.8 cm; (– × –) 28 cm; (– Δ –) 39.2 cm.

TABLE 2. Mean Characteristics of the Interaction of a Beam of Protons with Energy T (Normalized to one primary proton) with a Block of Natural Uranium

Characteristics	T, MeV 300	400	500	660
N^t	700	1290	1990	3030
$N^t(<10{,}5)$	3,0	4,0	5,8	8,5
N^{in}	100	184	280	430
$N^{in}(<10{,}5)$	1,7	2,1	3,1	4,6
N^8_{cap}	17	32	48	74 (60)
N^5_{cap}	0,18	0,36	0,5	0,8 (—)
N_{esc}	1,1	2,5	3,3	5,4 (4)
N	18	35	52	80 (64)
$\nu(>10{,}5)$	1,4	1,6	2,4	3,7 (3,6)
$\nu^8(<10{,}5)$	2.6	5,6	8,6	13,4 10,2)
$\nu^5(<10{,}5)$	1,0	1,8	3,0	4,6 (—)
ν	5,0	9,0	14,0	21,7 (13,8)
Q, GeV	1,2	2,2	3,4	5,0 (3,4)

high energy component which is not included in the contribution of the "evaporated particles" (T > 10.5 MeV). The histograms of Fig. 3 show the change in the quantity N^t (z, r) as a function of the distance from the central axis of the block.

When normalized to each other, the distributions associated with the interactions with the U^{235} nuclei are the same as those associated with the U^{238} nuclei; however, as will be shown below, there are significant differences in the absolute magnitudes of these distributions.

The distributions N^t and N^{in} characterize the distribution within the block of the flux of particles (primarily neutrons) which are generated by a primary proton with energy T, and determine the distributions of the fundamental physical quantities: the number of fissions and the yields of the various isotopes (in particular, Pu^{239}), the heat release, etc.

From the figures presented it is apparent that all the distributions have a marked maximum in an annular zone with radius $r \approx \lambda_{n.i}/2$ at a distance $z - z_0 \approx \lambda_{n.i}/2$ from the proton source. For T in the interval between 300 and 700 MeV this result does not depend on the magnitude of the energy T (Fig. 4 and Fig. 5).

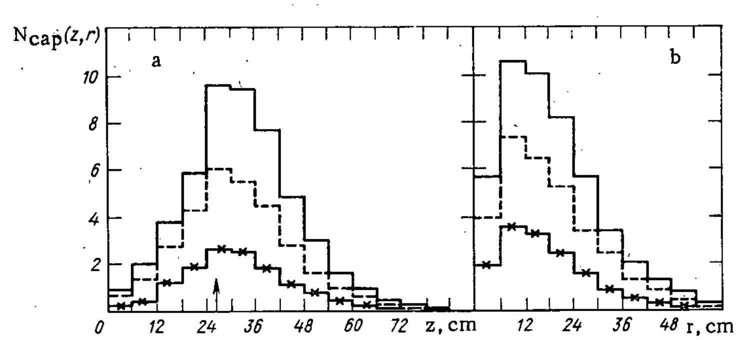

Fig. 4. The dependence in the longitudinal (a) and radial (b) directions of the number of radiative captures of neutrons $U^{238}(n, \gamma)U^{239}$ on the energy of the primary proton T for a block of a natural mixture of uranium isotopes (normalized the same as in Fig. 1). (—) 500 MeV; (– – –) 400 MeV; (– × –) 300 MeV.

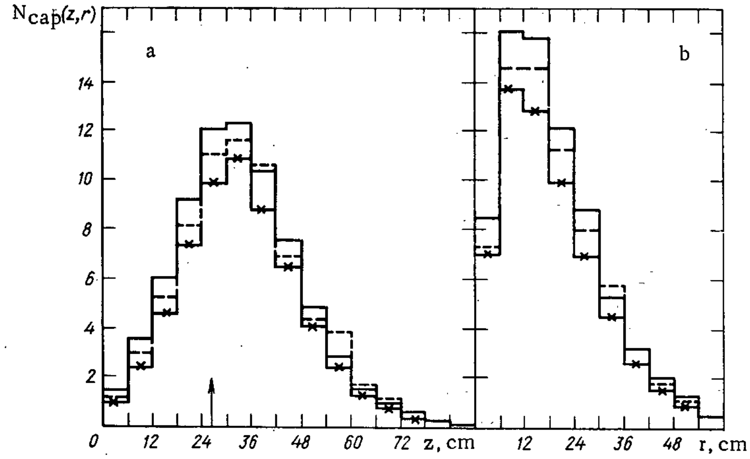

Fig. 5. The distribution of the number of radiative captures of neutrons in the longitudinal (a) and radial (b) directions for a uranium block irradiated by protons with energy T = 660 MeV (normalized the same as in Fig. 1). The histograms represent calculations for a natural mixture of uranium isotopes with the parameter a equal to 0.05 MeV^{-1} (the — line) and a equal to 0.1 MeV^{-1} (the – – – – line); the line —— × —— is for the calculation for pure U^{238} with a = 0.05 MeV^{-1} and η = 0. The arrow gives the position z_c of the proton source.

As the calculations show, the distributions of the basic physical quantities depend very weakly on the value of the nuclear level density parameter a (see Fig. 5). The histograms of Figs. 1 to 4 and all the results presented below were calculated with a = 0.05 MeV^{-1}.

The shape of the energy spectrum of the nucleons generated in the block is also characterized by a weak dependence on the primary energy T. However, as is evident from Table 1, the mean energy of the nucleons increases appreciably with increase in T, although it always remains of the order of 1 MeV. Failure to take this fact into account can lead to serious errors in experiments which use the $(n-\gamma)$ reaction as an indicator, since the probability of this reaction depends significantly on the shape of the energy spectrum of the neutrons.

The most interesting mean characteristics of the interaction of a beam of protons with a block of uranium are presented in Table 2. In this table $N^t = 2\pi \int_0^R rdr \int_0^L N^t(z, r)dz$ is the total number of elastic

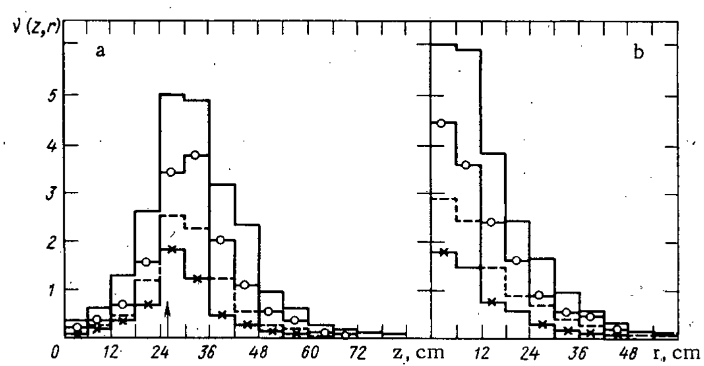

Fig. 6. The dependence on the primary proton energy of the distribution of the number of fission events in a block consisting of a natural mixture of uranium isotopes: (—) 660 MeV; (– ○ –) 500 MeV; (– – –) 400 MeV; (– × –) 300 MeV.

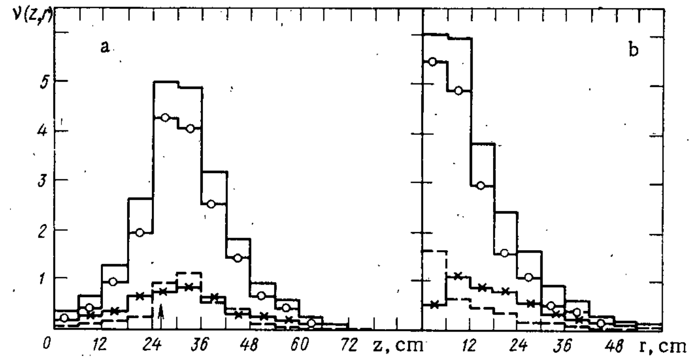

Fig. 7. The distribution in a block of a natural mixture of uranium isotopes of the number of fission events initiated by a proton with energy T = 660 MeV. (—) ν^{8+5}; (– – –) ν^5 for T < 10.5 MeV; (– × –) ν^8 for T < 10.5 MeV; (– ○ –) ν^8.

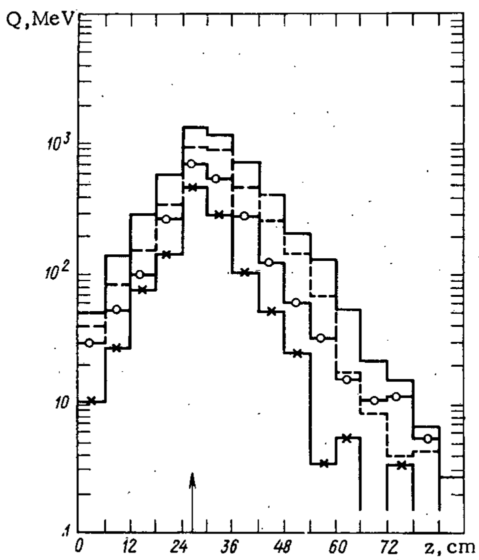

Fig. 8. The distribution of heat release in a block of natural uranium irradiated by protons with energy T: (—) 660 MeV; (– – –) 500 MeV; (– ○ –) 400 MeV; (– × –) 300 MeV.

and inelastic collisions in the block of the particles from a cascade generated by one primary proton, N^{in} is the corresponding number of inelastic interactions, N^8_{cap} and N^5_{cap} are the number of radiative captures of neutrons by the nuclei U^{238} and U^{235} respectively, N_{esc} is the number of neutrons escaping from the block, N is the total yield of neutrons, ν^8 and ν^5 are the number of fission events of the nuclei U^{238} and U^{235}, ν is the total number of fissions, and Q is the heat release in the block. Quantities which characterize the interactions of particles with energies E < 10.5 MeV and E > 10.5 MeV are presented separately. For T = 660 MeV the quantities associated with a block of pure U^{238} are shown in parentheses. The statistical error in the data presented in Table 2 is 5 to 10%.

The number of interactions N^t and N^{in} is a measure of the degree of branching ("strength") of the cascade in the block. The strength of the cascade increases rapidly with increase in the energy T. The number of neutrons captured in U^{238} is equal to the number of Pu^{239} nuclei produced.

The total yield of neutrons from one primary proton is computed from the number of neutrons escaping from the block through its sides and end faces, and from the "internal escape" defined as the number of radiative captures of neutrons by the isotopes U^{238} and U^{235}:

$$N = N^8_{cap} + N^5_{cap} + N_{esc}.$$

This quantity increases by a factor of four when the proton energy is increased by a factor of two (from 300 to 600 MeV). The number of fissions ν increases in approximately the same proportion.

The distribution of the fission events in the block and the dependence of this distribution on the proton energy and the isotopic composition of the block is shown in Figs. 6 and 7.

In order to estimate the influence of the addition of the U^{235} nuclei the calculation was performed for a block of pure U^{238}. As is evident from Table 2, the presence of only 0.72% admixture of U^{235} in natural uranium increases the neutron yield and the number of fissions by almost 1/4.

The last row of Table 2 gives the magnitude of the thermal energy released in the block by the cascade of particles initiated by one proton with energy T. This energy is computed from the ionization loss, from the energy released in nuclear fission, and from the energy of particle emission. Since the fission

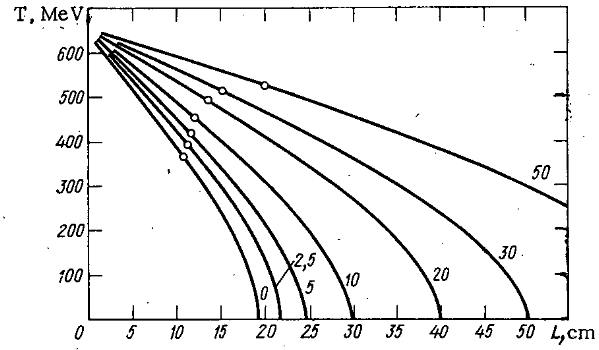

Fig. 9

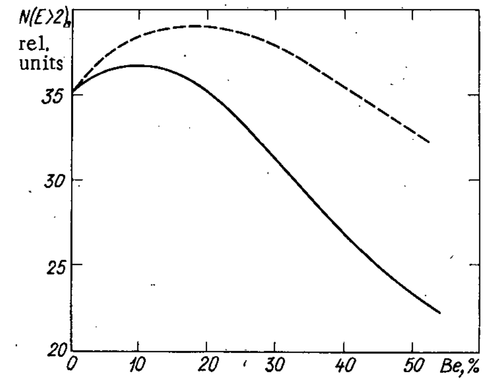

Fig. 10

Fig. 9. The energy of a proton after it has travelled a distance z in a block consisting of a homogeneous mixture of U^{238} and Be^9. The initial energy of the proton is T = 660 MeV. The numbers on the curve represent the percent content of Be^9; ○ gives the value of the proton energy after it has traversed a distance $z = \lambda_{n.abs}$.

Fig. 10. The dependence of the yield (in relative units) of fast neutrons (E < 2 MeV) on the amount of the admixture of Be^9 in a block of uranium U^{238}. (—) Yield of neutrons from U^{238} only; (– – –) yield of neutrons taking into account the multiplication of neutrons knocked out of the Be^9 nucleus by the primary proton.

energy release is the principal contributor, the distribution of heat release is found to be very close to the distribution of the number of fission events $\nu(z, r)$.

All the quantities presented in Table 2 and in Figs. 6 to 8 were computed with the nuclear level density parameter a equal to 0.05 MeV^{-1}. Doubling the value of a results in decreasing the neutron yield by 10 to 15%.* In particular, for a block of a natural mixture of uranium isotopes when T = 660 MeV one has $N^8_{cap} = 64$ and $N_{esc} = 4$, so that $N \approx 68$. Moreover, one has $\nu^8(< 10.5) = 9.5$ and $\nu^5(< 10.5) = 4.1$, in this case.

The yield of neutrons N depends extremely strongly on the magnitude of ionization loss of the beam of primary protons. One can try to decrease these losses (thereby increasing the yield of neutrons) by placing in front of the block of uranium a layer of a material (e.g., Be^9) with a large yield for a reaction of the type (p, xn). However, experimental studies [5] have shown that this method does not yield a positive result: the yield of neutrons is found to be even smaller than for direct irradiation of the uranium.

Another possibility consists in decreasing the density of the uranium block per ionization mean free path of the primary proton by a homogeneous admixture of a light material. When this admixture is increased the ionization mean free path increases significantly more rapidly than the nuclear mean free path because the beam of primary protons is more completely utilized. This is seen clearly in Fig. 9 which gives, for various concentrations of an admixture consisting of Be^9, the mean energy of the primary proton at a distance equal to the nuclear mean free path $\lambda_{n.abs}$ for a proton in the block.

Figure 10 presents the dependence of the mean number of "fast" neutrons with energies T ≥ 2 MeV on the percent of Be^9 in the block, for a primary proton energy T = 660 MeV. An admixture of approximately 20% of Be^9 is found to be optimal. At T = 660 MeV this gives a gain of approximately 10 or 12 neutrons out of a total yield N.

One should mention that there is still another interesting possibility for increasing the yield of neutrons by decreasing the ionization loss. This consists in using a beam of deuterons so that from the very start one has a nonionizing particle – the neutron. Estimates show that the yield of neutrons is increased

*The value $a = 0.05$ MeV^{-1} gives the best agreement with the known experimental data for nucleon–nucleus interactions; however, agreement can be obtained even for $a = 0.1$ MeV^{-1}. One should note that a greater number of neutrons are produced in a nucleon–nucleus interaction when $a = 0.1$ MeV^{-1} than when $a = 0.05$ MeV^{-1}; on the other hand, a larger number of neutrons are produced in the block when $a = 0.05$ MeV^{-1}. The cause of this apparent contradiction is that when $a = 0.05$ MeV^{-1} the evaporated neutrons have a harder energy spectrum, and this significantly influences their behavior in the reactor energy region.

by 15 to 20% in the energy range T ≈ 300 to 700 MeV (i.e., for T ≈ 150 to 350 MeV/nucleon). At high energies the advantage of using deuterons will evidently not be so marked, inasmuch as the proton ionization mean free path is significantly larger than the proton nuclear mean free path.

LITERATURE CITED

1. R. G. Vasil'kov et al., Atomnaya Énergiya, 29, 151 (1970).
2. V. A. Davidenko, ibid., p. 158.
3. S. M. Feynberg, ibid., p. 162.
4. L. P. Abagyan et al., Group Constants for Nuclear Reactor Calculations [in Russian], Atomizdat, Moscow (1964).
5. W. Crandall and G. Millburn, UCRL-2063 (1953) and UCRL-4931 (1957).

CHANGES IN THE STRENGTH CHARACTERISTICS OF GRAPHITE DUE TO NEUTRON IRRADIATION

P. A. Platonov, Yu. S. Virgil'ev,
V. I. Karpukhin, A. L. Zaitsev,
and I. F. Novobratskaya

UDC 621.039.532.21

A neutron field causes changes in the properties of graphite which affect the serviceability of graphite components.

It is known, for example [1-3], that neutron irradiation leads to marked increase (at low temperatures) in the strength characteristics of graphite, i.e., in the compressive strength and modulus of elasticity.

The amount of radiation strengthening diminishes with rise of irradiation temperature, and depends on the perfection of the crystal structure of the graphite. We investigated the radiation behavior of two grades of graphite, experimental and reactor (Table 1).

The measurements were made on specimens 4-6 mm in diameter and 40-45 mm in length. They were irradiated in sealed capsules filled with nitrogen or helium, in the fuel channels of an MR reactor [4] at temperatures up to 1000°C, and in the reflector block at about 100°C. All the doses (φt) are given with respect to neutrons with energies above 0.18 MeV. The temperature was monitored by means of thermocouples and diamond indicators [5]. The neutron fluxes in the fuel channels were calculated from the power of the fuel element in which the investigation was performed.

Measurements of the modulus of elasticity, the electrical resistivity, and the change of length before and after irradiation were made on the same specimens, so as to eliminate errors due to fluctuations in the properties of the graphite due to the production technology. In addition, for some specimens we determined the compressive and tensile strengths. In this case the specimens were broken.

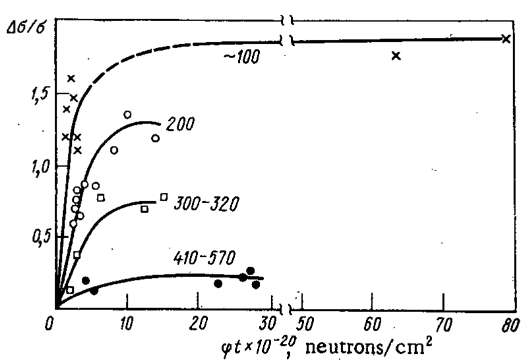

Fig. 1

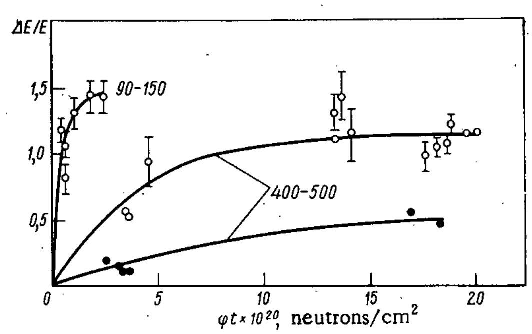

Fig. 2

Fig. 1. Relative change in compressive strength of reactor graphite vs integral flux. Irradiation temperatures marked on curves in degrees Celsius.

Fig. 2. Relative change in modulus of elasticity of reactor graphite (○) and its semifinished products (●) vs integral flux.

Translated from Atomnaya Énergiya, Vol. 35, No. 3, pp. 169-172, September, 1973. Original article submitted February 9, 1973; revision submitted March 27, 1973.

TABLE 1. Principal Properties of Grades of Graphite

Material	Method of shaping	Density, g/cm^3	Direction of cut relative to extrusion axis	Compressive strength, kg/cm^2	Modulus of elasticity, $\times 10^{-5}$, kg/cm^2	Electrical resistivity, $\Omega \cdot$ mm^2/m	Thermal expansion coefficient $\alpha_{20-100} \times 10^6$, (deg C)$^{-1}$
Reactor graphite	Punching	1,70	$\perp$	390	0,70	15	3,6
			$\parallel$	430	0,98	11	2,8
Experimental graphite	Pressing	1,73	$\perp$	440	0,95	17,5	4,1
			$\parallel$	340	0,65	19,5	4,9

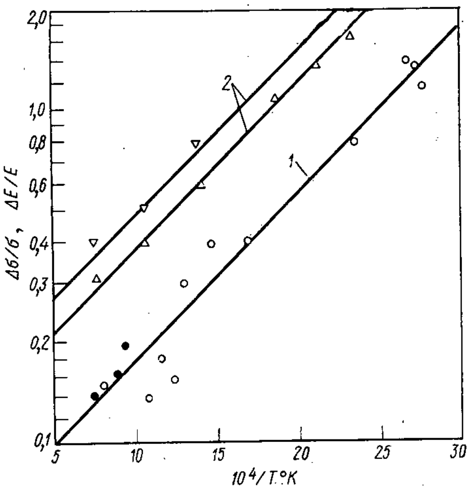

Fig. 3. Relative change in compressive strength (1) and modulus of elasticity (2) of graphite, corresponding to the "saturation" level of these characteristics, plotted vs irradiation temperature. (○) Reactor graphite; (●) experimental graphite. Orientations of specimens during measurement of modulus of elasticity; ▽) parallel; △) perpendicular.

The moduli of elasticity before and after irradiation were measured by a dynamic method in an RIU-2 apparatus with an error of ±5% [6]. The compressive and tensile strengths σ_{comp} and σ_{tens} were determined in an electronic tensometer* designed for mechanical testing of ÉTU1MIP-1000 polymers with recording on paper strip. The accuracy of the instrument was 3% at σ_{comp} = 400-500 kg/cm^2. To eliminate the influence of the scale factor we simultaneously determined the same characteristics on nonirradiated control specimens and took the relative changes in the measured properties as the results.

Irradiation of reactor graphite at 90-150°C causes considerable strengthening, which becomes stable after an accumulated dose of about $5\text{-}8 \cdot 10^{20}$ neutrons/cm^2 (Fig. 1). Prolonged irradiation to a dose of about $7 \cdot 10^{21}$ neutrons/cm^2 at these temperatures did not alter the strengths of the specimens. Rise of irradiation temperature reduced the observed effect.

The changes in the modulus of elasticity of the reactor graphite, measured on several specimens from one batch and separate specimens from another, were similar to the changes in strength (Fig. 2). The rise in the modulus of elasticity during low-temperature irradiation (90-150°C) is also rapidly stabilized at accumulated doses of $2.5 \cdot 10^{20}$ neutrons/cm^2. Rise of irradiation temperature to 400-500°C reduces this effect, and stabilization occurs at a high neutron dose of $10\text{-}15 \cdot 10^{20}$ neutrons/cm^2. The relative increase in modulus for material with imperfect crystal structure (e.g., semifinished products of reactor graphite) is half that for reactor graphite.

The temperature dependences of the radiation strengthening corresponding to the saturation level and the increase in modulus of elasticity are exponential curves (Fig. 3). The two characteristics fall practically with rise of irradiation temperature, showing that the changes in strength and elasticity modulus are due to a single type of defect.

Allowing for fluctuations in the properties due to natural technological inhomogeneity of the material, the relative changes in the strengths of the reactor and experimental graphite materials were the same.

The relative changes in the compressive and tensile strengths were also practically the same within the error of measurement. However, as σ_{comp} and σ_{tens} were measured on specimens irradiated above 600°C, at which the strengthening is slight, this conclusion must be regarded as somewhat tentative.

The difference between the changes in modulus of elasticity in graphitized and nongraphitized (semifinished) materials, mentioned above (see Fig. 2), impelled us to assess the influence of crystal structural perfection of carbon materials, i.e., the degree of graphitization, on the radiation-induced changes in the above properties. For this purpose, specimens of semifinished reactor graphite, after annealing, were subjected to heat treatment at 1300-3000°C. Figure 4 shows how the treatment temperature (i.e.,

*Designed by G. P. Ushakov.

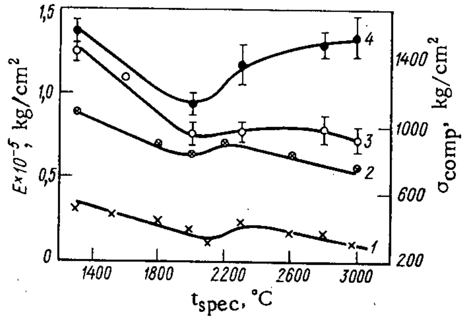

Fig. 4. Properties plotted vs treatment temperature of semifinished reactor graphite. 1) Compressive strength before irradiation at 230°C; 2) after irradiation at 230°C; 3) modulus of elasticity before irradiation at 400-500°C; 4) after irradiation at 400-500°C.

ultimately the crystalline structural perfection) affects the change in the modulus of elasticity and strength after irradiation by an integral flux of $3.6 \cdot 10^{20}$ neutrons/cm^2. The relative increase in compressive strength does not vary much with the crystalline structural perfection of the graphite over the whole tested range of heat treatments, i.e., for various carbon materials the relative changes in strength $\Delta\sigma/\sigma_{comp}$ can be taken as the same within ±10-15%. Thus they are governed only by the irradiation conditions – the temperature and the accumulated dose – and at high doses at which the process is stabilized, by the temperature alone.

On the other hand, the relative change in modulus of elasticity depends on the crystalline perfection; the more perfect the graphite, the more marked is the change of modulus.

The fact that the crystalline structural perfection has little influence on the relative change in strength of the material and the fact that $\Delta E/E$ depends on the structural perfection are due to the fact that these characteristics have different relations with the crystallite diameter L_a. Thus it has been shown [7] that $\sigma_{comp} \sim L_a^{-1/2}$. At the same time, the dependence of the modulus of elasticity on the crystallite diameter is more complex. For graphitized materials, there is a linear relation between the relative change in modulus of elasticity and the compressive strength at a given irradiation temperature (Fig. 5). This makes it possible to cancel out the kinetics of the radiation-induced strength changes against the kinetics of the changes in modulus of elasticity, and, using nondestructive methods of monitoring, to estimate the strength changes during irradiation. As the temperature rises (see Fig. 5) the effect of strengthening of graphite decreases more rapidly than the rise in its elastic characteristics.

The nonuniformity of the rate of change of the linear dimensions of the reactor structural elements, together with the elastic properties and creep, determines the level of internal stress. It is therefore of interest to compare data on the radiation-induced changes of dimensions and the modulus of elasticity during irradiation (Fig. 6). Owing to the linear relation between the strength and modulus of elasticity, the dependence of the changes in dimensions on the strength is roughly similar.

In Fig. 6 we distinguish three temperature ranges for the above properties of graphite: moderate growth $\Delta l/l < 1\%$ (T_{irr} = 150-300°C); marked growth (T_{irr} < 150°C); and shrinkage (T_{irr} > 300°C).

To each range there corresponds a characteristic change in the structure and properties of the graphite. The most interesting range is that of moderate growth of the graphite. Here the strength and elastic

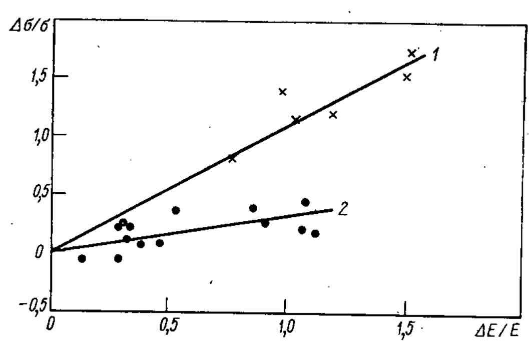

Fig. 5

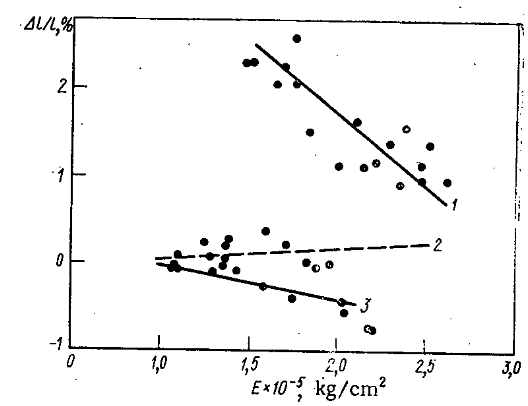

Fig. 6

Fig. 5. Relative changes in compressive strength and modulus of elasticity of reactor graphite irradiated at: 1) about 100; 2) 400-900°C.

Fig. 6. Relative change of length of reactor graphite specimens vs modulus of elasticity. Irradiation temperatures: 1) below 150°C; 2) 150-300°C; 3) above 300°C.

characteristics and the electrical resistivity change rapidly, but the linear dimensions change only slowly. We can suppose that microfissures "grow together" in the material during radiation-induced grain growth, leading to an increase in the modulus of elasticity and strength due to wedging together of the grains. In addition, accumulation of simple defects which fix dislocations prevents their slip over basal planes, also increasing the elastic and strength properties of the graphite [8]. In this temperature, x-ray investigations reveal a three-dimensional crystal lattice with finely-dispersed inclusions which cause blurring of the $(00l)$ diffraction lines. In the temperature range with moderate growth of the graphite, the nonsteady stage of radiation creep develops and terminates.

The temperature range with marked growth of graphite is characterized by a two-dimensional lattice: the x-ray diffraction patterns contain lines of type $(00l)$. In the lattice, only short-range order is preserved in the basal planes containing a large concentration of defects – interstitial atoms and vacancies. The concentration of simple defects reaches equilibrium, and their constantly-forming excess creates more complex defects.

As the dimensions of these defect complexes increase, the equilibrium concentration of simple defects falls. For this reason the modulus of elasticity and strength can even fall somewhat owing to the reduced concentration of interstitial atoms capable of fixing dislocations and preventing slip over basal planes, and also to the large number of vacancies in the basal planes. All this creates conditions for failure of the graphite under smaller loads, and must lead to a reduction in the modulus of elasticity. However, in our work the strength did not decrease, even for low-temperature irradiation by doses of up to $7 \cdot 10^{21}$ neutrons $/\mathrm{cm}^2$.

For the temperature range with decreasing dimensions (shrinkage) of the graphite, the three-dimensional crystalline structure is preserved up to high integral neutron doses of over 10^{21} neutrons/cm^2. The bulk contraction of the graphite causes its density to increase. We observe an increase in the modulus of elasticity and a slight increase in the compressive strength.

Thus the strengthening of highly-graphitized materials under irradiation depends comparatively slightly upon the original strength, the orientation of the specimens, or their crystalline structures. This enables us to use data obtained from reactor graphite to estimate the changes in the properties of other grades of graphite. The changes in the elastic properties of carbon materials under irradiation are largely governed by their crystalline structural perfection.

The correlation between the elastic properties and the changes in the linear dimensions shows that, by altering its modulus of elasticity, we can vary the dimensional stability of graphite within certain limits. The physical basis of the correlation is obscure and requires further investigation.

LITERATURE CITED

1. W. K. Woods et al., in: Metallurgy of Nuclear Power Production and Action of Radiation on Materials [Russian translation], Metallurgizdat, Moscow (1956), p. 593.
2. B. Kelly et al., J. Nucl. Mat., 7, 279 (1962).
3. T. Mantell, Carbon and Graphite: Handbook, LST, New York (1968).
4. V. V. Goncharov et al. (USSR): Third Geneva Conference (1964), Report No. 323.
5. V. I. Karpukhin and V. A. Nikolaenko, Temperature Measurement by Means of Irradiated Diamond [in Russian], Atomizdat, Moscow (1971).
6. P. S. Shukin et al., in: Structural Materials Based on Graphite, Fourth Issue [in Russian], Metallurgiya, Moscow (1969), p. 168.
7. Yu. S. Virgil'ev, in: Structural Materials Based on Graphite, Seventh Issue [in Russian], Metallurgiya, Moscow (1972), p. 52.
8. S. E. Vyatkin et al., Nuclear Graphite [in Russian], Atomizdat, Moscow (1967), p. 208.

STUDYING Be—Fe—C ALLOYS BY NUCLEAR GAMMA-RESONANCE METHOD

L. A. Alekseev, Yu. F. Babikova,
V. P. Gladkov, V. S. Zotov,
V. I. Kondar', and D. M. Skorov

UDC 539.144:546.45

Carbon and iron are the most widespread impurities in beryllium and, thus, they fundamentally determine the properties of this metal. Studying the interaction among impurities in the metallic matrix can aid the understanding of the processes taking place in beryllium.

The present work studied beryllium–carbon alloys, enriched with Fe^{57}, by the nuclear γ-resonance (NGR) method.

Samples were prepared from distilled beryllium having electrical purity* $\delta = \rho_{293°K}/\rho_{77°K} = 10$ by arc melting in a water-cooled copper hearth with subsequent cutting on an electric-spark apparatus.

*Evaluation of the overall purity of beryllium in relation to electrical resistivity at room temperature and 77°K was introduced in accordance with a proposal by participants in the International Conference on Beryllium (Grenoble, 1965).

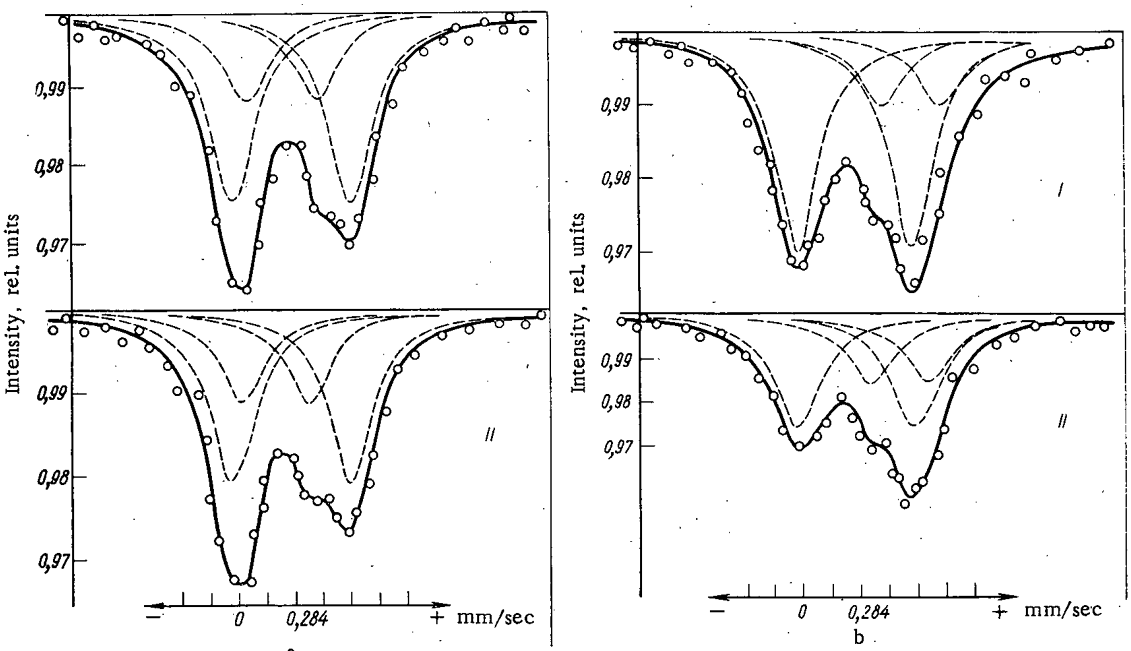

Fig. 1. Absorption spectra for samples containing 0.11 (I) and 0.39 (II) wt % carbon after annealing at 850°C with annealing time 4.5 h (a) and at 1130°C with annealing time 1.5 h (b).

Translated from Atomnaya Énergiya, Vol. 35, No. 3, pp. 173–174, September, 1973. Original article submitted May 18, 1972.

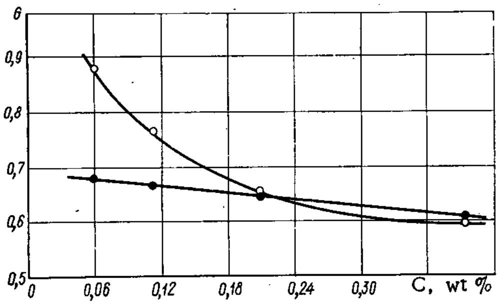

Fig. 2. Variation of the relative quantity of iron in a beryllium solid solution G as a function of the carbon concentration. Annealing at: ●) 850°C; ○) 1130°C.

Spectroscopically pure carbon was used as an admixture. Thermal processing was conducted in vacuum ($\sim 10^{-4}$ torr), using a zirconium chip as a getter. Mossbauer spectra were recorded on an electrodynamic-type spectrometer in the transiènt regime with a single-channel analyzer AI-256. The radiation source was Co^{57} enclosed in palladium.

Absorption spectra were obtained for samples containing 0.06, 0.11, 0.20, and 0.39 wt % carbon. The iron content in all samples was 0.05 wt %. As an example, Fig. 1a, b shows absorption spectra for alloys containing 0.11 and 0.39 wt % carbon after annealing at 1130 and 850°C. All the spectra can be viewed as superpositions of two doublets whose linewidths, corrected for the source linewidth and the absorber thickness, correspond to the natural width.

The presence of solid solutions in the Be–Fe system has been confirmed [1]. Therefore, one of the spectrum must be the doublet of iron dissolved in beryllium. This doublet was observed in [2-5]. The quadrupole splitting Q for the doublet of the iron solid solution in beryllium is 0.58 ± 0.07 mm/sec, and the isomeric shift is $\delta = 0.21 \pm 0.04$ mm/sec (relative to stainless steel).

After annealing at 850°C, besides the solid-solution doublet one observes a second doublet having Q = 0.36 ± 0.07 mm/sec and $\delta = 0.14 \pm 0.04$ mm/sec. According to the states diagram, there may form in the Be–Fe system the intermetallide $FeBe_{12}$ [6,7], i.e., the highest beryllide of iron with anisotropic crystalline structure (body-centered tetragonal). This structure can assure an electric-field gradient necessary for the appearance of a doublet having the above-mentioned parameters. We must remark that the NGR spectra obtained with control alloys of beryllium and iron (1 wt % Fe) showed that the doublet with Q = 0.36 mm/sec is due to the presence of the intermetallide $FeBe_{12}$. Additions of carbon did not change the form of the spectra, i.e., did not influence their qualitative composition (see Fig. 1a) and had a very weak effect on the relationship between iron in the solid solution and iron in the compound $FeBe_{12}$ (Fig. 2). Consequently, in the triple system Be–Fe–C at 850°C there exist a solid solution of iron in beryllium and the intermetallide $FeBe_{12}$; moreover, according to metallographic-analysis data, beryllium carbide (Be_2C) impurities are also observed.

The character of the spectra changed due to annealing at 1130°C. The $FeBe_{12}$ doublet is now absent (this agrees with the states diagram for Fe–Be [6,7]), but there appears a new doublet (its parameters: Q = 0.28 ± 0.07 mm/sec; $\delta = 0.43 \pm 0.04$ mm/sec) which cannot be attributed to the beryllide $FeBe_5$, since the latter is characterized by a single line [9]. Mozer and Kistner [3] observed a doublet with similar quadrupole splitting (Q = 0.29 mm/sec) on aging (600°C) and alloy Be + 0.1 wt % Fe, but with a Cu + Co^{57} source the isomeric shift of this doublet is somewhat less ($\delta = 0.05$ mm/sec). It probably is different in nature from the one observed in the present work.

Varying the carbon content in the alloys annealed at 1130°C produces decreased intensity in the solid-solution doublet (see Fig. 1b) while correspondingly leading to increased intensity in the new doublet.

This interrelationship may be evidence of the fact that there appeared in the alloys a phase component containing all three elements: beryllium, iron, and carbon. Apparently, some compound of the type $Be_m \cdot Fe_nC_p$ or a solution of iron in beryllium carbide can be such a phase. On the basis of Fig. 2, one can form hypotheses concerning either the oriented composition of an as-yet unknown compound in the system Be–Fe–C (probably about 0.2 wt % Fe) or the possible limit of iron's solubility in beryllium carbide at 1130°C.

LITERATURE CITED

1. I. I. Papirov and G. F. Tikhinskii, Physical Metallurgy of Beryllium [in Russian], Atomizdat, Moscow (1968).
2. B. Kistner et al., Bull. Amer. Phys. Soc., 7, No. 4 (1962).
3. O. Mozer and B. Kistner, Bull. Amer. Phys. Soc., 7, No. 7 (1962).
4. C. Janot et al., Comptes-rendus Acad. Sci., B-955, 267 (1968).
5. C. Janot and P. Deloroix, Acta Metallurgica, 20, 637 (1972).

Declassified and Approved For Release 2013/01/22 : CIA-RDP10-02196R000400020003-6

6. J. Darwin and J. Badderi, Beryllium [Russian translation], IL, Moscow (1962).
7. D. White and D. Berk, Beryllium [Russian translation], IL, Moscow (1960).
8. G. Samsonov, Beryllides [in Russian], Naukova Dumka, Kiev (1966).
9. Keizo Ohta, J. Appl. Phys., 39, 2123 (1968).

SWELLING OF IRRADIATED BERYLLIUM DURING ISOTHERMAL ANNEALING

G. A. Sernyaev, V. P. Gol'tsev,
and Z. I. Chechetkina

UDC 621.039.532.5

Gas swelling is one of the reasons which restricts the use of beryllium as moderator and reflector in nuclear reactors and also as a component of dispersion-hardened composite materials. The mechanism of gas swelling in beryllium is extremely complicated. The phenomenon is based on a number of processes, the relative importance of which is determined both by the original structure of the material and by the conditions of irradiation. In view of this, any elucidation of the part played by individual processes in the general picture of the gas swelling of beryllium may well promote a better understanding of the phenomenon as a whole, and also (and this is a matter of no mean importance) methods of combating its effects.

In the present investigation we studied the laws governing the swelling of metalloceramic beryllium. Special attention was devoted to determining the function of grain boundaries. The material so studied is primarily of interest in view of the well-developed technology of its production and the possibilities of its use on the industrial scale.

Material and Conditions of Irradiation. As subject for study we took hot-pressed beryllium made from powder with a particle size of $\leq 600\mu$. The original samples had the form of cylinders 6 mm in diameter and 10 mm long. The samples were irradiated in an SM-2 reactor at 60°C with an integrated flux of fast ($E \geq 0.8$ MeV) neutrons equal to $5.1 \cdot 10^{21}$ neutrons/cm^2.

Methods of Investigation. After irradiation, the samples were subjected to isothermal annealing at 750-1000°C. While so doing, we monitored both the swelling and the changes in structural state.

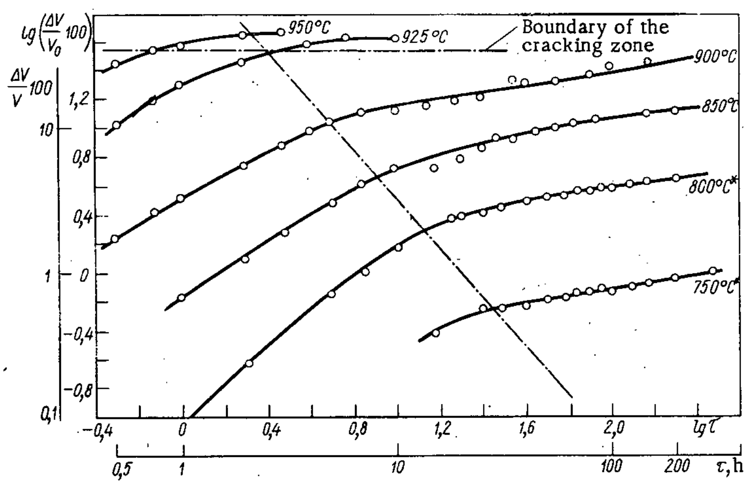

Fig. 1. Relationship between the swelling and the annealing time (the asterisk signifies that the swelling was determined from the results of the dilatometric analysis).

Translated from Atomnaya Énergiya, Vol. 35, No. 3, pp. 175-178, September, 1973. Original article submitted November 9, 1972.

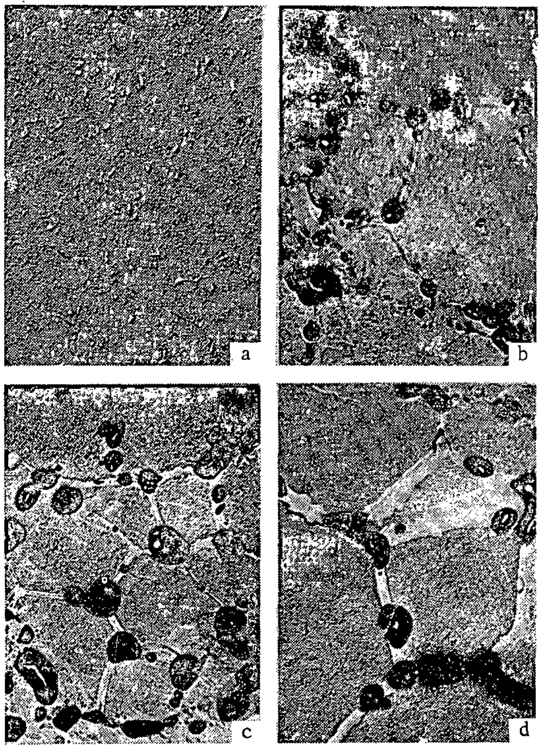

Fig. 2. Porosity structure of the samples after irradiation and annealing at 900°C: a) 30 min (replica from microsection, × 11,500); b) 3 h (× 500); c) 5 h (× 500); d) 10 h (× 500).

Annealing took place in the working space of a vacuum dilatometer, or else in a vacuum furnace. The specified temperature was maintained to an accuracy of ±5°C.

The swelling was monitored either by recording the changes in sample length (annealing in the dilatometer) or by periodically measuring the sample density (annealing in the furnace). The swelling was calculated from the expressions

$$\frac{\Delta V}{V_0}=3\left(\frac{\Delta l}{l_0}\right)+3\left(\frac{\Delta l}{l_0}\right)^2+\left(\frac{\Delta l}{l_0}\right)^3; \quad \frac{\Delta V}{V_0}=\frac{\gamma_0}{\gamma}-1,$$

where Δl is the change in sample length on swelling, l_0 is the original length, γ_0 and γ are the sample densities before and after annealing respectively. In order to determine the final swelling of the samples annealed in the dilatometer, both the foregoing methods were employed. This enabled us to estimate the accuracy of the readings of the dilatometer and to determine the limits of its applicability. The results subsequently presented were averaged over two or three samples. The microsections for metallographic investigation were prepared by grinding and then electropolishing in a reagent containing 120 ml of H_3PO_4, 10 ml of a 50% aqueous solution of CrO_3 and 70 ml of glycerin. The electron-microscope examination was conducted by the method based on two-stage lacquer-carbon replicas.

Experimental Results. Kinetic Swelling Curves. Figure 1 shows the relationships

$$\lg\left(\frac{\Delta V}{V_0}\right)_T=f(\lg\tau)$$

based on the results of the investigation. We see from this that the swelling increases with rising temperature and increasing annealing period. In the swelling/time relationship there are two easily-distinguished stages: one of intensive, and one of moderate swelling. The duration of the first stage is short (~ 10 h at 800°C) and diminishes with increasing annealing temperature. The duration of the second stage is only restricted by the limiting value of the permissible swelling (in the present case $\Delta V/V_{0\,max} \approx$ 34-36%). On reaching this value, the samples crack.

Both the first and the second stages in the swelling/anneal period relationship may be closely described by an expression of form

$$\frac{\Delta V}{V_0}=A\tau^B,$$

where A is a coefficient depending on the dose of irradiation and the annealing time. In the first stage the index B is close to unity (~0.8-1.2) and in the second exactly equal to 0.25.

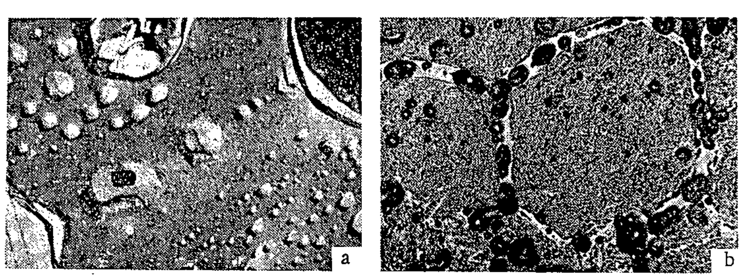

Fig. 3. Porosity structure of the samples after irradiation and annealing at 950°C: a) 30 min (replica with a break, × 18,000); b) 3 h (× 500).

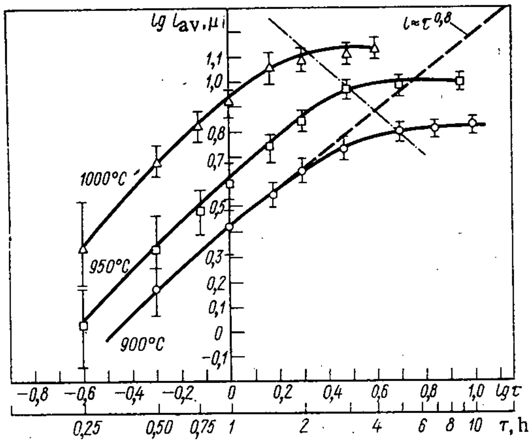

Fig. 4. Width of the pore-free zone as as a function of annealing time.

Change in the Structural State of the Material. Metallographic and electron-microscope examinations showed that, in all cases considered, the swelling of the material was due to the generation and growth of a large number of pores. In speaking of the porosity structure, it is first of all essential to point out the great difference between the sizes of the pores inside the grains and at the grain boundaries, and also the marked reduction in the number of pores in regions adjacent to the boundaries (Figs. 2 and 3). We see from the figures that, with increasing annealing time and temperature, there is a general growth of the pores and a widening of the regions of low pore content close to the boundaries. The latter fact directly indicates the migration of pores to the grain boundaries and is therefore of first-rate interest. We accordingly attempted to follow the kinetic characteristics of the process in question by preparing microsections after each anneal and measuring the width of the pore-free zones around 100-200 different boundaries. The averaged results of these measurements are shown in Fig. 4. We see from this figure that an intensive increase in the width of the pore-free boundary zones only occurs in the initial periods of annealing. Subsequently the rate of growth falls sharply. In addition to this, the final width of the pore-free zone is the greater, the higher the annealing temperature. One also notices the fact that the time during which the intensive growth in the width of the pore-free zone occurs shortens with increasing annealing temperature, and approximately coincides with the duration of the stage of intensive swelling.

Discussion of Results. Earlier it was predicted on the basis of the concept of the migration and union of bubbles* that the swelling of samples annealed after low-temperature irradiation should be described by the expression

$$\frac{\Delta V}{V_0} = A\,(FD_s t)^{0.25}, \tag{1}$$

where F is the force acting on the pores, D_s is the coefficient of surface self-diffusion.

We see from Fig. 1 that such a relationship does in fact hold for long annealing times (stage of moderate swelling). However, in the first moments of annealing (stage of intensive swelling), the index of t is not equal to 0.25, but may be estimated as ~1. This kind of behavior fails to obey the simplified Barnes theory. One of the shortcomings of this model (in our own opinion) is the fact that it only describes the behavior of materials with homogeneous structures and compositions. This in turn assumes the uniformity of the diffusion constants, the forces acting on the pores (motive forces of coalescence), and hence the swelling. However, real materials rarely satisfy these assumptions. This is also indicated by the results of the present structural investigation. The clearly-expressed difference between the rates of pore coalescence in the regions close to the boundaries and within the grains observed in the present case directly indicates a different tendency toward swelling in the corresponding localized regions. This difference may be a consequence of the difference in the motive forces of coalescence and the diffusion coefficients. An analogous situation may occur in composite materials.

Thus for real materials the total volume of the sample may more correctly be considered as the sum of individual subsidiary volumes with differing properties, i.e., we may consider that

$$V_{\text{sam}} = \sum_{i=1}^{n} V_i.$$

The swelling of the sample is thus defined as

$$\frac{\Delta V}{V_0}(\text{sam}) = \sum_{i=1}^{n} \frac{\Delta V_i}{V_{0i}}\, n_i,$$

where $n_i = V_{0i}/V_0$ is the volumetric proportion of the i-th subsidiary volume.

* By R. Barnes, in "A theory of swelling and gas release for reactor materials," J. Nucl. Materials, 11, No. 2, 135-148 (1964).

In the more general case in which $n_i = n_i(t)$,

$$\frac{\Delta V}{V_0}(\mathrm{sam}) = \sum_{i=1}^{n} \frac{\Delta V_i}{V_{0i}} n_i(t).$$

In the case under consideration, we may distinguish two essentially differing subsidiary volumes: that including the zones close to the boundary $[V_1(t)]$ and that including the centers of the grains $[V_2(t)]$. Hence the swelling of the samples under consideration should in general be described by the expression

$$\frac{\Delta V}{V_0}(\mathrm{sam}) = \frac{\Delta V_1}{V_{01}} n(t) + \frac{\Delta V_2}{V_{02}} [1 - n_1(1)].$$

Using Eq. (1) to describe the swelling of any of the subsidiary volumes so distinguished, and also considering that, in the first moments of annealing, the swelling of the samples is mainly determined by the development of porosity at the grain boundaries, we may consider that, for the first stage

$$\frac{\Delta V}{V_0}(\mathrm{sam}) \approx n_1(t)\, t^{0.25}.$$

Remembering that at this stage $n_1(t) \approx l_{av}(t) \approx t^{0.8}$ (Fig. 4), we find $\Delta V/V_0(\mathrm{sam})_{\mathrm{I}} \approx t^{0.8}t^{0.25} \approx t$, in good agreement with the experimental law of swelling obtained for this stage.

In the second stage, in which $n_1(t) \to \mathrm{const}$, the swelling will be described by the law

$$\frac{\Delta V}{V_0}(\mathrm{sam})_{\mathrm{II}} \approx t^{0.25}$$

independently of the contributions of the two subsidiary volumes.

SWELLING OF BERYLLIUM AT HIGH TEMPERATURES UNDER LARGE DOSES OF IRRADIATION

V. P. Gol'tsev, Z. I. Chechetkina,
G. A. Sernyaev, and V. A. Ol'khovikov

UDC 621.039.532.5

The present necessity of increasing the working parameters of atomic installations makes a study of the behavior of various materials, including beryllium, which are subjected to irradiation at high temperatures very important. However, any investigations of this kind are beset by serious technical difficulties, relating to the production, maintenance, and measurement of the high temperatures. This has largely restricted the accumulation of the desired factual material.

In the last decade a number of communications have appeared in relation to the high-temperature irradiation and examination of beryllium samples outside the Soviet Union. A detailed discussion of these investigations may be found in an earlier review [1].

The present investigation is a continuation of work started earlier [2] and contains experimental data characterizing the behavior of certain types of Soviet-produced beryllium subjected to large doses at high temperatures of irradiation.

Characteristics of the Material, Conditions of Irradiation, and Methods of Investigation. We studied hot-pressed and hot-extruded beryllium samples (obtained from 600 and 400μ powder respectively). Irradiation was carried out in channel 2 of an SM-2 reactor, using a special hermetically-sealed ampoule system, which was filled with commercially-pure helium before irradiation. The samples were heated solely by the absorption of the reactor irradiation. The required temperature was reached by making a specified gap between the surface of the channel and the body of the ampoule, and was monitored by means of Chromel–Alumel microthermocouples calked into the samples.

The samples of hot-extruded beryllium were irradiated at 550, 650, and 800°C with an integrated neutron flux of $5.7 \cdot 10^{21}$ neutrons/cm^2 ($E_n \geq 0.8$ MeV): the irradiation time (period of action of the high

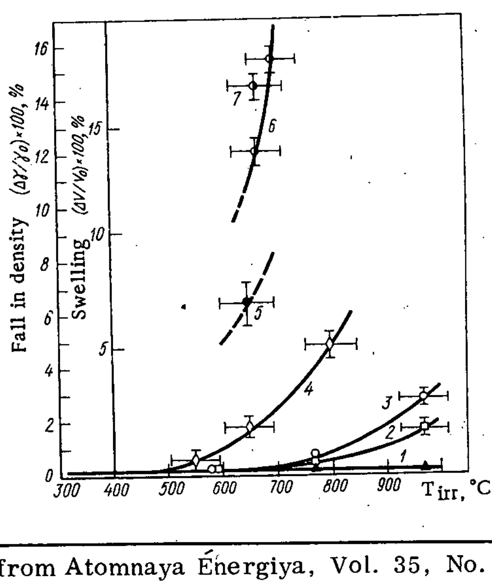

Fig. 1. Temperature dependence of the swelling of bicrystalline (1), hot-pressed [2) $\leq 56\mu$; 3, 5–7) – $\leq 600\mu$] and hot-extruded [4) – ≤ 400 μ] beryllium for the following fast neutron fluxes in neutrons /cm^2: 1,2,3) $6 \cdot 10^{20}$ [2]; 4,5) $5.7 \cdot 10^{21}$; 6) $8.9 \cdot 10^{21}$; 7) $1 \cdot 10^{22}$.

Translated from Atomnaya Énergiya, Vol. 35, No. 3, pp. 178–180, September, 1973. Original article submitted November 9, 1972.

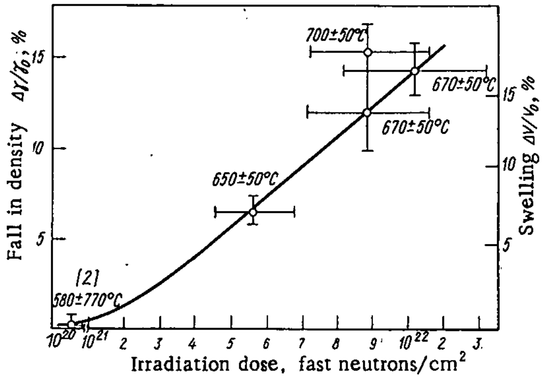

Fig. 2. Dose dependence of the swelling of hot-pressed ($\leq 600\mu$) beryllium.

temperature) was in this case 6700 h. The samples of hot-pressed beryllium were irradiated with fast-neutron integrated fluxes of $5.7 \cdot 10^{21}$ ($T_{irr} \approx 650°C$), $9 \cdot 10^{21}$ ($T_{irr} \approx 670$ and $700°C$) and $1 \cdot 10^{22}$ ($T_{irr} \approx 670°C$) neutrons/cm^2. The period of irradiation for a dose of $5.7 \cdot 10^{21}$ neutrons /cm^2 was 6700 h and for $9 \cdot 10^{21}$ and $1 \cdot 10^{22}$ neutrons/cm^2 9600 h.

The density of the samples was determined after the reactor tests by hydrostatic weighing in ethyl alcohol. Before this, the surface was cleaned in a 30% aqueous solution of hydrofluoric acid. The density values were averaged over three to five samples. The microsections for metallographic examination were electropolished in a reagent containing 120 ml H_3PO_4, 10 ml 50% aqueous solution of CrO_3, and 70 ml glycerin. For the electron-microscope investigation the method of lacquer-carbon replicas was employed.

RESULTS AND DISCUSSION

The experimental results are presented in Fig. 1 in the form of curves giving the change in density (swelling) expressed as a function of the irradiation temperature. For convenience of discussion the results of [2] are also reproduced here. It follows from the figure that, under the influence of high-temperature irradiation, the density of the samples in considerably reduced, the more so the greater the integrated flux and the higher the irradiation temperature.

The change in density also depends very much on the form of the material. Thus in single-crystal and bicrystalline material it is smaller than in metalloceramic samples; the swelling of the latter in turn increases with increasing coarseness of the original powder.

The results obtained in the present investigation and in [2] also give a fair idea of the effect of dose on the change in the density of hot-pressed beryllium in the practically important temperature range (600-700°C). Existing data are presented in Fig. 2 as a relationship between $\Delta\gamma/\gamma_0$ and the irradiation dose. The continuous line gives the relation

$$\frac{\Delta\gamma}{\gamma_0} = -\frac{k\Phi^{3/2}}{1 + k\Phi^{3/2}},$$

where Φ is the integrated dose of fast ($E \geq 0.8$ MeV) neutrons and $k = 1.58 \cdot 10^{-34}$ is a constant for the particular temperature.

A study of the structure of the irradiated and nonirradiated samples showed that the change in density was in all cases associated with the generation and growth of a large number of pores in the material, while comparison of the porosity patterns of various irradiated samples showed certain common features

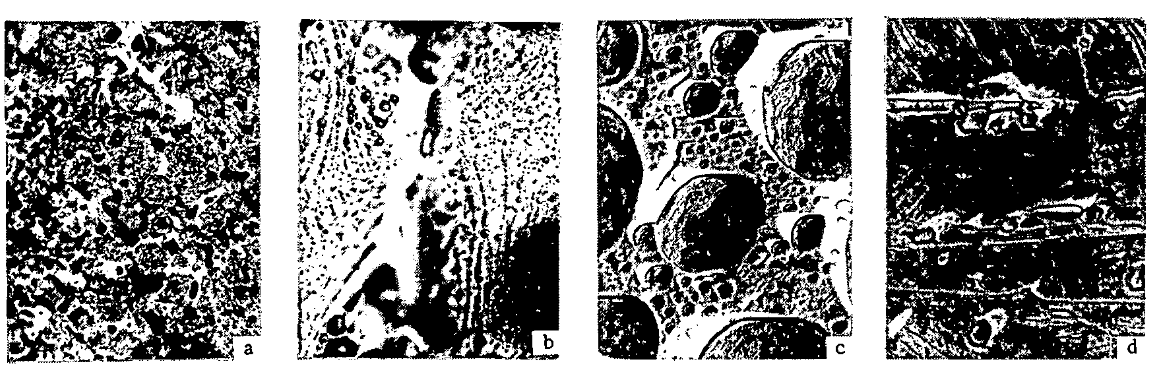

Fig. 3. Microstructure of hot-pressed beryllium ($\leq 600\mu$) irradiated at 650°C with an integrated flux of fast neutrons, $5.7 \cdot 10^{21}$ neutrons/cm^2. a) Microsection (× 200); b) microsection (× 800); c) fracture along the grain boundary (× 10,000); d) fracture through the body of the grain (× 10,000).

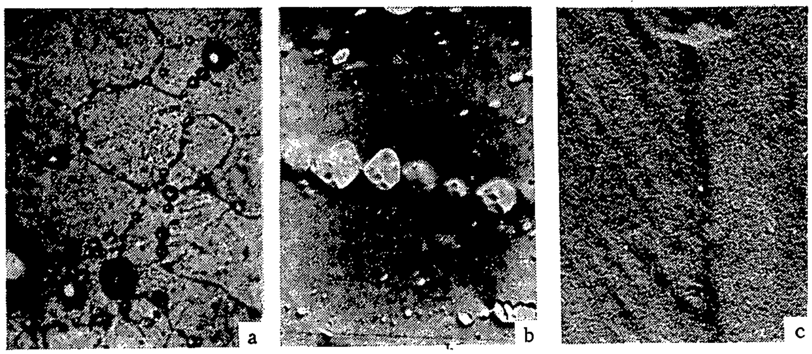

Fig. 4. Microstructure of hot-extruded (a, b) and bicrystalline (c) samples after irradiation with integrated fast-neutron fluxes of $5.7 \cdot 10^{21}$ (T_{irr} = 650°C) and $6 \cdot 10^{20}$ (T_{irr} = 580°C) neutrons/cm^2 respectively: a) microsection (× 800); b) replica from microsection (× 7500); c) replica from microsection (× 20,000).

for most of the materials. First of all, one notices great differences in the size of the pores (Fig. 3a). The largest pores lie at the triple points and along the grain boundaries. The intragranular pores are finer, and often form up into chains, which may be a result of the decoration of individual dislocations and subgranular boundaries by the pores (Fig. 3b). The local porosity of the material varies greatly from place to place. Thus the porosity at the grain boundaries is always higher than within the grains (Fig. 3c, d), while immediately next to the boundaries there is a pore-free zone (Fig. 3a, b).

There is a general growth in the pores as the temperature and dose of irradiation increase. However, the rate of pore growth within the grains and on the grain boundaries is quite different; the pores at the boundaries increase more rapidly with increasing irradiation dose. The width of the pore-free zone close to the boundary increases with increasing irradiation temperature.

There are also certain differences in the porosity structure of the different materials. Thus the width of the pore-free zone close to the boundary and the rate of growth of the pores at the grain boundaries are the smaller, the finer the powder used for the preparation of the material, or ultimately the finer the grain of the finished material.

Figure 4a, b shows some micrographs of the structure of hot-extruded beryllium. On comparing Figs. 3a and 4a, we see that the grain of the hot-extruded material is three or four times finer than that of the hot-pressed material. The widths of the pore-free zones close to the boundaries and the pore size at the grain boundaries differ accordingly.

In this respect the structure of the bicrystals constitutes an exception; there are hardly any pore-free zones at the boundaries of these (Fig. 4c).

The foregoing results show that the "gas" atoms accumulated in the material during irradiation at high temperatures have a considerable mobility, and unite to form gas bubbles (pores). The generation of the pores naturally affects the density of the material. Under the influence of different motive forces the bubbles migrate and collide. The coalescence of the bubbles in turn leads to an additional swelling of the material. A model of swelling under high-temperature irradiation based on these concepts [3] gives the following expression, which is in reasonable agreement with the results obtained (Fig. 2):

$$\frac{\Delta V}{V_0} = k\Phi^{3/2}.$$

Here K is a function of the irradiation temperature and the motive force of coalescence.

The foregoing data indicate a clear relationship between the grain size and the swelling of the material. Thus with increasing grain size the width of the zone feeding the grain boundaries with gas increases, and so do the rate of pore growth at the grain boundaries and the swelling of the material. This behavior may, in our own view, be explained by considering that the migration of the bubbles is in this case largely due to the stress fields arising at the grain joints as a result of the anisotropy of the linear expansion coefficients of individual crystallites.

LITERATURE CITED

1. J. Beeston, Nucl. Engineering Design, 14, 445 (1970).
2. Z. I. Chechetkina et al., At. Énerg., 30, 434 (1971).
3. R. Barnes, J. Nucl. Materials, 11, 135 (1964).

ELECTRON BEAMS WITH MOMENTA UP TO 46 GeV/c IN THE SERPUKHOV ACCELERATOR

S. S. Gershtein, A. V. Samoilov, Yu. M. Sapunov, A. M. Frolov, A. I. Alikhanyan, G. L. Bayatyan, G. S. Vartanyan, S. G. Kzyanyan, A. T. Margaryan, A. S. Belousov, N. P. Budanov, B. B. Govorkov, E. V. Minarik, S. V. Rusakov, E. I. Tamm, P. A. Cherenkov, and P. N. Shareiko

UDC 621.384.635.5/6

Proton accelerators yield particles with energies ten times exceeding those capable of being achieved in electron accelerators. Thus proton accelerators may be used to create electron beams of energies which electron accelerators themselves could as yet never hope to attain. The creation of such beams offers excellent prospects for extending experimental investigations into the physics of electromagnetic interactions in the high-energy field.

The fundamental process underlying the generation of electrons (positrons) in proton accelerators is the conversion of the photons arising from the decay of π^0 mesons generated in the target by the protons ($\pi^0 \to 2\gamma$, $\gamma \to e^+e^-$). The fluxes of γ quanta arising in the targets of proton accelerators may be estimated from the known cross sections relating to the formation of pions by protons. Theoretical estimations carried out in relation to the 70-Gev Serpukhov proton synchrotron [1-3] and also the 500-GeV proton accelerator in Batavia (USA) [4] showed that these accelerators might indeed prove to be fairly strong sources of high-energy electrons.

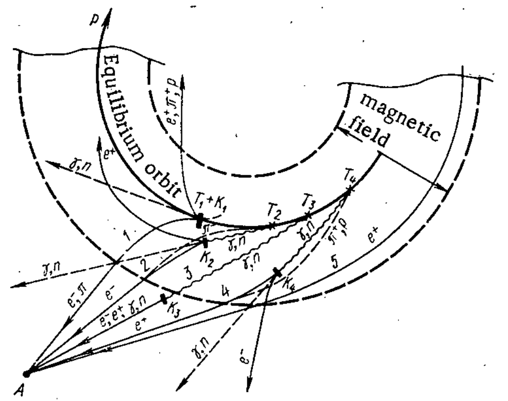

Fig. 1. Methods of generating electron and positron beams at a point in the outer zone of the magnetic ring of the accelerator, based on the use of internal targets (angle of formation of the γ quanta $\theta_\gamma = 0°$: T, target: K, converter: paths 1 and 5, limiting trajectories for the possible extraction of electrons or positrons to meet in the point A).

The present investigation is aimed at a realization of this idea in the Serpukhov accelerator, in which electron beams were obtained for the first time with energies of up to 45.5 GeV, more than twice as great as the most powerful contemporary electron accelerators.

Electron beams are intended to be created in the proton accelerator of the National Accelerator Laboratory of the USA in Batavia, and also in the 300-GeV proton accelerator being constructed in CERN. Superpowerful proton accelerators will clearly provide unique sources of electron (positron) beams in the energy range between hundreds and thousands of GeV.

An obvious method of creating strong, pure electron beams is the conversion of photons from a target placed in the beam of primary protons extracted from the accelerator.

Translated from Atomnaya Énergiya, Vol. 35, No. 3, pp. 181-187, September, 1973. Original article submitted December 28, 1972.

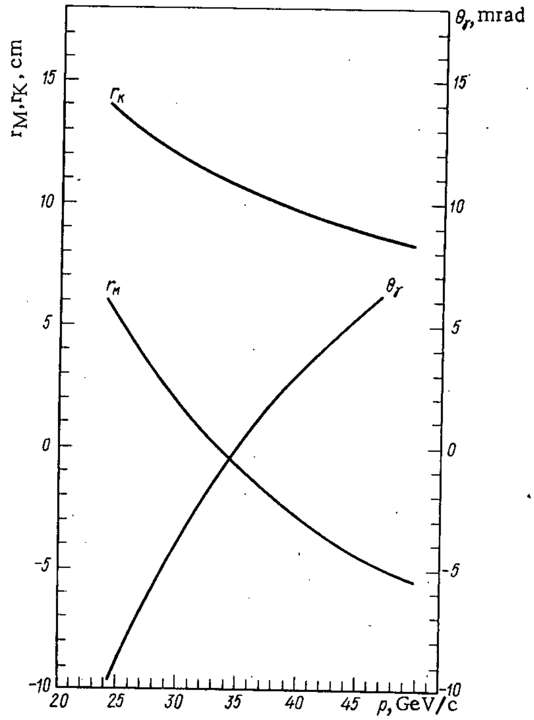

Fig. 2

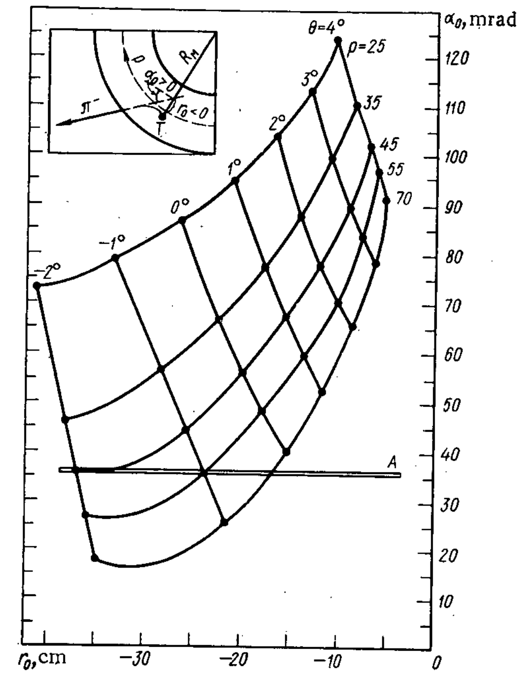

Fig. 3

Fig. 2. Radial positions of the target r_M and converter r_K relative to the equilibrium orbit of the protons in the accelerator, and angle of formation of the photons in the target θ_γ as functions of the momentum p of the conversion electrons in channel No. 2B (r and θ are positive for displacements and angular deviations relative to the equilibrium orbit in the direction of the outer zone of the magnetic ring of the accelerator; E_0 = 70 GeV).

Fig. 3. Diagram of the trajectories in the zone of channel No. 2B for negatively-charged particles generated in the target (photon source) with E_0 = 70 GeV (A is the horizontal acceptance of the channel for the electrons from the converter).

However, this method requires a special channel for working with the electron beam, and this is a complicated problem in present accelerators.

In the Serpukhov accelerator, the efforts of a team of workers from the Institute of High-Energy Physics, the Physical Institute of the Academy of Sciences, and the Erevan Physical Institute were directed into a search for effective practical means of creating electron beams using internal targets sited in the magnetic field of the accelerator [5].

Using internal targets, there are three possible means of generating conversion electrons (positrons). These are illustrated in Fig. 1. In the first method (path 1), photon conversion takes place in the same target in which the π^0 mesons are generated. In this case the electrons constitute only a small proportion, not exceeding a few percent, of the beam of charged hadrons from the target [5-7]. A slight increase in this proportion may be achieved on using a target comprising a mixture of light and heavy substances [5]. Experiments in such mixed beams require the separation of the electrons from a high background of hadrons. The second method (path 3) is based on the use of a neutral beam drawn from the target, and enables a pure electron beam to be formed [1]. However, a special magnetic channel has to be made for this. Furthermore, in view of the long path of the neutral beam in the accelerator, this method cannot realize the maximum acceptance of the magnetic channel. A method based on the spatial separation of the target and converter in the magnetic field of the accelerator (paths 2,4), free from the disadvantages of the foregoing methods, was proposed in the Institute of High-Energy Physics with a view to creating pure electron (positron) beams [5].

On using a target and converter spatially separated in the magnetic field of the accelerator, charged hadrons from the target also arrive at the entrance into the magnetic channel in which the electron (positron) beam is formed (Fig. 1). However, the electron and hadron momenta are in general completely different, so that the hadrons may be drawn out of the channel with a magnetic analyzer. In the beam so

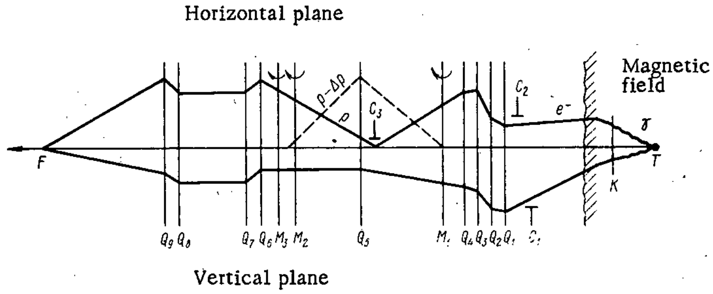

Fig. 4. Optical scheme for the formation of the electron beam in channel No. 2B.

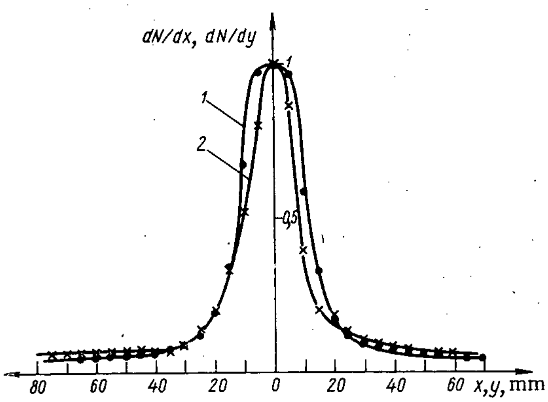

Fig. 5. Vertical (1) and horizontal (2) profiles of the electron beam at the final image in channel No. 2B (target diameter 2 mm; lead converter 0.5 rad. units thick; $E_0 = 70$ GeV; p = 31 GeV/c; $\Delta p/p = \pm 3\%$; N is the intensity; x and y are the horizontal and vertical coordinates relative to the beam axis).

formed there will only be a slight trace of charged hadrons, namely, those generated in the converter under conditions identical with those governing the capture of electrons (positrons) into the channel. Clearly the amounts involved will be smaller in the case of electron beams than in that of positron beams.

This method enables us to make an independent choice of the optimum parameters of the target and converter so as to obtain the greatest possible electron (positron) current density. Using this method, strong electron beams may be formed in the outer zone of the magnetic ring of the accelerator and positron beams in the inner zone. In order to realize the method, careful matching of the rectilinear trajectory of the photon and the curvilinear trajectory of the electron (positron) is essential. In this way, after placing the target and converter at specific points in the magnetic field of the accelerator, we may obtain an electron (positron) beam in any magnetic channel designed for hadron beams. By providing for radial motion of the target and the converter, we may vary the electron (positron) energy over a fairly wide range in the channel of the outer (or inner) zone of the magnetic ring for a constant energy of the accelerated protons.

An electron beam was obtained in the Serpukhov accelerator on the basis of the method just described at the end of 1971, using magnetic channel No. 2B. The channel was created in experimental areas external to the accelerator, intended for the formation and transportation of beams of negatively-charged hadrons with momenta up to 60 GeV/c [8, 9].

A special target was placed in the 24th magnetic unit of the accelerator for the generation of the photons. The lead converter was placed at a distance of some 6.64 m from the target in the direction of circulation of the proton beam.

The vertical and radial dimensions of the converter were equal to 60 and 70 mm. The main positions of the target and converter were chosen so that, for the capture of electrons with a momentum of p = 35 GeV/c into the channel, the converter was irradiated with photons formed at an angle of $\theta_\gamma = 0^0$ (θ is the angle of generation of the particles), with an accelerated proton energy of $E_0 = 70$ GeV. Radial displacements of the target and converter in the accelerator enabled the momentum of the electrons introduced into the channel to be varied over the range p = 26-46 GeV/c (Fig. 2). However, conditions were not optimum for the generation of electrons with $p \neq 35$ GeV/c, since in these cases $\theta_\gamma \neq 0^0$. The introduction of electrons with p < 26 GeV/c into the channel was achieved by using a reduced energy of the accelerator.

Figure 3 shows the so-called Mikhaélis diagram for the trajectories of negatively-charged particles generated in the target and extracted from the accelerator. The variable parameters in this are θ and p. Superposed on the diagram is the horizontal acceptance of the channel A for an electron beam arriving from the converter, referred to the azimuthal coordinate of the target in the accelerator. This acceptance

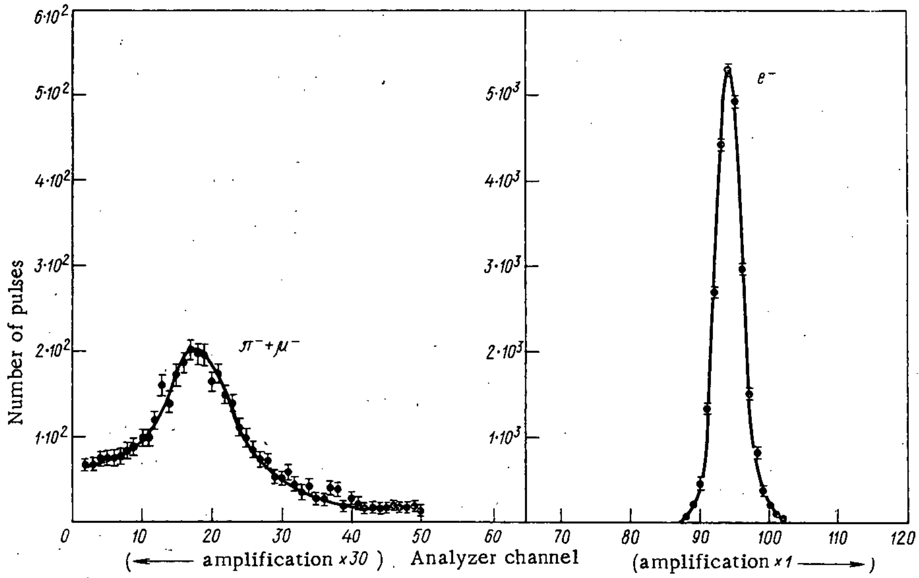

Fig. 6. Pulse-amplitude spectrum of the total-absorption Cerenkov spectrometer in an electron beam with p = 45.5 GeV/c in channel No. 2B (E_0 = 70 GeV, $\Delta p/p = \pm 2\%$).

varies little over the whole range of electron momenta p ≈ 26-46 GeV/c. We see from the diagram that in the electron beam so formed with p ≈ 26-40 GeV/c no traces of hadrons generated in the target should appear. For p > 40 GeV/c, the beam may be expected to contain less than 10% of hadrons from the target. The purification of the electron beam with respect to hadrons is aided by the fact that these particles have different focusing characteristics in the magnetic field of the accelerator: the positions and characteristics of the virtual sources corresponding to the electrons and hadrons extracted from the accelerator are quite different. The electron beam extracted from the accelerator has an imaginary source in the vertical plane, lying at a distance of some 13 m from the first quadrupole lens of channel No. 2B, while in the horizontal plane this beam has a very small angular divergence.

The electron beam was formed in the optical scheme illustrated in Fig. 4. At the entrance into the channel the beam is limited by the aperture collimators C_1 and C_2. A doublet of four quadrupole lenses

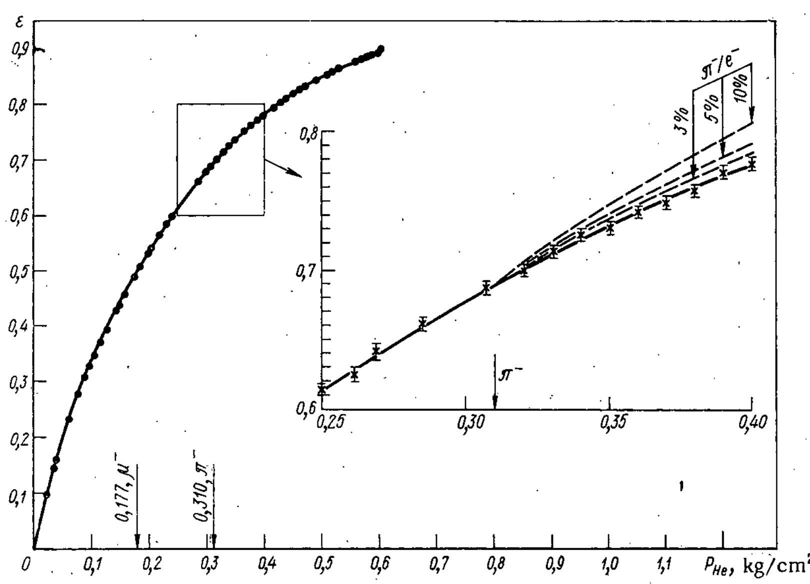

Fig. 7. Particle-recording efficiency for a threshold-type gas Cerenkov counter ε in an electron beam with p = 31 GeV/c in channel No. 2B, expressed as a function of the pressure of the working gas p_{He} (E_0 = 70 GeV, $\Delta p/p = \pm 3\%$).

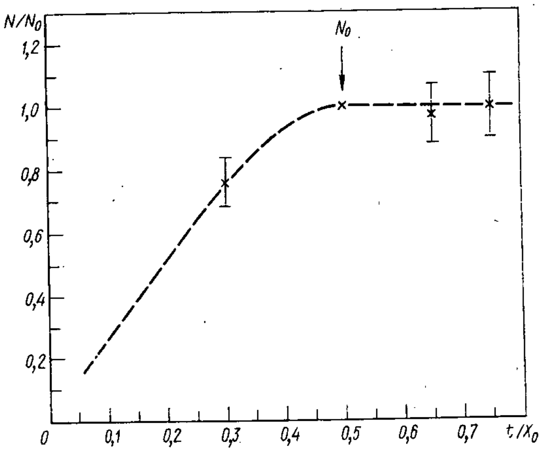

Fig. 8. Relative yield of electrons N/N_0 as a function of the thickness of the lead converter t/X_0 (the thickness of the converter is expressed in rad. units; p = 31 GeV/c).

Q_1-Q_4 creates an image of the converter in the collimator C_3 in the horizontal plane, while in the vertical plane a beam converging behind the lens Q_5 is formed. The deflecting magnet M_1 disperses the image of the target in the collimator C_3 with respect to particle momentum. The collimator C_3 selects the particles in the desired momentum range $p \pm \Delta p$. The field lens Q_5 and the deflecting magnets M_2 and M_3 reduce the linear and angular dispersion of the beam particles in the momentum range selected. All three magnets M_1-M_3 deflect the beam toward the accelerator. In the vertical plane the beam travels in a parallel manner in the section between lenses Q_5 and Q_6. The quadruplet of quadrupole lenses Q_6Q_7-Q_8Q_9 creates a beam traveling parallel in both planes between lenses Q_7 and Q_8, and forms a stigmatic final image F in the experimental target (at a distance of about 29 m from lens Q_9). The coefficients of linear magnification of the optical system in the section between the target T and the image F, including the magnetic field of the accelerator, equal 2.15 and 6.60 in the horizontal and vertical planes respectively. The linear dispersion of the image of the target in collimator C_3, allowing for the dispersion of the electron beam in the magnetic field of the accelerator, equals 5 mm/($\Delta p/p$) = 1%. The coefficient of linear magnification of the optical system in the horizontal plane in the section between the target T and the collimator C_3 equals 1.30. On using a target with a cross section (diameter) of approximately 3 mm and a converter with a thickness of about 0.5 rad. units, the effective cross section of the target for p = 26-46 GeV/c will be increased to a mean square diameter of ~4.5 mm, owing to the multiple Coulomb scattering of the electrons in the converter material. This corresponds to an image size of ~5.7 mm in the collimator C_3 and a minimum range of momentum resolvable in the channel of $(\Delta p/p)_{min} \approx 1\%$. In the final image in the horizontal plane there remains an uncompensated linear dispersion of 4.2 mm/($\Delta p/p$) = 1%. For the conversion electrons which are drawn into the channel, the solid angle of formation of photons in the target equals $\Delta\Omega_\gamma \approx 40\mu$ sr for the average momentum, while the mean solid angle is equal to $(\Delta\Omega_\gamma)_{av} \approx 27\mu$ sr for the maximum range of electron momenta $\Delta p/p = \pm 3\%$. The total length of the beam from the converter to the final image is ~118 m. The electron beams may be expanded in time, giving a pulse lasting up to $\tau \approx 2$ sec.

Investigations into the characteristics of the electron beams in the channel were carried out for p values of 26.6, 31, 40, and 45.5 GeV/c, and an acceleration energy of E_0 = 70 GeV. Matching of the paths of the photons and electrons was achieved by varying the radial position of the target in the accelerator until the maximum flux of particles was achieved at the output of the pulse analyzer of the channel (behind lens Q_7, Fig. 4). The operating conditions of the optical elements of the pulse analyzer of the channel and the position of the converter in the accelerator were set in accordance with calculations. It should be noted that the area of the converter was made slightly larger than the area from which the electrons were drawn into the channel. The experimental positions of the target and converter agreed closely with the calculated values. The electron beams in the channel for $\Delta p/p = \pm 3\%$ were formed into a spot some 30 mm in diameter in the final image, with an angular divergence of approximately ±1 mrad (Fig. 5). Over the greater part of their path the electrons traveled in vacuo.

The composition of the beams was determined by means of a telescope of scintillation counters in the channel and a total-absorption Cerenkov spectrometer. The spectrometer had a radiator 22 rad. units thick. The dependence of the spectrometer pulse amplitude on the energy of the electrons recorded was linear; the energy resolution over the whole working energy range was no worse than 5% (total width of the peak at half height).

The electrons leave a considerable part of their energy in the radiator of the spectrometer (owing to the formation of showers), while the hadrons lose only a small part of their energy in the radiator (ionization loss). Hence separation of the electrons and hadrons is easily effected by amplitude analysis of the Cerenkov spectrometer pulses.

A wide range of energy measurement was ensured by varying the amplitude of the pulse from the spectrometer. For p = 26-40 GeV/c the proportion of hadrons and muons in the electron beam was less

Declassified and Approved For Release 2013/01/22 : CIA-RDP10-02196R000400020003-6

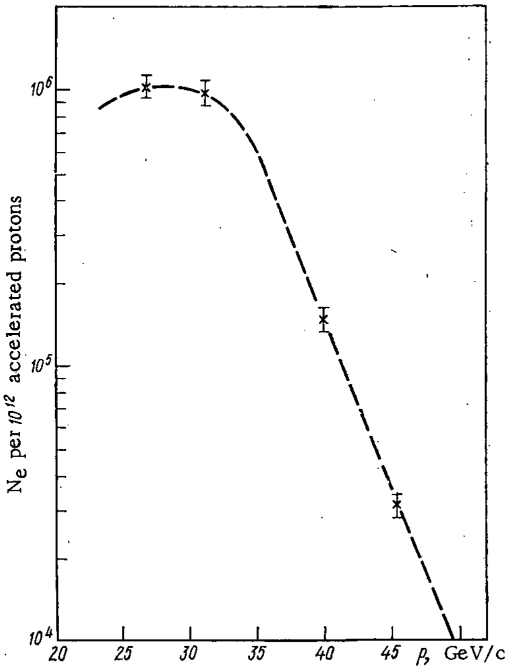

Fig. 9. Electron fluxes with various momenta in channel No. 2B (beryllium target 3 mm in diameter and 40 mm long, lead converter $0.5X_0$, $E_0 \doteq 70$ GeV, $\Delta p/p = \pm 3\%$).

than 1%, while for p = 45.5 GeV/c it was 3.6%. The characteristic pulse-amplitude spectra obtained from the Cerenkov spectrometer for the hadrons and electrons are shown in Fig. 6. Control measurements of traces of pions and muons in the electron beam with a momentum of p = 31 GeV/c were also carried out using a threshold-type gas Cerenkov counter [10]. As in the previous measurements, these never exceeded 1% of the flow of electrons in the channel (Fig. 7).

The electron fluxes were measured with the same spectrometer. In these measurements the pulses from the spectrometer, passing through an integral discriminator of the SAIP-VDI/21 type with a rapidity of action of 100 MHz, were recorded in coincidence with the pulses from the telescope counters. In measuring the electron fluxes, the number of accelerated protons passing into the target was recorded at the same time. The statistical error of the measurements was low (under ±1%). The accuracy in measuring the number of protons passing into the target was ±(5-10)%. In order to obtain the most intensive electron beams, special investigations were carried out in an electron beam with a momentum of p = 31 GeV/c.

The optimum thickness of the lead converter $t_{opt} \approx 0.5$ rad. units was determined experimentally (Fig. 8). For thinner converters the electron yield diminished, for thicker converters the electron yield hardly increased at all, while the flux of hadrons from the converter had to be made greater. We measured the yields of photons from the $\pi^0 \to 2\gamma$ decay for several targets: beryllium (diameter 3 mm, length 40 mm); aluminum (diameter 2 mm, length 20 mm); Duralumin (diameter 2 mm, length 50 mm). The relative yields for these targets were respectively 1, 0.67 ± 0.07, 0.60 ± 0.06; these allow for the dynamic characteristics of the interaction of the accelerated proton beam with the target, involving the repeated passage of protons through the latter. We note that the efficiency of the nuclear interaction of the proton beam with the aluminum target (for a slow application of protons to the target) equals ~0.4 [11]. The electron fluxes in channel No. 2B were measured for a beryllium target 3 mm in diameter and 40 mm long and a lead converter 3 mm thick (0.5 rad. units). In the range $\Delta p/p = \pm 3\%$ with $(\Delta\Omega_\gamma)_{av} \approx 27\mu$ sr, these fluxes amounted to approximately 10^6–$3 \cdot 10^4$ electrons per pulse (for a momentum of p = 26-46 GeV/c) to every 10^{12} accelerated protons (Fig. 9). Owing to the deflection of the channel path toward the accelerator, in the region of the final image there was a considerable lateral muon background, amounting to ~10^2 particles/cm^2.

The electron beam of the Serpukhov accelerator was used for experiments relating to the total cross sections representing the hadron absorption of photons by nucleons at energies of 12-30 GeV [12]. The creation of these electron beams was a basic necessity in order to examine the possibility of using the Serpukhov accelerator in order to produce a beam of photons "tagged" with respect to energy up to 35 GeV, and also a beam of quasi-monochromatic, linearly-polarized photons with energies up to 20 GeV for studying electromagnetic interactions in the two-meter hydrogen bubble chamber "Lyudmila" (Joint Institute for Nuclear Research) [13].

In conclusion, the authors wish to express their sincere thanks to A. A. Logunov, A. A. Naumov, Yu. D. Prokoshkin, V. A. Yarbe, R. M. Sulyaev, V. I. Kotov, and S. P. Denisov (Institute of High-Energy Physics) for constant interest and very real support and assistance at all stages in the creation of the Serpukhov electron beam. The authors are grateful to A. L. Zhadkevich, V. G. Rogozinskii, N. M. Tarakanov, V. P. Sakharov, R. S. Shuvalov (Institute of High-Energy Physics), P. A. Zaitsev, N. G. Kotel'nikov, E. I. Malinovskii, V. P. Plaksin, V. P. Finogenov, I. V. Mikhailov, V. I. Sergienko, V. G. Dolgalev (Physical Institute of the Academy of Sciences), G. A. Akopdzhanov, L. S. Bagdasaryan, O. M. Vinnitskii, K. A. Ispiryan, and G. A. Oganesyan (Erevan Physical Institute) for help at various stages in realizing the beam project, and also Z. G. T. Kirakosyan (USA) for useful discussions.

LITERATURE CITED

1. A. I. Alikhanyan et al., Preprint, Erevan Physical Institute É4-1(70) [in Russian], Erevan (1970).
2. V. V. Makeev and V. N. Folomeshkin, Preprint, Institute of High-Energy Physics 71-51 [in Russian], Serpukhov (1971).
3. A. S. Belousov et al., Preprint, Physical Institute of the Academy of Sciences 71 [in Russian], Moscow (1970).
4. C. Halliwell et al., Nucl. Instrum. and Methods, 102, 51 (1972).
5. A. I. Alikhanyan et al., Contribution to the International Conference on Apparatus in High-Energy Physics [in Russian], Dubna (1970); preprint, Institute of High-Energy Physics 70-105 [in Russian], Serpukhov (1970).
6. F. Binon et al., Phys. Lett., 30B, 506 (1969); Yadernaya Fizika, 11, 3 (1970); preprint, Institute of High-Energy Physics 69-78 [in Russian] (1969).
7. V. A. Kachanov et al., Preprint, Institute of High-Energy Physics 71-89 [in Russian], Serpukhov (1971).
8. K. I. Gubrienko et al., in Transactions of the Seventh International Conference on High-Energy Accelerators (Erevan, Vol. 1 1969) [in Russian], Izd. AN ArmSSR, Erevan (1970), p. 471; preprint, Institute of High-Energy Physics 69-77 [in Russian], Serpukhov (1969).
9. I. A. Aleksandrov et al., At. Énerg., 29, 29 (1970); preprint, Institute of High-Energy Physics 69-36 [in Russian], Serpukhov (1969).
10. S. Denisov et al., Nucl. Instrum. and Methods, 85, 101 (1970); Pribory i Tekh. Éksperim., No. 3, 117 (1970).
11. Yu. B. Bushnin et al., Phys. Lett., 29B, 48 (1969); Yadernaya Fizika, 10, 585 (1969); preprint, Institute of High-Energy Physics 69-18 [in Russian], Serpukhov (1969).
12. A. S. Belousov et al., Contribution to the Sixteenth International Conference on High-Energy Physics in Batavia (USA); preprint, Physical Institute of the Academy of Sciences 19 [in Russian], Moscow (1973).
13. A. M. Baldin et al., Preprint, Joint Institute for Nuclear Research–Physical Institute of the Academy of Sciences–Institute of High-Energy Physics R1-6202 [in Russian], Dubna (1972).

DYNAMICS OF AQUEOUS HOMOGENEOUS PULSE REACTORS

A. N. Sizov and V. F. Kolesov

UDC 621.039.522.042.46

A derivation of a system of equations describing the dynamics of aqueous homogeneous pulse reactors is given. The system comprises equations for radiolytic gassing and neutron kinetics.

The process of radiolytic gassing is distinguished by the diffusion of a radiolytic gas, which is formed as a result of the radiolysis of water, into the gas bubbles arising on the tracks of the fission fragments. The equations describing the radiolytic gassing have the form:

$$C_{in} - \frac{2B\sigma(t)}{R(\xi,t)} - B\{p(t)-\varphi(t)\}$$
$$-\frac{\sqrt{t-\xi}}{4\sqrt{3\pi D(t)}\,R^2(\xi,t)}\cdot\frac{\partial m(\xi,t)}{\partial t}$$
$$= N\rho(t)\int_0^t m(\xi,t)\,d\xi,\quad t>\xi;$$
$$\frac{2\sigma(t)}{R(\xi,t)}+p(t)-\varphi(t)=\frac{T(t)}{R^3(\xi,t)}\left\{A+\frac{3F}{4\pi}m(\xi,t)\right\},$$
$$m(\xi;\xi)=0,$$

where C_{in} is the initial concentration of radiolytic gas in solution; A, B, F are constants; D is the coefficient of diffusion of the gas in solution; m is the amount of gas (in grams) which entered a given bubble at a specified moment of time; N is the average number of bubbles arising during a single fission event; n is the output (in fissions), separable in 1g of solution; p is the pressure; R is the radius of the bubble; T is the temperature; t is the time; ξ is the moment of creation of the bubble; ρ is the density of the solution; σ is the coefficient of surface tension; φ is the water vapor pressure on the saturation line.

Weak pulses (the pressure during the occurence of the pulse fluctuates slightly) for a KEWB reactor [1] were calculated on the basis of the equations derived. From a comparison of the results of the calculation with the experimental data, it is found that the average number of gas bubbles formed in a single fission is 1.5.

The nature of the effect of the initial values of pressure, temperature, and the concentration of radiolytic gas in the reactor mixture on the processes occurring in the behavior of the pulse is explained. It is shown that, with an increase in the initial temperature and concentration of radiolytic gas in solution, the total energy release decreases, but with an increase in pressure it increases, which agrees with the experimental data.

It is found that of the two pulses, having the same initial reactivity, recurrent one after another in a short time interval, the second will be weaker, since at the start of the second pulse not all of the radiolytic gas generated in the first pulse succeeds in escaping from the solution, but the solution itself after this time is not yet sufficiently cool.

The calculations allowed one to utilize the temporal behavior of the gas bubbles. It is established that only part of the bubbles created during the pulse grow with time; in the course of growth, these bubbles decrease the concentration of radiolytic gas in the solution so much, because of the diffusion into them of the latter, that, starting at some moment, all of the created bubbles are gradually destroyed again.

Translated from Atomnaya Énergiya, Vol. 35, No. 3, pp. 189-196, September, 1973. Original article submitted November 29, 1972.

LITERATURE CITED

1. M. Remli et al., Second Geneva Conference [in Russian], Vol. 3, Atomizdat, Moscow (1959), p. 585.

SMOOTHING OF CONTOUR RADIOMETRIC MEASUREMENTS AT A HIGH LEVEL OF FLUCTUATION NOISE

I. D. Savinskii, É. Ya. Ostrovskii, and V. S. Blashchinskii

UDC 543.52

A new method of smoothing, based on the idea of minimizing the norm in L_2 by curve averaging, is discussed. The problem thus arises to match the increments ΔN_j of the smoothed values for the original $N_j(x)$ at n points of the contour so that a minimum for the norm was achieved with preservation of the prescribed quantity $\beta^2 = 1/n \sum_{j=1}^{n} \Delta N_j^2$. With utilization of expressions presented in [1], the problem of the extremum of a function of n variables is solved. The expressions obtained for the ΔN_j ensure the solution of the problem so much better than the smaller β, other conditions being equal: in connection with this, an iteration procedure for smoothing with fairly small β (on the order of 0.1 of the level of the fluctuations) is specified. The proposed iteration smoothing procedure is essentially different from other widespread methods applying linear filters: during the smoothing of the curve for a function, the effects of the values at neighboring points on the value at a given point is determined not only by the distance between the points, but also by the values at the points themselves.

Using as an example of the smoothing of model curves cases involving known effective signals and noise, and representing the most important in the field of radiometric surveys, the iteration procedure is compared with the method of curve reconstruction by a truncated Fourier series and the slipping average technique with a reiterated smoothing procedure. The results obtained attest to the fact that the smoothing

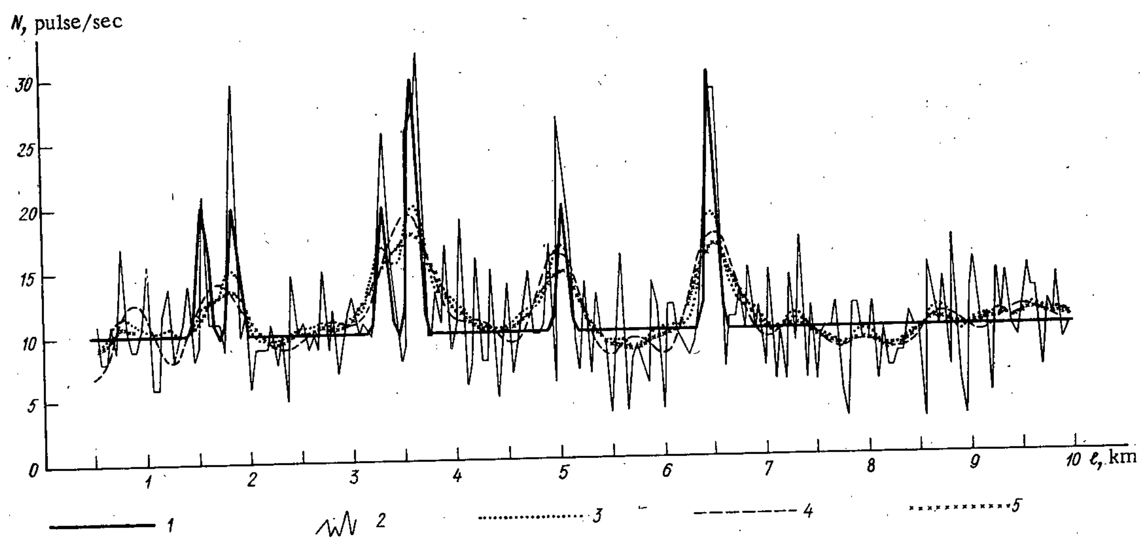

Fig. 1. Smoothing of a model curve with the presence of "spike" signals: 1) effective signal; 2) signal noise; 3) iteration procedure; 4) truncated Fourier series; 5) delta filter.

Original article submitted July 14, 1972; revision submitted December 28, 1972.

operation allows one to reduce by two to three times the root-mean-square deviation between the effective signal curve and the recorded curve. The smoothing is virtually a compulsory operation, the advantages of which are especially well manifested during the code recording of discrete measurements along the contour [2]. The iteration procedure in all cases gave results not inferior to the results with the utilization of other procedures; in the case of "spike" signals with a frequency spectrum close to the noise spectrum, the iteration procedure gives noticeably better results (see Fig. 1).

The iteration procedure has important advantages for the automatic processing of data on an electronic computer. It ensures effective filter discrimination with the same filter parameters for the different character of the signals and the noise, an arbitrary length of the contour which does not require the interruption of the computational process for its correction by the operator, but also a significant expenditure of machine time. The data presented in the paper, in the same way as the significant experience in the efficient processing of data from aero-γ-spectrometric surveys, allows one to recommend an iteration smoothing procedure for the mass processing of the results of radiometric and other kinds of measurements on an electronic computer.

LITERATURE CITED

1. I. D. Savinskiii, Fizika Zemli, No. 6, 72.
2. F. É. Apel'tsin, S. F. Lugov, and E. Ya. Ostrovskii, Sov. Geologiya, No. 12, 107 (1967).

MONTE CARLO CALCULATION OF THE ESSENTIAL FEATURES OF BREMSSTRAHLUNG DETECTION

A. V. Pokrovskii and G. P. Tarasov

UDC 539.166.3

In the present article we present an algorithm and the results of our calculations of several integral characteristics of a radiation detection technique which uses a scintillation detector shielded by an opaque collimator. We examined both monoenergetic sources (Cs^{137}, Co^{60}) as well as a bremsstrahlung source (E_{max} = 6 MeV); point perpendicular, conical, and disk geometries were used, in each case homogeneous. A cylindrical NaI (Ta) detector was used. The source and detector were separated by a plane layer of absorber (iron).

The quantities which were calculated were the energy of the radiation impinging on the crystal, the energy dissipated by the crystal, and the cutoff level of the radiation scattered in the absorber (the ratio of the energies at the output of the collimator). The rms relative error in the calculations averaged between 3% and 6%. The migration in the absorber was modeled by a specially chosen chain in order to sample the important trajectories. The characteristic difference between the algorithm considered here from those already known lies in the fact that here one initially develops the overall direction angles of the new transition, and subsequently determines the cosine of the angle of the change of direction (from which one calculates the new value of the quantum energy).

Original article submitted July 17, 1972; revision submitted February 6, 1973.

HIGH-TEMPERATURE NEUTRON DETECTORS CONTAINING IRON, NICKEL, AND COBALT

M. A. Kolomiitsev, T. S. Ambardanishvili,
G. I. Kiknadze, T. Ya. Zakharina,
V. Yu. Dundua, and I. G. Brovkina.

UDC 539.1.074.8

Iron, cobalt, and nickel detectors are widely used to measure neutron densities and integrated neutron fluxes. These detectors are generally pure metal foils or homogeneous mixtures of neutron-sensitive elements with matrices of aluminum and magnesium oxides and polyethylene which are weakly activated by neutron bombardment.

An activity of the isotope formed in the irradiation of the detector sufficient for radiometric measurement can frequently be obtained with less than 10^{-4}-10^{-5} g of the element per detector.

The article discusses the special features of the manufacture and the main characteristics of activation detectors based on the mixing of an alcoholic solution of a phenolformaldehyde resin (PFR) and an alcoholic solution of the nitrate of the metal, with a subsequent conversion of the true solution obtained into polymeric tablet monitors. This method of manufacture eliminates most of the disadvantages of earlier methods and permits an extension of the range of control of the concentration of the neutron-sensitive element in the matrix from 1 to 10^{-8}%.

The specific content of the elements in the detectors obtained was determined, and by using photocolorimetric methods of analysis and by studying the infrared spectra it was shown that the elements are uniformly distributed in the PFR. The error in the determination of the number of nuclei of the elements is no more than 2-3%. PFR based detectors are heat resistant to 250°C, radiation resistant to integrated fluxes of up to 10^{19} neutrons/cm^2, capable of operating in water and superheated steam, and are mechanically strong.

The polymeric detectors were subjected to pyrolysis at temperatures from 250 to 1600°C in an argon atmosphere to increase their radiation and heat resistance. The loss of weight of the polymer was found as a function of the pyrolysis temperature, and the specific content of the elements in the carbonized detectors was determined. The specific content of the elements relative to the weight of the initial PFR tablet was calculated from these determinations and the thermogravimetric relation. The results obtained establish 1500°C as the high temperature limit for the use of carbonized monitors.

An analysis of the PFR and the carbonized detectors showed that oxygen is removed from the matrix at 800°C. At 1300°C there is no more than 1 at. % of hydrogen in the pyrolysis product, i.e., the material obtained is practically pure carbon with a radiation resistance slightly different from that of graphite. These data indicate that 1300°C is an optimum temperature for the pyrolysis of PFR based detectors.

Carbon detectors can be used in water at 100°C, as indicated by a study performed by the method of isotopic exchange, and in superheated steam since iron, cobalt, and nickel are not washed out of the matrix.

Because of the high activation purity of PFR and its pyrolysis products the measurements can be begun from one to three hours after cessation of irradiation of the detectors by high integrated neutron fluxes of 10^{17}-10^{19} neutrons/cm^2.

Original article submitted October 23, 1972; abstract submitted February 1, 1973.

THE EFFECT OF RESONANCES ON THE NONSTATIONARY NEUTRON SPECTRUM

E. V. Metelkin and G. Ya. Trukhanov

UDC 539.125.5.173.162.3:539.125.5.162.3

We investigate the effect of resonances on the nonstationary spectrum of neutrons in an infinite homogeneous medium from a uniformly distributed instantaneous source for the simplest model taking account of the resonance structure of the absorption cross section: in the energy ranges $E > E_1$ (the first region) and $E < E_2$ (the third region) there is no absorption, i.e., $\Sigma_{tot}^{(1)} = \Sigma_s^{(1)} = \Sigma_{tot}^{(3)} = \Sigma_s^{(3)} = \text{const}$; in the range $E_2 \le E \le E_1$ (the second region) the neutron absorption is controlling, i.e. $\Sigma_{tot}^{(2)} = \Sigma_a^{(2)} = \text{const}$ with $\Sigma_a^{(2)} \gg \Sigma_s^{(1)}$. The calculations are performed in the "narrow resonances" approximation. The criterion for the applicability of this approximation is that the absorption probability in an individual resonance be small and have the form $E_1 - E_2 \ll 2E_1/M$, where M is the mass number of a moderator nucleus. The neutron spectrum is determined under the assumption that the moderator nuclei are stationary, which is valid for neutron energies above 10 MeV, and that the scattering is spherically symmetric in the center of mass system.

It is shown that the neutron flux in the resonance region is maximum at the time $t(E) = 2/\xi\nu\Sigma_s^{(1)}$, which agrees with the result in [1] to within terms of the order 1/M. This shows that the presence of resonances does not affect the slowing down time.

The neutron flux is found to be

$$\Phi(E,\ t) = \Phi_0(E)\frac{[t/\tau_1(E)]^{2/\xi}\exp\{-t/\tau_1(E)\}}{\tau_1(E)\,\Gamma\left(\frac{2}{\xi}+1\right)}, \tag{1}$$

where $\Phi_0(E) = (1/\xi E\Sigma_{tot})\exp[-\int\limits_E^{E+}(\Sigma_a/\Sigma_{tot})\cdot(dE/\xi E)]$ is the solution of the corresponding stationary problem, $\tau_1(E) = 1/\nu\Sigma_s^{(1)}$ is the mean free time of neutrons of energy E, ξ is the average change in lethargy in an elastic collision, and $\Gamma(2/\xi + 1)$ is the gamma function. It is clear from (1) that the neutron flux has dips in the resonance region and the collision density ($\Psi = \Sigma_{tot}\Phi$) is a smoothly varying function as in the stationary case.

The result is generalized to an arbitrary number of sufficiently widely spaced resonances. It is shown that in this case the resulting absorption can be considerable.

The final result, taking account of the effect of resonances on the nonstationary neutron energy spectrum for narrow resonances, is obtained by multiplying the nonstationary neutron distribution function calculated in the absence of resonances by the resonance escape probability calculated for the stationary case, taking account of the resonances. It should be noted that the narrow resonances approximation is valid for a number of substances [2].

LITERATURE CITED

1. M. V. Kazarnovskii, "The theory of the nonstationary elastic slowing down of neutrons in a heavy medium", Trudy FIAN, 11, 176 (1957).
2. L. Dresner, Resonance Absorption in Nuclear Reactors, Pergamon, New York (1960).

Original article submitted November 20, 1972; abstract submitted April 2, 1973.

AMPLITUDE MODULATION OF THE ACCELERATING FIELD IN A LINEAR ACCELERATOR WITH ASYMMETRIC VARIABLE-PHASE FOCUSING

V. V. Kushin and V. M. Mokhov

UDC 621.384.64

One can increase the capture of particles in an accelerator with asymmetric variable-phase focusing, if, simultaneously with periodic variation longitudinally of the synchronous phase of the accelerator ($\varphi_s = \varphi_0 \pm \varphi_1$), one also varies the amplitude of the accelerating waves [$E_m = E_0(1 \pm \varepsilon)$].

The transverse and longitudinal (phase) oscillations of a particle in the dimensionless coordinates ρ, $\sigma \sim \Delta\varphi$, z are described by the equations:

$$\frac{d^2\rho}{dz^2} + [-A_\rho \pm G_\rho]\,\rho = 0; \tag{1}$$

$$\frac{d^2\sigma}{dz^2} + [-A_\varphi \pm G_\varphi]\,\sigma = 0, \tag{2}$$

where

$$\left.\begin{aligned} A_\rho &= B\,[\sin(\varphi_0 + \Delta\varphi)\cos\varphi_1 + \varepsilon\cos(\varphi_0 + \Delta\varphi)\sin\varphi_1], \\ \sigma_\rho &= B\,[\cos(\varphi_0 + \Delta\varphi)\sin\varphi_1 + \varepsilon\sin(\varphi_0 + \Delta\varphi)\cos\varphi_1], \\ A_\varphi &= -2A_\rho\,|_{\Delta\varphi=0}, \quad G_\varphi = 2G_\rho\,|_{\Delta\varphi=0}, \end{aligned}\right\} \tag{3}$$

$$B = \frac{\pi e E_0 (1 - \beta_s^2)^{3/2} L^2}{m_0 c^2 \lambda \beta_s^3}. \tag{4}$$

Here e, m_0 are the charge and rest mass of the particle; λ is the wavelength; L is the focusing period; $\beta_s = v_s/c$, where v_s is the equilibrium velocity, c is the velocity of light. The well-known stability diagram in the A, G plane corresponds to Eqs. (1) and (2). Provided that the phase shift of the particle $\Delta\varphi = \varphi - \varphi_s$ fluctuates in the limits from $-\Delta\varphi_m$ to $+\Delta\varphi_m$, a representative point of the transverse oscillations A_ρ, G_ρ performs oscillatory motion along the arc of an ellipse, which is described in parametric form by Eqs. (3).

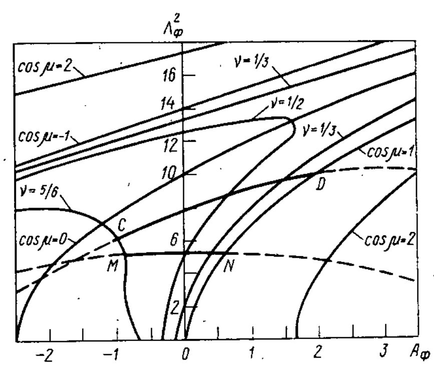

Fig. 1. Trajectories of a representative radial point for the cases $\varepsilon = 0$ and $\varepsilon \neq 0$.

The radial stability of the particles is maintained as long as the representative point does not go outside of the limits of the stability region, which is bounded in Fig. 1 by the lines $\cos\mu = 1$ and $\cos\mu = -1$. In the case $\varepsilon = 0$, this point moves along the arc of an ellipse, whose axes coincide with the coordinate axes (arc MN). Therefore, a representative point approaches the $\cos\mu = 1$ stability limit by the shortest path. The introduction of amplitude modulation of the field $\varepsilon \neq 0$ allows one to rotate the axes of the ellipse relative to the coordinate axes and thereby to displace noticeably the point of intersection of the trajectory with the stability limits (arc CD). Thus, one succeeds in increasing the admissible peak-to-peak amplitudes of the phase oscillations and the phase holding device of the accelerator up to values which usually occur during phase stability. However, the consumption of radio frequency power, which during asymmetric variable-phase focusing is spent on the creation both of the accelerating and of the focusing field, is found to be noticeably higher than during phase stability.

Original article submitted November 29, 1972.

CONCENTRATION OF RADIOACTIVE FERRIC HYDROXIDE SLUDGE AND RECYCLE SOLUTIONS BY COMBINED EVAPORATION

D. I. Trofimov and A. I. Barabanov

UDC 66.049.1

Until recently [1], concentration of radioactive wastes in the form of $Fe(OH)_3$ hydroxide sludge and recycle solutions forming in deactivation of effluents has been carried out by such methods as centrifugation and evaporation. Centrifugation cannot produce a sludge of less than 90% moisture content, resulting in higher burial disposal costes. Evaporation of recycle solutions is accompanied by intense frothing, and the maximum bulk reduction factor is in the 10-12 range.

It has been established experimentally [2] that the evaporation ratio can be increased to 25 through mixing hydroxide sludge and recycle solutions. Frothing is kept to a level well below that encountered when recycle streams only are evaporated, and froth removal is no longer a serious problem. Conventional equipment, e.g. including an outboard heating chamber, is used in the combined evaporation process. The process is a quiescent one, with no surges or impulses. $Fe(OH)_3$ micellar particles are not observed to stick to the heating surface of the process equipment.

When hydroxide sludge is mixed with recycle solution containing mostly $NaNO_3$, in all likelihood a process of substitution of water ions in the adsorptive layer of the sludge by Na^+ and NO_3^- ions ensues, i.e., a salting-out process gets under way. In the combined evaporation process, the heat transfer coefficient K is 20-25% higher than in evaporation of recycle alone. The heat transfer coefficient increases as ferric hydroxide sludge with its enhanced thermal conductivity is added to the stream. The resulting condensate does not exceed the norms set for wastes that can be dumped in an open reservoir, in terms of content of radioactive isotopes.

Table 1 shows results of investigations of combined evaporation of ferric hydroxide sludge and recycle solutions.

On the basis of these investigations and the work done in adapting this arrangement to production, it was shown that the separate concentration of hydroxide sludge and recycle slurry makes it possible to reduce waste bulk by only 250 times, whereas combined evaporation brings the concentration ratio up to 500. This results in a significant reduction in the costs of reprocessing radioactive waste slurries.

TABLE 1. Results of Investigations of Combined Evaporation of $Fe(OH)_3$ Sludge and Recycle Solutions

Characteristics of process	Evaporation of recycle	Mixture of recycle and hydroxide sludge (1 : 1)
Boiling point, °C	114-116	115-117
Evaporation ratio	11-12	24-26
Rate of heat removal, kg evaporated moisture per m^2 per h	40-50	60-70
Still residue:		
salt concentration, g/dm^3	800-850	950-1000
density, g/cm^3	1.30-1.40	1.50-1.60
total β-activity, Ci/kg	$(2-4)\cdot 10^{-4}$	$(3-5)\cdot 10^{-4}$

LITERATURE CITED

1. D. I. Trofimov et al., IAEA Symposium on the Reprocessing of Low-Level and Medium-Level Radioactive Wastes, Vienna, 1965. IAEA, Vienna (1966), p. 449 [Russian edition].
2. A. I. Barabanov and E. I. Zhiguleva, Byull. Izobret., No. 32 (1973).

Original article submitted January 15, 1973; revision submitted March 28, 1973.

THERMAL CONDUCTIVITY OF METAL DODECABORIDES WITH A UB_{12} STRUCTURE

V. V. Odintsov, M. I. Lesnaya, and S. N. L'vov

UDC 536.21:546.271

Dodecaborides are suitable for use in the nuclear power industry, thanks to their high boron content and the presence of rare earths. These materials must also exhibit sufficiently high thermal conductivity, in addition to their other properties.

The article deals with an investigation of the temperature dependence of the electrical resistivity and thermal conductivity of certain dodecaborides (YB_{12}, ZrB_{12}, DyB_{12}, HoB_{12}, ErB_{12}, TmB_{12}), in the range of temperatures from 300° to 1000°K. Dodecaborides used in this work were obtained by reducing the metallic oxides of boron in vacuum, and were found to be single-phase materials on the basis of x-ray phase analysis and metallographic analysis.

The following conclusions were arrived at on the basis of these findings (see diagram): the temperature dependence of the electrical resistivity is linear in all of the phases studied; the thermal conductivity varies inversely with temperature, and adopts a constant value when temperatures are reasonably high.

The high thermal conductivity exhibited by dodecaborides of metals with a type UB_{12} structure, which is higher than that of the metals, can be accounted for in terms of a peculiar feature in the structure of these compounds, and the strong covalent bonds linking boron atoms [2-4]. The existence of a fairly rigid lattice appears to be the primary reason for the higher thermal conductivity of the dodecaborides: first, the fraction of the phonon component in the thermal conductivity is enhanced; secondly, the distance between conduction electrons is narrowed, so that the electron fraction in the thermal conductivity is enhanced.

The Wiedemann–Franz law holds for the metal dodecaborides, but the value of the Lorentz function departs from the theorectical.

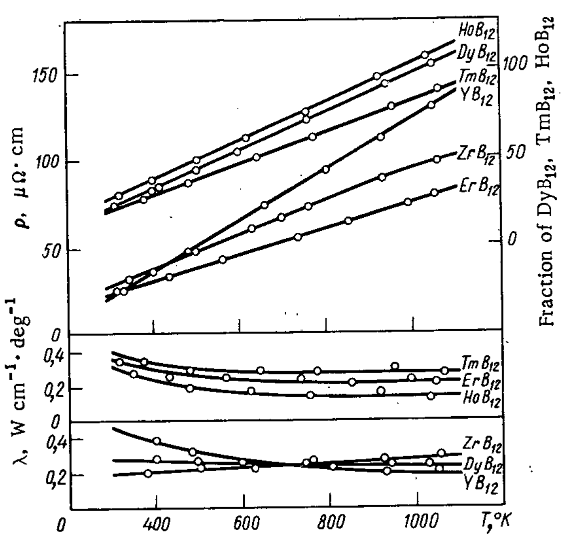

Fig. 1. Temperature dependence of electrical resistivity and thermal conductivity of metal dodecaborides.

LITERATURE CITED

1. Yu. B. Paderno and V. V. Odintsov, Metallothermal Processes in Chemistry and in Metallurgy [in Russian], Nauka, Novosibirsk (1971), p. 39.

Original article submitted January 23, 1973; revision submitted May 10, 1973.

Declassified and Approved For Release 2013/01/22 : CIA-RDP10-02196R000400020003-6

2. Yu. M. Goryachev, V. V. Odintsov, and Yu. B. Paderno, Metal Physics, No. 37 [in Russian], Naukova Dumka, Kiev (1971), p. 29.
3. V. V. Odintsov, et al., Teplofiz. Vys. Temp., 2, 216 (1971).
4. E. V. Yukhimento, et al., Poroshkovaya Met., No. 11, 52 (1971).

INTERACTION UNDER NON-EQUILIBRIUM CONDITIONS OF ALUMINUM WITH SALT MELTS CONTAINING URANIUM

A. B. Zolotarev, I. N. Kashcheev, and G. P. Novoselov

UDC 546.791.4

Salt concentrates containing uranium and plutonium are evolved from the alkali metal fluorides in a number of pyrochemical processes [1,2]. These metals are treated with metallic melts in order to extract them from the salts. We have studied the interaction of aluminum with UF_4–LiF and UF_4–NaF salt mixtures for an initial uranium concentration of 15% by weight and a temperature of 1150°C under non-equilibrium conditions.

It was found that the extraction of uranium from a UF_4–LiF mixture increases continuously as the holding time is increased, becoming almost 100% for an experiment lasting 150 min. Uranium extraction in the UF_4–NaF system reaches a maximum within 15 min and thereafter decreases (see Fig. 1).

The difference in these results can be explained by the fact that in addition to the reaction

$$4Al + 3UF_4 \rightleftarrows 4AlF_3 + 3U \tag{1}$$

which occurs in systems containing NaF, reduction of uranium by sodium ion pairs also occurs; the sodium ion pairs are formed under non-equilibrium conditions in the reaction

$$Al + 3NaF \rightarrow AlF_3 + 3Na. \tag{2}$$

In this case the principal process of uranium reduction is by the sodium ion pairs and occurs throughout the volume of the salt. The metallic uranium coagulates into drops which descend quite rapidly. Under non-equilibrium conditions, however, not only aluminum interacts with sodium fluoride, but also uranium [2]. This causes a decrease in the uranium extraction for long holding, since part of it again enters the salt melt.

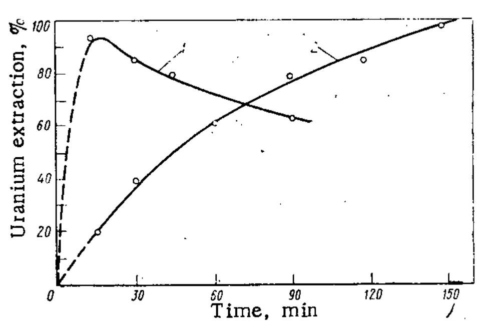

Fig. 1. Uranium extraction from salt melts as a function of holding time. 1) From UF_4–NaF salt mixtures; 2) from UF_4–LiF salt mixtures.

Original article submitted February 7, 1973; revision submitted October 5, 1973.

Aluminum and the salt melt have practically no interaction in LiF systems, since metallic lithium has negligible volatility under these conditions. In these systems, the alkali metal is not separated out, and the extraction of uranium occurs only at the phase interface, in accordance with reaction (1).

We also studied the extraction of microscopic quantities of plutonium (the concentration of Pu in the salt was 10^{-3}% by weight) together with uranium from UF_4–NaF–PuF_4 mixtures, with the reduction caused by aluminum. The behavior of the plutonium in these salt systems was found to be similar to that of uranium, and its extraction in the metallic phase was identical to that of uranium.

LITERATURE CITED

1. N. P. Galkin et al., The Chemistry and Technology of the Compounds of Uranium with Fluorine [in Russian], Gosatomizdat, Moscow (1961).
2. G. P. Novoselov et al., The Interaction of Certain Metals with Sodium Fluoride [in Russian], Proceedings of the Economical Mutual Aid Council (COMECON) Symposium on the Treatment of Nuclear Fuel, Karlovy Vary (1968).

DETERMINATION OF THE FORMS IN WHICH RADIOISOTOPES OCCUR IN PRECIPITATION

M. I. Zhilkina, L. I. Gedeonov, and A. G. Trusov

UDC 621.039.7

A study of the forms in which radioisotopes of artificial origin occur was conducted at the V. G. Khlopin Radium Institute in two stages.

In the first stage we studied the distribution of radioisotopes among the fractions of the precipitation. Precipitation samples were collected during the years 1961-1972. The solid and liquid fractions were separated immediately after collection, in order to preclude any errors arising from possible changes in the physicochemical characteristics of the water during storage. The fractions were separated by filtration and centrifugation. The solid fraction consisted of suspended particles of organic and inorganic origin ranging in size from 1μ to 1 mm; the liquid fraction, in addition to ions, molecules, colloids, and pseudocolloids of the precipitation components, also contained a finely dispersed suspension in the 0.1-1μ size range. The total volume of precipitation collected was 8,800 liters, representing a total of 57 samples.

The results of a decade of observation showed that the radioisotopes Mn^{54}, Sr^{90}, Y^{91}, Zr^{95} + Nb^{95}, Ru^{103}, Ru^{106}, Sb^{125}, Cs^{137}, Ce^{144}, Ce^{141}, and Eu^{155} were present in precipitation (Leningrad district) in water-soluble and water-insoluble forms. We determined the relative fraction of each radioisotope in each of these forms.

In the second stage of the investigation we studied the forms in which the radioisotopes occurred in each precipitation fraction. To determine the radioisotope composition in the liquid fraction of the precipitation, we used the method of adsorption on synthetic resins; we prevented the soluble forms of the radioisotopes from being sorbed by the filter material when the fractions were separated by filtration.

The composition of the radioisotopes in the solid fraction of the precipitation was studied by the method of volatilization for the following series: Mn^{54}, Be^7, Zr^{95} + Nb^{95}, Ru^{106}, Sb^{125}, Cs^{137}, Ce^{144}, and Eu^{155} at various temperatures (200-1,000°C) and with various processing times (1-4 h). The volatilization was carried out in an oxidative medium (air). The age of the fission-product mixture was 300 days or 600 days.

Original article submitted February 1, 1973.

In order to study the composition of the radioisotopes in the solid fraction, we also used the method of leaching with mineral acids: HCl, HNO_3, HCl + HNO_3, HCl + HF, HF + HNO_3, and H_2SO_4 + HF. We measured the concentrations of the acids (2 N, 6 N, and 12 N) and the contact times (0.5 h, 1 h, 5 h and 20 h).

An analysis of our extensive experimental data showed that the relative amount of the sum of the fission products and individual radioisotopes Zr^{95} + Nb^{95}, Ru^{106}, Ru^{103} + Ru^{106}, and Ce^{144} and macrocomponents present in the acid-insoluble residue was much less than the relative amount in the original solid fraction of the precipitation. The relative amount of Sr^{90} and Cs^{137} in the solid fraction was close to the amount in the acid-insoluble residue. Increasing the concentration of the acids and the contact time did not produce any notable increase in the degree of leaching of the radioisotopes (including Sr^{90} and Cs^{137}) and macrocomponents. The radioisotopes, including Sr^{90} and Cs^{137}, were observed to go into solution only when all the macrocomponents were completely dissolved after repeated processing of the samples with a mixture of concentrated acids, HNO_3 + HF or HCl + HF.

THE EFFICIENCY OF ATOMIC HEAT SUPPLY PLANTS

Yu. D. Arsen'ev, M. E. Voronkov, and N. M. Sinev

UDC 621.039.003

Under present-day conditions it is possible to obtain a considerable saving of organic fuel by making use of some of the nuclear fuel in nuclear reactors or so-called atomic heat supply plants, rather than using it in atomic electric power plants.

This is explained by the fact that because there is no heat loss from the exit gases, the thermal efficiencies of atomic heat supply plants η_{ahs} are higher than the thermal efficiencies η_b of industrial and regional boiler-type heating plants (not to mention those of block and local boilers). The efficiencies η_{app} of atomic electric power plants using saturated steam and thermal neutron reactors are at most 31-32%, which are considerably less than the efficiencies η_{cpp} of condensing electric power plants using organic fuel (especially gas); those of the latter are ~41%.

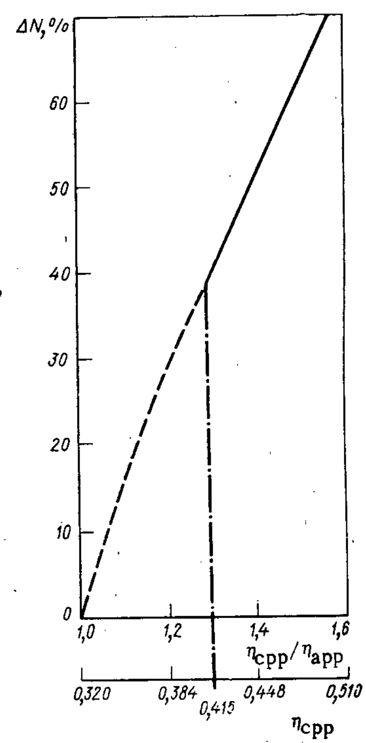

Fig. 1. Additional output ΔN of a gas-fueled condensing electric power plant, as a function of η_{cpp}/η_{app} and as a function of the condensing electric power plant efficiency η_{cpp} (for η_{app} = 0.32).

We consider two variants of energy systems, each supplying the same electrical and thermal energy output. The first variant uses atomic electric power plants, condensing electric power plants, and gas-fired boilers (with outputs denoted by $N_{app,I}$, $N_{cpp,I}$, and $Q_{b,I}$ respectively); the second variant uses atomic electric power plants, condensing electric power plants, gas-fired boilers, and atomic heat supply plants (with outputs denoted by $N_{app,II}$, $N_{cpp,II}$, $Q_{b,II}$, and Q_{ahs} respectively). The nuclear fuel consumption is the same for both variants. Letting the yearly number of hours of use of maximum output be denoted by τ_{app}, τ_{cpp}, τ_{ahs}, and τ_b, we have the following system of equations:

$$\frac{\Delta N_{app}}{\eta_{app}}\tau_{app}=\frac{Q_{ahs}\tau_{ahs}}{\eta_{ahs}} \text{ (nuclear fuel balance);} \quad (1)$$

$$(N_{cpp,II}-N_{cpp,I})\tau_{cpp} =\Delta N_{app}\tau_{app} \text{ (electrical energy balance);} \quad (2)$$

$$(Q_{b,I}-Q_{b,II})\tau_b =Q_{ahs}\tau_{ahs} \text{ (heat energy balance),} \quad (3)$$

where $\Delta N_{app} = N_{app,I} - N_{app,II}$.

The thermal energy of the fuel W_I and W_{II} for the two variants is made up as follows:

$$W_I=W_{cpp,I}+W_{b,I}+W_{app,I} =\frac{N_{cpp,I}\tau_{cpp}}{\eta_{cpp}}+\frac{Q_{b,I}\tau_b}{\eta_b}+\frac{N_{app,I}\tau_{app}}{\eta_{app}};$$

Translated from Atomnaya Énergiya, Vol. 35, No. 3, pp. 197-198, September, 1973. Original article submitted November 27, 1972; revision submitted February 12, 1973.

$$W_{II} = W_{cpp,\,II} + W_{b,\,II} + W_{app,\,II} + W_{ahs}$$
$$= \frac{N_{cpp,\,II}\tau_{cpp}}{\eta_{cpp}} + \frac{Q_{b,\,II}\tau_b}{\eta_b}$$
$$+ \frac{N_{app\,II}\tau_{app}}{\eta_{app}} + \frac{Q_{ahs}\tau_{ahs}}{\eta_{ahs}}. \tag{4}$$

The annual savings in thermal energy ΔW and consumption of arbitrary fuel ΔG which are obtained by replacing atomic electric power plants by nuclear reactors are found from Eqs. (1)-(4):

$$\Delta W = W_I - W_{II} = 0.86 \cdot 10^{-3} \Delta N_{app}\tau_{app}\left(\frac{\eta_{ahs}}{\eta_b\,\eta_{app}} - \frac{1}{\eta_{cpp}}\right) \text{ Gcal/year;} \tag{5}$$

$$\Delta G = 0.123 \cdot 10^{-3} \Delta N_{app}\tau_{app}\left(\frac{\eta_{ahs}}{\eta_b\,\eta_{app}} - \frac{1}{\eta_{cpp}}\right) = G_{ahs}\left(\frac{\eta_{ahs}}{\eta_b} - \frac{\eta_{app}}{\eta_{cpp}}\right) \text{ tons of arb. fuel/yr,} \tag{6}$$

where ΔN_{app} is the electrical output in kW of the atomic electric power plants which are being replaced by atomic heat supply plants, and G_{ahs} is the annual consumption in tons of an arbitrary fuel which is equivalent to the quantity of nuclear fuel used by the atomic heat supply plants.

If we take $\eta_{ahs} = 0.97$, $\eta_{app} = 0.32$, $\eta_b = 0.9$, $\eta_{cpp} = 0.41$, and $\tau_{app} = 7000$ h/yr, then the annual saving of arbitrary fuel becomes $\Delta G = 0.8\Delta N_{app} = 0.3\ G_{ahs}$ tons/yr.

For example, if $\Delta N_{app} = 30$ million kW, the annual saving in organic fuel obtained by replacing thermal neutron atomic electric power plants by atomic heat supply plants amounts to 24 million tons of arbitrary fuel. The additional output of condensing power plants which can be introduced by using the fuel saved is determined by the equation

$$\Delta N = \frac{\Delta W \eta_{cpp}}{\tau_{cpp}} = \Delta N_{app}\frac{\tau_{app}}{\tau_{cpp}}\left(\frac{\eta_{cpp}\eta_{ahs}}{\eta_{app}\eta_b} - 1\right). \tag{7}$$

For $\tau_{app} = \tau_{cpp}$, and the values listed above for the efficiencies, $\Delta N = 0.38\Delta N_{app} = 11.4$ million kW. It is interesting to note (see Fig. 1) the significant increase in the efficiency of the condensing power plant (for example, due to MGDG) which occurs with such a redistribution in the employment of nuclear fuel. A certain reorganization of the atomic power engineering can therefore result in a substantial saving of organic fuel which is much greater than can be obtained by improving the thermodynamic efficiency of the atomic electric power plants. It should also be noted that because of the reduced parameters ($p < 60$ kg/cm^2, and $t < 200$°C) and the rather small unit output of the reactor, atomic heat supply plants can be quite safe, and can meet the requirements of urban location.

The wide-scale introduction of atomic heat supply plants, which are completely automated and require moderate investment for each unit of heat output from the reactors, makes it possible to improve the state of the atmospheric reservoir of cities. The question of the development of atomic power engineering can only be resolved on the basis of an engineering and economic analysis of the possible variants of the satisfaction of electrical energy and heat requirements, taking into account the structure of the additional electrical and heating loads, the stand-by reserves, and the operating regime of the generating plants. A preliminary analysis of the fuel–energy balance of Moscow showed that even if all heat and electric power plants were replaced by condensing electric power plants located far from the city and atomic heat supply plants, over-consumption of organic fuel would not result (given the same yield of electrical and thermal energy).

PERMISSIBILITY OF BOILING IN DOWNCOMERS OF A CIRCULATION LOOP OF A COOLING REACTOR

A. V. Bondarenko and M. E. Minashin

UDC 621.039.53

In boiling reactors of the channel type (Beloyarskaya and Bilibinskaya Atomic Electric Power Plants) in the boiling reactor vessels under normal operating conditions a nonboiling single-phase coolant flows in the conducting channels. However, for certain starting and emergency regimes it is difficult to guarantee the absence of temporary boiling of water in the downcomers of the circulation loop, especially if we take into account that heat is supplied on part of the downcomers. We must therefore solve the question of whether or not such boiling is generally permissible, and, if it is, under what conditions. The requirement that boilding not be permitted in the downcomers for all regimes can considerably complicate the schematic solution of the plant. The answer to the posed question is most important for reactors that are cooled by the natural circulation of the coolant, and having Π-shaped sections on the downcomers, which under adverse conditions can contribute to the buildup of vapor in the conducting channels and the stoppage of circulation.

Estimates of the possibility of the start of boiling in the downcomers as a result of the decrease in pressure were made in [1], where the conditions for the start of boiling in such regimes were determined, and the inadmissibility of the start of boiling in the downcomer was indicated if the velocity of the coolant in the downcomer is comparable with the velocity of advance of the vapor. However, no account was made for the features resulting from the existence of heating sections in the downcomers.

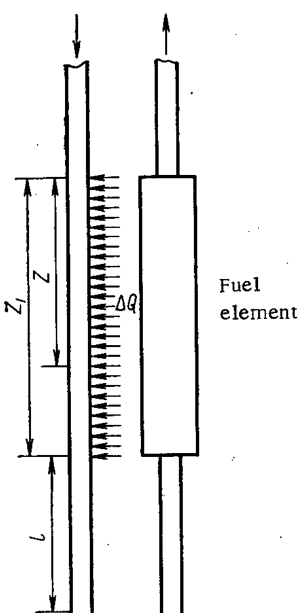

Fig. 1. Reference diagram.

In the present study we make an attempt, by using a calculation method, to estimate the possible criteria for the permissibility of boiling in the heating sections of the downcomers, including below the heating section in sufficiently long nonheating sections. The start of boiling in the downcomer depends on the rate of variation of water temperature at its input, the rate of pressure variation, the water velocity, the variation in heating, and the geometry of the channels.

There are great difficulties associated with the complete mathematical description of the process of the start of boiling in the reference diagram (see Fig. 1); therefore, for the heating section we assume a model of boiling with a variable velocity of water at the input to the section of constant length, initially filled with water at the saturation temperature or a steam–water mixture having steam content constant along the length, i.e., the thermal charge acts from the initial moment ($t = 0$). The dependence of the parameters of the water and of the vapor on the pressure, which varies along the height, can be neglected. Such a model enables us to obtain qualitative estimates for the case in which the boiling in the heating downcomer results from the oscillations of the thermal load for a practically constant pressure (this is correct when we can neglect the pressure variation) or when the boiling results from the pressure drop, but the length of the sections along the height are not very great and the heating on the heating sections is greater than the difference in saturation temperatures for the

Translated from Atomnaya Énergiya, Vol. 35, No. 3, pp. 198–200, September, 1973. Original article submitted February 7, 1972; revision submitted January 19, 1973.

pressure on the section and the pressure in the upper part of the loop (in the separator), i.e., boiling with a pressure drop occurs at first on the heating section. We take into account the effect of the variation in flow rate.

Taking these assumptions into account, the linearized system of equations of the law of conservation of energy and continuity in the case of small perturbations has the form

$$(\gamma'-\gamma'')\frac{\partial\Delta\varphi}{\partial\tau}-\gamma'\frac{\partial\Delta w'}{\partial z}+\varphi_0\left(\gamma'\frac{\partial\Delta w'}{\partial z}-\gamma''\frac{\partial\Delta w''}{\partial z}\right)+(\gamma' w_0'-\gamma'' w_0'')\frac{\partial\Delta\varphi}{\partial z}=0; \quad (1)$$

$$(\gamma' i'-\gamma'' i'')\frac{\partial\Delta\varphi}{\partial\tau}+\left(\gamma' i'\frac{\partial\Delta w'}{\partial z}-\gamma'' i''\frac{\partial\Delta w''}{\partial z}\right)\varphi_0-\gamma' i'\frac{\partial\Delta w'}{\partial z}+(\gamma' i' w_0'-\gamma'' i'' w_0'')\frac{\partial\Delta\varphi}{\partial z}=-\Delta Q. \quad (2)$$

If we assume that the mean velocity of the relative motion of the phases of a one-dimensional two-phase flow is determined by the type of liquid, the pressure, and the volume vapor-content, but depends weakly on the flow characteristics, then the relative velocity of the vapor can be expressed in terms of data on the slippage of the vapor during bubbling [2]. In such a case for motion through a downcomer:

$$w_{\text{rel}}=w''-w'=-\frac{a}{1-\varphi}, \quad (3)$$

where $a(p) = (0.65-0.0039p)(d/63)^{1/4}$ (30 mm < d < 240 mm is the hydraulic diameter, 11 abs. atm < p < 125 abs. atm is the pressure).

For deviation of the vapor velocity from the initial value

$$\Delta w''=\Delta w'-\frac{a\Delta\varphi}{(1-\varphi_0)^2}. \quad (4)$$

Using this model for $\Delta w''$, we pose the problem. For transfer functions of the variation of vapor content, the velocities of the aqueous and vapor phases for variation of velocity at the input and heat supply on the heating part of the downcomer, the solution using the method of Laplace transformations of Eqs. (1), (2), and (4), for initial values of the coolant parameters that are independent of the coordinates, is expressed in the following manner.

A. Heating section

$$\Delta\varphi_1(s,z)=\frac{\Delta\bar{Q}(s)[\gamma'-\varphi_0(\gamma'-\gamma'')]}{s\gamma'\gamma'' r}\left(1-e^{-\frac{sz}{w_0''}}\right); \quad (5)$$

$$\Delta w_1'(s,z)=\Delta w'_{\text{in}}(s)+\frac{(\gamma'-\gamma'')}{\gamma'\gamma'' r}\Delta\bar{Q}(s)z$$

$$+\frac{a}{1-\varphi_0}\left(1+\frac{\gamma''}{\gamma'}\frac{\varphi_0}{1-\varphi_0}\right)\frac{1}{s}\frac{\Delta\bar{Q}(s)}{\gamma'' r}\left(1-e^{-\frac{sz}{w_0''}}\right); \quad (6)$$

$$\Delta w_1''(s,z)=\Delta w'_{\text{in}}(s)+\frac{(\gamma'-\gamma'')}{\gamma'\gamma'' r}\Delta\bar{Q}(s)z. \quad (7)$$

B. Nonheating section below boiling

$$\Delta\varphi_2(s,l)=\Delta\varphi_1(s,z_1)e^{\frac{-sl}{w_0''}}; \quad (8)$$

$$\Delta w_2'(s,l)=\Delta w_1'(s,z_1)-\frac{a}{(1-\varphi_0)^2}\Delta\varphi_1(s,z_1)\left(1-e^{-\frac{sl}{w_0''}}\right); \quad (9)$$

$$\Delta w_2''(s,l)=\Delta w_1'(s,z_1)-\frac{a}{(1-\varphi_0)^2}\Delta\varphi_1(s,z_1)$$

$$=\Delta w'_{\text{in}}(s)+\frac{(\gamma'-\gamma'')}{\gamma'\gamma'' r}\Delta\bar{Q}(s)z_1. \quad (10)$$

The transfer function (7) shows that on the boiling section with increasing coordinate there is an increase in the velocity of the vapor phase for increasing heat supply and velocity of the aqueous phase (6), with the buoyancy of the vapor leading to an additional increase in the velocity of the aqueous phase. The time characteristics of this additional increase are characterized by a delay time, determined by the velocity of motion of the vapor.

On the section of the downcomer below the heating zone (9), (10) for increase in vapor content at the input to this section there is observed a slowing of the aqueous and vapor phases relative to the velocity of the aqueous phase at the output of the heating zone. For the aqueous phase the slowing occurs during the variation of the vapor content at the output of the heating zone and over the time interval following this, equal to the time of flow of the vapor along the nonheating section. For the vapor phase the slowing is determined by the increase in vapor content at the output of the heating zone at the given moment of time. However, if we substitute (5) and (6) for $z = z_1$ into (10), i.e., if we find the transfer function of the variation of vapor velocity on the nonheating section from the variation of the water velocity at the input to the heating section and the heat supply to it, we obtain an expression [the second half of Eq. (10)], showing the acceleration of the vapor on the nonheating section relative to the water velocity at the input to the heating section. The decrease in velocity of the vapor phase does not exceed the decrease in velocity of the water if it occurs at the input to the heating section.

Thus, in dynamic regimes related to the start of boiling in downcomers, over the entire length of the heating and occurring below the nonheating parts, the minimum velocity of motion of the vapor is observed at the input to the heating section, which is correct near the point of the start of boiling.

In order to maintain normal circulation and to prevent dangerous results due to the stoppage of the vapor and its subsequent buildup, the water velocity at the input to the downcomer, where the start of boiling is possible, should not be reduced in value close to the value of the slippage factor.

Results of an experimental study of accident regimes of the Bilibinskaya Atomic Electric Power Plant on a specialized stand gave qualitative estimates, which allow us to assume the above condition relative to the velocity at the input to the section with the start of boiling necessary for elimination of the dangerous consequences of boiling of the coolant in the downcomers for nonstationary regimes. In order to refine our results it is necessary to formulate special experiments.

LITERATURE CITED

1. A. Ya. Kramerov and Ya. V. Shevelev, Engineering Calculations of Nuclear Reactors [in Russian], Atomizdat, Moscow (1964), p. 471.
2. A. Ya. Kramerov and Ya. V. Shevelev, ibid., p. 321.

OPTIMAL EQUALIZING OF THE HEAT RELEASE OVER THE REACTOR VOLUME

T. S. Zaritskaya and A. P. Rudik

UDC 621.039.51

A number of problems have recently been solved, using the maximum principle of L. S. Pontryagin [1-9]. In the present paper, still another problem is solved: that of the optimal equalizing of the heat release over the reactor volume.

The problem is formulated as follows. We have a reactor of given power without a reflector, in which it is possible to redistribute the nuclear fuel over the reactor volume (neglecting the depth of depletion). It is thus required to distribute the nuclear fuel so that the standard deviation of the heat release over the reactor volume will be a minimum. We consider the simplest mathematical model: a single group of neutrons, a linear dependence of the Laplacian on the nuclear-fuel concentration, and a one-dimensional reactor without a reflector. The geometry of the reactor is: the center at z = 0, and the boundary at z = H.

The initial equations has the usual form [10]

$$\frac{d^2N}{dz^2}+[U(z)-\bar{U}]N=0, \tag{1}$$

where N is the thermal-neutron density; U(z) is the "control" (as assumed in [5]), proportional to the concentration of the nuclear fuel; U is constant. The control U(z) must be satisfied by the following constraints:

$$U_{\min}\leqslant U(z)\leqslant U_{\max}. \tag{2}$$

The total power of the reactor $\overline{W}$ is assumed given:

$$W=\int_0^H U(z)N(z)\,dz. \tag{3}$$

Furthermore, it is possible for the following thermotechnical constraint to exist:

$$P(z)=U(z)N(z)-D\leqslant 0, \tag{4}$$

where D is a given constant (or a function of the coordinate z).

We must select U(z) such that the functional $\mathcal{J}$ attains a minimum:

$$\mathcal{J}=\int_0^H\left[U(z)N(z)-\frac{W}{H}\right]^2 dz. \tag{5}$$

Taking account of the condition (3) we transform the functional (5) to the form

$$\mathcal{J}=\int_0^H U^2(z)N^2(z)\,dz-\frac{W^2}{H}. \tag{6}$$

The canonical system of equations corresponding to expressions (1)-(6) has the form [5]

$$\frac{dx^{(0)}}{dz}=U^2[x^{(1)}]^2;\quad \frac{dx^{(1)}}{dz}=x^{(2)};$$

Translated from Atomnaya Énergiya, Vol. 35, No. 3, pp. 200-202, September, 1973. Original article submitted July 21, 1972.

$$\frac{dx^{(2)}}{dz}=-[U-\tilde{U}]\,x^{(1)};\quad \frac{dx^{(3)}}{dz}=1;\quad \frac{dx^{(4)}}{dz}=Ux^{(1)}. \tag{7}$$

Here $x^{(1)} \equiv N$; $x^{(2)} \equiv dN/dz$; $x^{(0)}$ is related to the functional to be minimized; $x^{(3)}$ takes into account that the dimension of the reactor is given; $x^{(4)}$ corresponds to the condition (3). The system (7) corresponds to the Hamiltonian $\mathscr{H}$:

$$\mathscr{H}=\psi_0U^2\,(x^{(1)})^2+\psi_1x^{(2)}-\psi_2\,(U-\tilde{U})\;x^{(1)}+\psi_3+\psi_4Ux^{(1)}. \tag{8}$$

The adjoint functions ψ_i are satisfied by the following equations [under the assumption that the absolute inequality in the expression (4) is satisfied]:

$$\frac{d\psi_i}{dz}=-\frac{\partial\mathscr{H}}{\partial x^{(i)}};\quad \frac{d\psi_1}{dz}=-2\psi_0U^2x^{(1)}+\psi_2\;(U-\tilde{U})-\psi_4U;\quad \frac{d\psi_2}{dz}=-\psi_1. \tag{9}$$

Here the function $\psi_0 = -1$, and the functions ψ_3 and ψ_4 are constants, the values of which are determined from the solution of the optimization problem. The equations for the function ψ_2 can conveniently be transformed to a form similar to the form of Eq. (1):

$$\frac{d^2\psi_2}{dz^2}+[U-\tilde{U}]\,\psi_2=2\psi_0U^2x^{(1)}+\psi_4U. \tag{10}$$

The phase variables $x^{(i)}$ are satisfied by the usual boundary conditions, and the adjoint functions ψ_i are satisfied by the boundary conditions generated from the transversality principle [5]:

$$\left.\begin{aligned}&\psi_1\,(0)=0;\; x^{(2)}\,(0)=0;\; x^{(3)}\,(0)=0;\; x^{(4)}\,(0)=0;\\ &x^{(1)}\,(H)=0;\; \psi_2\,(H)=0;\; x^{(3)}\,H=H;\; x^{(4)}\,(H)=W.\end{aligned}\right\} \tag{11}$$

To solve the problem we assume that constraints (2) and (4) are absent. Then it is obvious that the optimal solution will be the classical control $U_0(z)$, which is obtained from the condition

$$\frac{\partial\mathscr{H}}{\partial U}=2\psi_0U_0\,[x^{(1)}]^2-[\psi_2-\psi_4]\;x^{(1)}=0, \tag{12}$$

which leads to the relations

$$U_0x^{(1)}=\frac{\psi_2-\psi_4}{2\psi_0};\quad U_0=\frac{\psi_2-\psi_4}{2\psi_0x^{(1)}}. \tag{13}$$

We note that for $U(z) = U_0$ the maximum of the Hamiltonian $\mathscr{H}$ is actually attained as a function of U, since

$$\frac{\partial^2\mathscr{H}}{\partial U^2}=2\psi_0\,[x^{(1)}]^2<0. \tag{14}$$

To determine $U_0(z)$ and $x^{(1)}(z)$ we must find ψ_2. Substituting U_0 from (13) into expression (10), we obtain

$$\frac{d^2\psi_2}{dz^2}-\tilde{U}\psi_2=0. \tag{15}$$

Taking account of Eq. (9) and the boundary conditions (11) for ψ_1 and ψ_2, we arrive at a conclusion; if the control $U_0(z)$ holds for the entire reactor, then

$$\psi_1\,(z)=\psi_2\,(z)=0. \tag{16}$$

Then from Eqs. (13) we have

$$x^{(1)}\,(z)\,U_0\,(z)=-\frac{\psi_4}{2\psi_0}=\lambda, \tag{17}$$

where λ is some positive-definite constant, whose numerical value is determined from the condition (3):

$$\lambda=\frac{W}{H}. \tag{18}$$

We should note that the functional to be minimized (5) [or (6)] vanishes.

A basic feature of the considered problem without the constraints (2) and (4) is that the solution is determined within the framework of classical calculus of variations [see Eqs. (12) and (14)] and that the obtained optimal control (17) corresponds to a constant heat release over the entire reactor volume.

We note that in the problem under consideration the constant heat release corresponds to the realization of the classical control (13), whereas in the problem on the minimum of the critical dimensions [2] the constant heat release is a consequence of the thermotechnical constraint (4).

We introduce into the consideration the constraint (2). Then the solution (17) will contradict this constraint, since

$$U_0\,(z\to H)=\frac{\lambda}{x^{(1)}\,(z\to H)}\to\infty. \tag{19}$$

From physical considerations and from experience in using the Pontryagin maximum principle [1-4] it is obvious that for the presence of constraints (2) we can expect that the optimal arrangement is two-zone: a central zone $U(z) = U_0(z)$, $0 \le z \le h$, and a peripheral zone $U(z) = U_{max}$, $h \le z \le H$.

We can also present mathematical reasons that indicate that the two-zone arrangement is optimal. To do this we consider in the Hamiltonian (8) terms that depend on the control. Taking into account that as $z \to H$ the functions $x^{(1)}(H)$ and ψ_2 (H(approach zero, we obtain that the principal term in the Hamiltonian $\mathscr{H}$ will be $\psi_4 U x^{(1)}$. However, according to Eqs. (17) and (18), the constant ψ_4 is positive; hence, on the boundary of the reactor there must be a zone with $U(z \to H) = U_{max}$.

We verify the proposed two-zone arrangement for optimality. To simplify the calculations we introduce an assumption that is insignificant in principle: that the constant $\tilde{U}$, which appears in the Laplacian (1), equals zero. Then, in the central zone, owing to the condition $\tilde{\psi}_1(0) = 0$ in agreement with (9), (15) we obtain $\psi_2(z) = \text{const}$ and $x^{(1)}(z)U(z)$ again equals the constant $\tilde{\lambda}$ [although the value of $\tilde{\lambda}$ is now different from that in (18)]. Denoting $U_{max} \equiv \alpha^2$ and $\delta = h/H$, taking account of the continuity of the control for $z = h$ we obtain

$$
\begin{gathered}
U_0(h-\varepsilon)=U_{max};\\
0 \leqslant z \leqslant h;\ x^{(1)}(z)=\\
=\frac{\tilde{\lambda}H^2}{\alpha^2H^2}\left\{1+\frac{\alpha^2H^2\delta^2}{2}-\frac{\alpha^2H^2}{2}\cdot\frac{z^2}{H^2}\right\};\\
x^{(1)}U_0(z)=\tilde{\lambda};\\
h \leqslant z \leqslant H;\ x^{(1)}z=\frac{\tilde{\lambda}H^2}{\alpha^2H^2}\sqrt{1+\alpha^2H^2\delta^2}\sin\alpha H\,(1-z/H);\\
U(z)=U_{max}=\alpha^2.
\end{gathered}
\tag{20}
$$

The ratio δ is determined from the criticality equation:

$$\operatorname{tg}\alpha H\,(1-\delta)=\frac{1}{\alpha H\delta}. \tag{21}$$

From Eq. (3) we obtain the constant $\tilde{\lambda}$:

$$\tilde{\lambda}=\frac{W}{H}\cdot\frac{\alpha H}{\sqrt{1+\alpha^2H^2\delta^2}}. \tag{22}$$

Using (20) and (22), we determine the value of the functional I to be minimized, and from (6) we obtain

$$\frac{IH}{W^2}=\frac{1}{2}\cdot\frac{\alpha^2H^2}{(1+\alpha^2H^2\delta^2)}[1+\alpha^2H^2\delta^2(1-\delta)]-1. \tag{23}$$

To estimate the order of the effect we carried out calculations based on Eq. (23) for $\alpha H = 2.32$, obtaining the following values: $\delta = 0.785$; $IH/W^2 = 0.06$. We note that for the case of uniform distribution of fuel over the reactor volume $IH/W^2 = (\pi^2/8)-1 = 0.24$, i.e., optimization leads to a decrease in the quadratic deviation (6) by a factor of four.

In conclusion we consider the case in which the constraint (4) is significant. We expect that the optimal arrangement will be three-zone: a central zone $0 \le z \le h_1$, $U(z) = D/x^{(1)}$; an intermediate zone $h_1 \le z \le h_2$, $U(z) = U_0(z)$; and a peripheral zone $h_2 \le z \le H$, $U(z) = U_{max}$. We note that in this case the classical control $U_0(z)$ is determined from the general equation (13), and even if $U = 0$, from (15), generally speaking, we do not obtain $\psi_2 = \text{const}$, i.e., $U_0(z)x^{(1)}(z) \ne \text{const}$. For the calculations we assumed that the specific form of a classical control can depend on the general nature both of the arrangement and also of the entire reactor.

The authors thank B. I. Il'ichev for a discussion of the results.

LITERATURE CITED

1. B. P. Kochurov, At. Énerg., 20, 243 (1966).
2. T. S. Zaritskaya and A. P. Rudik, At. Énerg., 22, 6 (1967).
3. T. S. Zaritskaya and A. P. Rudik, At. Énerg., 23, 218 (1967).
4. B. P. Kochurov and A. P. Rudik, At. Énerg., 22, 40 (1967).
5. L. S. Pontryagin et al., Mathematical Theory of Optimal Processes [in Russian], Fizmatgiz, Moscow (1961).
6. M. Melice, Nucl. Sci. and Engng., 37, 451 (1969).

7. D. Wade and W. Terney, Nucl. Sci. and Engng., 45, 199 (1971).
8. W. Terney, ibid., p. 226.
9. R. Koga et al., Nucl. Sci. Technol., 8, 267 (1971).
10. A. D. Galanin, Theory of Nuclear Reactors Using Thermal Neutrons [in Russian], Atomizdat, Moscow (1959).

THE SOLUBILITIES OF TITANIUM ALLOYS AND ALLOY STEELS IN LIQUID INDIUM AND LIQUID INDIUM–GALLIUM ALLOY

D. M. Zakharov, S. P. Yatsenko, G. I. Kiknadze, L. V. Mel'nikova, É. N. Dieva, and É. P. Danelyan

UDC 669.295.018:669.87

To create radiation loops it is necessary to study the compatibility of the most promising constructional materials with liquid-metal gamma-carriers in the form of indium and indium–gallium alloy. In this connection we investigated the solubilities of constructional materials in liquid indium and in indium–gallium eutectic (20.5 wt. % indium) at 350°C in static experimental conditions. We used commercial VT1-1 titanium with a single-phase α-structure, two-phase $\alpha + \beta$ titanium alloys VT6 and VT14, containing the beta-stabilizers V and Mo, and steels of the classes 1Kh18N10T (austenitic), 0Kh21N6M2T (ferrite-austenitic), and Kh25 (ferrite) classes. The gallium and indium were of high purity (total determined impurities $\leq 5 \cdot 10^{-4}$ wt. %). Specimens of the constructional materials were polished and carefully prepared for testing in the form of cylinders 1.5 mm in diameter or rectangular plates 1 mm thick; they were placed in separate quartz capsules filled with the appropriate melt. They were kept at constant temperature (±5°C) with free access of air to the surface of the liquid metal, which had a volume-to-surface ratio of V/S = 2 or 4 cm. The concentrations of titanium, iron, and nickel in the indium and indium–gallium melts were determined by the photocolorimetric method [1], the sensitivity of which was $5 \cdot 10^{-5}$ for titanium, $2 \cdot 10^{-5}$ for iron, and $3 \cdot 10^{-6}$ wt. % for nickel.

The constructional materials for the tests were not subjected to any special heat treatment. However, some of the titanium alloy specimens were passivated in air at 550°C for 250 h. Prolonged low-temperature oxidation of titanium gives an oxide film on the surface consisting of TiO_2 with the rutile structure, which prevents rapid penetration of oxygen into the metal, which is undesirable owing to the possibility of embrittlement. In the given passivation conditions the thickness of the oxide film does not exceed a few hundred Ångstroms [2], so that we can neglect the changes in the surface areas of the titanium specimens during oxidation. It has been shown [3] that an oxide film of TiO_2 can block the formation of intermetallic compounds on the surface of VT1-1 titanium in contact with an indium–germanium alloy. The

TABLE 1. Concentrations of Titanium in Liquid Metals and Corrosion Rates of Titanium Alloys

Liquid metal	$C\times10^2/K\times10^6$*						Test duration, h
	Nonpassivated specimens			Passivated specimens			
	VT1-1, V/S = 2	VT6, V/S = 4	VT14, V/S = 4	VT1-1, V/S = 2	VT6, V/S = 4	VT14, V/S = 4	
Indium–gallium alloy	0.8/5,6	0.43/6,0	0.38/5,3	0.03/0.21	0.38/5.3	0.29/4.1	400
Indium	0.067/4,4	0.03/3,8	0.014/1.8	0.026/1.7	0.015/1.9	0.028/3.7	50

*Here and in Table 2, the numerator represents the concentration of solute element in wt. %, and the denominator represents the corrosion rate in mm/h.

Translated from Atomnaya Énergiya, Vol. 35, No. 3, pp. 202–204, September, 1973. Original article submitted November 13, 1972.

TABLE 2. Concentrations of Iron and Nickel in Indium–Gallium Alloy and Rate of Corrosion of Steel Specimens

Test duration, h	$C \times 10^2/K \times 10^6$		
	1Kh18N10T $V/S = 4$	0Kh21N6M2T $V/S = 2$	Kh25 $V/S = 2$
100	1,2 (Fe); 1,4 (Ni) / 77	0,3 (Fe); 0,24 (Ni) / 8,2	0,1 (Fe); 0,005 (Ni) / 3,2

influence of the oxide film on the other, equally important aspect of the corrosion process, namely the solubility of titanium, has not been previously studied. Our present experimental results are listed in Table 1. The corrosion rate was calculated by means of the formula $K = 0.1(V/S)(d_1/d_2)(C/t)$, where K is the corrosion rate in mm/h, d_1 and d_2 are the densities of the liquid metal and the metal solute, C is the concentration of solute metal in wt. %, and t is the test duration in hours. By a well-known method [1] we previously determined the limiting solubility of titanium in liquid indium and in indium–gallium alloy at 350°C: the results were respectively $1.7 \cdot 10^{-2}$ and $1.2 \cdot 10^{-2}$ wt. %. From Table 1 we see that the concentration of titanium in the melt is less than its limiting solubility.

In liquid indium the corrosion rates of the titanium alloys were practically independent of the passivation: the corrosion rates of all the specimens were comparable. In indium–gallium alloy, the corrosion rates of the nonpassivated specimens of VT1-1, VT6, and VT14 were also practically the same. Passivation has an appreciable effect only on the corrosion rate of VT1-1 titanium, and reduces it by a factor of about 25; however, it has no effect on the corrosion rates of VT6 and VT14. In this connection, at present we can make only some qualitative suggestions. In particular, alloyed titanium alloys oxidize more slowly than commercial titanium. Furthermore, the quality of the oxide film (strength, density, and adhesiveness) can be impaired by the complexity of its composition owing to the selective oxidation of the alloying elements. We must also take account of the thermodynamic possibility of reduction of rutile by aluminum, which may promote disruption of the oxide film. In the scale of corrosion stability [2], titanium alloys, which have a corrosion rate of $K \leq 10^{-5}$ mm/h, belong to the class of stable materials. All the grades of alloy used agree with this condition. However, the data on the concentration of titanium in the melt give an adequate characterization only of the solubility of commercial titanium VT1-1. The solution of alloys VT6 and VT14 is more complex owing to the possibility of diffusion of atoms of alloying elements in the melt. Thus the concentration of aluminum in liquid indium (after 50 h of keeping VT6 and VT14 specimens at 350°C) is about $0.2 \cdot 10^{-2}$ wt. %, which is greater than the concentration of dissolved titanium in the same test time (Table 1). We also found that aluminum is capable of selective solution in indium regardless of whether or not the titanium specimen is passivated. The concentration of aluminum in the indium–gallium alloys was not determined. However, we can expect that it is even higher in the alloy, because the solubility of aluminum in gallium at 350°C is greater than that of aluminum in indium. These results show that VT1-1 commercial titanium has several advantages in comparison with titanium alloys: it is "not contaminated" by the liquid aluminum, and besides, passivation of VT1-1 titanium can sharply reduce its solubility in indium–gallium alloy. This information permits us to correctly orient ourselves with regard to the properties of titanium alloys for the creation of radiation loops. However, a final estimate of the compatibility of titanium-based constructional materials with liquid-metal gamma-carriers can be obtained only by prolonged corrosion tests.

Table 2 lists data on the solubilities of alloy steels in indium–gallium alloy at 350°C. We did not study the solubilities of the components of the steel at times exceeding 100 h, because more prolonged contact of the specimens with the indium–gallium alloy at 350°C leads to rapid formation of brittle intermetallic compounds on their surfaces, which can easily break up and get into the alloy [3]. In this case the

TABLE 3. Concentrations of Iron and Nickel in Liquid Indium and Corrosion Rates of Steel Specimens

Time, h	Iron and nickel concentrations, $C \cdot 10^2$ wt. %			Corrosion rate, $K \cdot 10^{-7}$, mm/h		
	1Kh18N10T $V/S = 2$	0Kh21N6M2T $V/S = 2$	Kh25 $V/S = 4$	1Kh18N · 10T	0Kh21N6 · M2T	Kh25
5	0,021 (Fe) 0,05 (Ni)	0,18 (Fe) 0,01 (Ni)	0,14 (Fe) 0,005 (Ni)			
100	0,048 (Fe) 0,06 (Ni)	0 2 (Fe) 0,03 (Ni)	0,14 (Fe) 0,005 (Ni)			
1750	0,7 (Fe)	0,46 (Fe)	0,27 (Fe)	7,4	4,8	6,0
3500/	Not determined	0,6 (Fe)	0,35 (Fe)	—	3,0	3,7

solubilities of the components of the steel in the liquid metal will be too high. Table 2 shows that as the chromium content of the steel is increased, the corrosion rate due to the solubilities of the main components (iron and nickel) decreases. A similar phenomenon was observed in a study [4] of the compatibilities of alloy steels with liquid indium–gallium–tin alloy. Appreciable solubility of chromium itself in the melts was not observed. The beneficial influence of chromium on the stabilities of alloy steels is apparently due to the presence of the oxide of trivalent chromium in the surface film, at a concentration which rises with the total chromium content of the steel. The thickness of the protective film on the surface of stainless steel is usually only a few tens of Ångstroms; further increase in the oxide film thickness is undesirable owing to the formation of internal stresses which reduce its protective capacity [5].

According to the solubility data, the stabilities of the grades of steel investigated in indium–gallium alloy are fairly high. Thus on a five-point scale of stability [6] steels Kh25 and 0Kh21N6M2T are very stable ($K < 10^{-5}$ mm/h) and steel 1Kh18N10T is of stability suitable for constructional materials ($K = 10^{-5}$–10^{-4} mm/h). On the other hand, steels cannot work in contact with indium–gallium and indium–gallium–tin alloys at 350°C owing to rapid formation of intermetallic compounds on the surface [3,4]. Thus the temperature range of compatibility of alloy steels with indium–gallium alloys is limited by the rates of the processes governing the formation of intermetallic compounds on the surface of the constructional material. Data on the solubilities of steel specimens in liquid indium at 350°C are given in Table 3.

The nickel concentration in indium melts, corresponding to 100 h of isothermal holding of the specimens, is steady. The results, in Table 3, show that the influence of chromium on the stability of steel in liquid indium is not as definite as for indium–gallium alloy used as a liquid metal medium. At the same time the low corrosion rates in liquid indium show that all the grades of steel examined are in the very stable class. They apparently show promise as constructional materials for work in contact with liquid indium at high temperatures, since, in the first place, the solubilities of the main components of the steel in liquid indium are low, and, in the second place, the phase diagram of the system Fe–In [7] does not contain intermetallic compounds and shows negligible solubility of indium in solid iron – this is very important. In this respect the alloy system Fe–In differs to advantage from the systems Fe–Ga, Ti–Ga, and Ti–In, in which there are a whole group of intermetallic compounds. Thus we can expect that when steel interacts with liquid indium, the processes occurring on its surface will not have an appreciable influence on the corrosion rate, which is mainly limited by the process of solution of the components of the steel in liquid indium. Among the grades of steel considered, the greatest practical interest is presented by the austenitic steel 1Kh18N10T, because its technological properties are preferable.

LITERATURE CITED

1. S. P. Yatsenko and Yu. A. Anikin, Izv. Akad. Nauk SSSR, Metally, No. 4, 162 (1970).
2. A. S. Bai, D. I. Lainer, E. N. Slesareva, and M. I. Tsypin, Oxidation of Titanium and Its Alloys [in Russian], Metallurgiya, Moscow (1970).
3. G. I. Kiknadze, D. M. Zakharov, and L. V. Mel'nikova, At. Énerg., 19, No. 2, 177 (1965).
4. S. P. Yatsenko, V. I. Kononenko, V. N. Danilin, and E. P. Druzhinina, "Properties of gallium in aqueous solutions and melts," Tr. In-ta Khimii, Sverdlovsk, UFAN SSSR, No. 2, 122 (1966).
5. A. A. Babakov, Stainless Steels [in Russian], Goskhimizdat, Moscow (1956).
6. D. G. Tufanov, Corrosion Resistance of Stainless Steels: Handbook [in Russian], Metallurgizdat, Moscow (1963).
7. N. V. Ageev (editor), Phase Diagrams of Metallic Systems, No. 13, Izd. VINITI, Moscow (1969).

POSSIBLE USE OF Sn^{119m} SOURCES IN GAMMA RAY SAMPLING OF MOLYBDENUM ORES

A. P. Ochkur, E. P. Leman,
V. V. Kotel'nikov, V. M. Ivanov,
and Yu. P. Yanshevskii

UDC 550.835

A method for detecting tin in powder samples which is currently being widely used makes use of nuclear resonance fluorescence excited by an Sn^{119m} Mossbauer source emitting 23.8 keV photons. This source can also be used successfully in the x-ray analysis of many ores and of the products resulting from their processing [1]. The Sn^{119m} photons most effectively excite the characteristic 17.5 keV K-radiation of molybdenum, whose K absorption edge is at 20.0 keV.

The dimensions of Mossbauer sources make it difficult to use them in x-ray sampling detectors, and so a special Sn^{119m} source was prepared in a cylindrical aluminum ampule 5 mm in diameter and 3 mm high. The activity of the source was from 1 to 20 mCi. It was intended for use in the "Mineral-4", BRA-6, RPS4-01, "Gagara", and RRShA-1 types of x-ray apparatus for the analysis of powder samples and for ore sampling at the site of occurrence (in mine development walls and boreholes). The possibility of detecting molybdenum was studied with models of molybdenum ores. Figure 1a shows the secondary spectrum measured for these models, using a 5 mCi Sn^{119m} source. A "Mineral-4" apparatus was used in making the measurements, which were made in a wide solid angle without collimating the radiation. An SRPO-12 xenon proportional counter with 16% resolution at the 23.8 keV line was used as the detector. It is clear from the figure that the analytic molybdenum line and the peak corresponding to single scattering of the source radiation are completely resolved. The background of scattered radiation in the region of the analytic line is therefore quite small, and a change in the molybdenum concentration from 0 to 1% causes the counting rate to increase by a factor of thirty. If the method of spectral ratios is used in making the measurements, and the single scattering peak is chosen as an internal standard of the background, the analytic plot (see Figure 1b) turns out to be linear all the way up to 10-15% of molybdenum, and the measured value of the spectral ratio η/η_0 increases by a factor of forty as the molybdenum concentration increases from 0 to 1%. The threshold of sensitivity of the method for detecting molybdenum with a Sn^{119m} source is 0.005%. An analogous measurement technique, using a Cd^{109} source, provides a threshold of sensitivity to the molybdenum content which is from 0.01 to 0.02%, with an analytic plot which is nonlinear [2,3]. This is explained by the fact that when an Sn^{119m} source is used, the analytic 17.5 keV K-line of molybdenum and the peak corresponding to the singly scattered 22 keV radiation are completely separated by the detector, while the singly scattered quanta of the 20

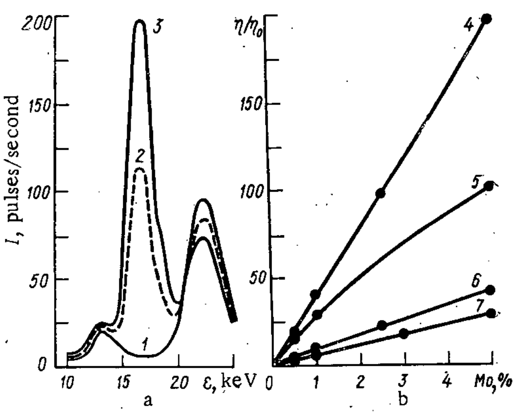

Fig. 1. Use of an Sn^{119m} source in the analysis of molybdenum ores. a) Secondary γ-spectra obtained for models of ores with various contents of molybdenum: 1) 0%; 2) 0.5%; 3) 1.0%. b) Analytic plots obtained for models of ores, using as a source Sn^{119m} (4, 6), Cd^{109} (5), and Tm^{170} (BaO) (7), detecting the secondary radiation with proportional (4, 5) and scintillation (6, 7) counters.

Translated from Atomnaya Énergiya, Vol. 35, No. 3, pp. 204-205, September, 1973. Original article submitted December 13, 1972; revision submitted March 13, 1973.

keV Cd^{109} source create a considerable background in the region of the analytic molybdenum line (because of the finite resolution of the detector).

The threshold of sensitivity is only 0.03 to 0.05% for other sources, such as Pm^{147} (38 keV) and S^{35} (32 keV).

A source on the basis of Sn^{119m} also is best in connection with recording the secondary spectrum by a scintillation detector. Figure 1b shows the curves obtained when the radiation is detected with a scintillation counter consisting of an FÉU-35 with an NaI (Tl) crystal 18 mm in diameter and 2 mm high with a lithium fluoride reflector and a beryllium end-window. The method of measurement and apparatus are the same as those used with a proportional counter. Results obtained [3] with a Tm^{170} source and a secondary BaO target under similar conditions of measurement are shown in Fig. 1b for comparison. It is clear that the Sn^{119m} source ensures the linearity of the analytic plots and maximum sensitivity to molybdenum content even when scintillation detectors are used.

It should also be noted that Sn^{119m} has an advantage over other sources (except for Cd^{109}) in testing molybdenum ores in that it enables one to detect other elements acompanying the molybdenum; i.e., copper (by the K-series) and tungsten (by the L-series).

LITERATURE CITED

1. G. L. Zhuravlev et al., "Possible application of Sn^{119m} sources in x-ray analysis" [in Russian], Proceedings of the Eighth Conference of Young Scientists of the All-Union Scientific Research Institute of Mineral Raw Materials, Part 2, published by the Department of Scientific and Technical Information, All-Union Scientific Research Institute of Mineral Raw Materials (Izd. ONTI VIMS), Moscow (1970), pp. 52-56.
2. E. P. Leman, N. G. Bolotova, and V. V. Kotel'nikov, "X-ray sampling of molybdenum ores in mine workings," Izv. Vuz. SSSR, Gornyi Zh., No. 11, pp. 3-7 (1971).
3. V. S. Nakhabtsev, V. A. Meier, and G. A. Pshenichnyi, "The conditions for detecting molybdenum with various radiation sources and radiation detectors as applied to the problem of using radioisotopes in logging by the x-ray fluorescence method," Uchenye Zapiski LGU, No. 361, Ser. Fiz. i Geol. Nauk, No. 21, pp. 56-62 (1971).
4. V. S. Nakhabtsev, V. A. Meier, and Yu. S. Medvedev, "Selection of optimum conditions for excitation and detection with scintillation counters of the x-ray fluorescence of molybdenum," Uchenye Zapiski LGU, No. 366, Ser. Fiz. i Geol. Nauk, No. 22, 82-89 (1972).

CHARACTERISTICS OF THE CALCULATION OF IDEAL CASCADES WITH ARBITRARY ENRICHMENT PER STAGE

N. I. Laguntsov

UDC 621.039.31

In [1, 2] we considered the theory of the construction of symmetric and asymmetric two-component cascades with arbitrary enrichment $c^+ - c = \delta^+ = f(c, \theta)$ on each separation stage. In principle, the equations obtained in this study are sufficient for determining all the parameters of the cascade. In addition, we can estimate in advance the overall characteristics of the cascade [3]. However, the calculations may involve difficulties owing to the fact that in one of the stages the value of the flow division coefficient θ, as has already been mentioned in [1], is selected arbitrarily. As a result of this, there exists a family of ideal cascades from which we must select the optimal one. In addition, since the enrichment function depends on θ, the convergence of the calculations will depend substantially on the direction of the count, i.e., from waste end to product end or vice versa. In the particular case in which δ^+ depends only on the concentration c (the case considered by Cohen [4]), the calculation of the ideal cascade is unique.

In the present study we consider the above-mentioned characteristics of the calculation and give a criterion for the choice of the optimum value of the flow division coefficient.

For the sake of simplicity, we shall consider the case of a symmetric cascade whose parameters are described by the following system of equations [1]:

$$c_{i+1} - c_i = f(c_i, \theta_i); \tag{1}$$

$$\theta_i = \frac{c_i - c_{i-1}}{c_{i+1} - c_{i-1}}; \tag{2}$$

$$L_i = \frac{P(c_p - c_i)}{\theta_i f(c_i, \theta_i)}. \tag{3}$$

In this system it is sufficient to have the first two equations, (1) and (2), for the calculation of c_i and θ_i. Making use of the criterion of non-mixing, we transform (2) to the form

$$\frac{\theta_i}{1-\theta_i} \delta^+(c_i, \theta_i) = \delta^-(c_i, \theta_i) = \delta^+(c_{i-1}, \theta_{i-1}). \tag{4}$$

In the cases in which the static coefficient of separation α_0 is not very large ($\alpha_0 < 2$), the concentration will change little, and therefore when we investigate the process, we may take $c_{i-1} \approx c_i$ in formula (4), i.e., the concentration will appear in (4) only as a parameter. This enables us to make the change from the system (1), (2) to a single equation in θ:

$$\delta^-(\theta_i) = \delta^+(\theta_{i-1}). \tag{5}$$

Formally, from the mathematical point of view, the solution of Eq. (5) can be treated as an iterative process for solving the equation

$$\delta^-(\theta) = \delta^+(\theta), \tag{6}$$

where, if the counting is done in the forward direction (from waste end to product end), the δ^- values will be determined from the δ^+ values, whereas if the counting is in the opposite direction, the δ^+ values will be determined from the δ^- values. Thus, if in the first stage of the cascade (the numbering of the stages is from waste end to product end) we take an arbitrary value θ_1, then the flow division coefficient in the second stage, θ_2, can be determined from the equation

$$\delta^-(\theta_2) = \delta^+(\theta_1), \tag{7}$$

Translated from Atomnaya Énergiya, Vol. 35, No. 3, pp. 205–207, September, 1973. Original article submitted April 19, 1973.

after which, using the expression (5), we find Q_3 from the value of $\delta^+(\theta_2)$, and so on until we reach the last (N-th) stage.

If the counting is done in the opposite direction, after having θ_N given arbitrarily, we determine θ_{N-1} from the equation

$$\delta^+(\theta_{N-1}) = \delta^-(\theta_N), \tag{8}$$

and the values of the subsequent θ_i for the i-th stages are found from $\delta^-(\theta_{i+1})$.

Since the derivatives of the functions δ^+ and δ^- with respect to θ are opposite in sign, it follows that, depending on the direction of the counting, the values of θ_i, oscillating about a specific value of θ which is the root of Eq. (6), will either converge to that value or diverge.

Let us investigate the process of solving (6) for a particular case of low enrichment values, when $\alpha_0 - 1 = \varepsilon_0 \ll 1$. Making use of the known expression for the enrichment function [4, 5],

$$\delta^+ = \varepsilon_0 \frac{1-\theta}{\theta} \ln \frac{1}{1-\theta} c(1-c) \tag{9}$$

(where we neglect infinitesimals of second order in δ^+), we write (6), for counting in the forward direction, in the form

$$\theta = \varphi(\theta) = 1 - \exp\left[-\frac{(1-\theta)\ln\frac{1}{1-\theta}}{\theta + \varepsilon_0(1-2c)(1-\theta)\ln\frac{1}{1-\theta}}\right]. \tag{10}$$

By a theorem on the convergence of an iterative process [6], the condition for convergence of (10) is

$$|\varphi'(\theta)| \leqslant M < 1, \tag{11}$$

where the oscillations of θ_i about the root $\tilde{\theta}$ of Eq. (10) can be estimated by the inequality

$$|\tilde{\theta} - \theta_i| < \frac{M_i}{1-M}. \tag{12}$$

Numerical investigation of Eq. (10) has shown that in the interval $0 < \theta < 1$ the iterative process is convergent, with $\tilde{\theta} \simeq 0.5$ and $M \leq 1/2$, i.e., in practice after five or six stages we have $\theta_i \approx \tilde{\theta}$.

If the counting process is carried out in the opposite direction, it will be divergent. We replace (10) by the equivalent equation

$$\theta = \psi(\theta), \tag{13}$$

where $\psi(\theta)$ is the inverse of the function $\varphi(\theta)$. Then, by some familiar theorems of mathematical analysis, we have

$$|\psi'(\theta)| = \left|\frac{1}{\varphi'(\theta)}\right| \geqslant \frac{1}{M} > 1, \tag{14}$$

i.e., the counting process in the reverse direction is divergent.

In Fig. 1 we show schemes for calculating the values of θ_i from Eq. (6) in the forward direction and the reverse direction in the general case of arbitrary α_0 and c. The figure confirms the conclusions arrived at for low enrichment values.

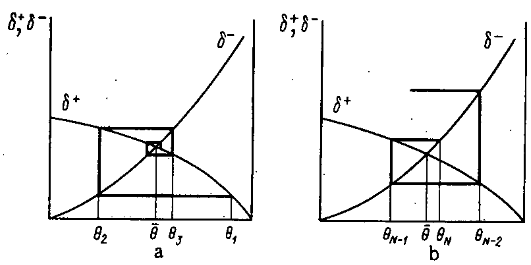

Fig. 1. Schemes for calculating the flow division coefficients θ in an ideal cascade [a) forward direction; b) reverse direction].

Thus, when the parameters of the cascade are calculated by means of finite-difference equations, the calculations can be carried out only from the waste end toward the product end.

Now we examine the problem of choosing the initial value θ_1. We consider the influence of θ_1 on the total flow of the cascade, confining our attention to the enrichment section. The values of θ_i converge rapidly to the root of Eq. (6), and therefore a change in θ_1 affects only the first stages. The sum of the flows in the first n stages can be written approximately in the form

$$\sum_{i=1}^{n} L_i = P(c_p - c) \sum_{i=1}^{n} \frac{}{\theta_i f(c, \theta_i)}, \tag{15}$$

Declassified and Approved For Release 2013/01/22 : CIA-RDP10-02196R000400020003-6

where c is the average concentration in the interval under consideration. The total flow will be minimal when the following condition is satisfied:

$$\sum_{i=1}^{n} \frac{1}{\theta_i f(c, \theta_i)} = \min. \tag{16}$$

When there is enrichment along the channel [3], the function $F = 1/\theta f(c,\theta)$ will be concave upward. The values of θ_i will oscillate about the root of (6), and for $M < 1/2$ the amplitude of the oscillations of θ_i in each stage will decrease by a factor of more than 2. Therefore, depending on the position of the root of Eq. (6) on the curve F and depending on the value of $\partial F/\partial\theta$, the total flow will be minimal at the point $\min_\theta F(\theta,c)$ or at the point $\tilde{\theta}$. Numerical calculations have shown that over a broad range of α_0 and c_i the value of the root $\tilde{\theta}$ is fairly close to $\min_\theta F(\theta,c)$, and the difference in the values for the total flow is less than 1%. Therefore we can recommend a choice of $\theta_1 = \tilde{\theta}$ for the initial value instead of a cumbersome analysis of the function F.

The value of θ can be found on the basis of the approximate explicit formulas obtained in [3] for δ^+ and δ^- for a known concentration c_1 in the first stage. To do this, we must solve the equation

$$\delta^+(c_1, \theta) = \delta^-[c_1 + \delta^+(c_1, \theta), \theta]. \tag{17}$$

In the present study we have considered the case of symmetric cascades; it can be shown that in asymmetric cascades, just as in this case, the counting must be carried out from the waste end toward the product end, and the values of θ_i will converge rapidly to the solution of an equation for $\tilde{\theta}$ which is analogous to (6).

The author wishes to express his sincere gratitude to N. A. Kolokol'tsov* for his guidance and his valuable advice, which made it possible to improve the work, and to G. A. Sulaberidze for his constant interest in the work.

LITERATURE CITED

1. N. A. Kolokol'tsov and N. I. Laguntsov, At. Énerg., 27, 560 (1969).
2. N. A. Kolokol'tsov and N. I. Laguntsov, At. Énerg., 29, 300 (1970).
3. N. A. Kolokol'tsov, N. I. Laguntsov, and G. A. Sulaberidze, At. Énerg., 35, 259 (1973).
4. K. Cohen, The Theory of Isotope Separation, New York (1951).
5. N. A. Kolokol'tsov, At. Énerg., 27, 9 (1969).
6. B. P. Demidovich and I. A. Maron, Fundamentals of Computational Mathematics [in Russian], Moscow (1970).

* Deceased.

EFFECT OF THE DEGREE OF GRAPHITIZATION OF A CARBON MATERIAL ON THE CHANGE IN MAGNETORESISTIVE EFFECTS DURING NEUTRON IRRADIATION

A. I. Polozhikhin, Yu. S. Virgil'ev, A. S. Kotosonov, G. F. Efremova, and I. P. Kalyagina

UDC 539.1:621.311:661.66

Graphites applicable in reactor construction are usually composite materials and are characterized by structural inhomogeneity, since regions with a different degree of structural perfection are present in the body of the material. Such inhomogeneity substantially affects the radiation changes in the properties of the graphite. During irradiation of pyrocarbons, a decrease in dimensional alterations with an increase in the degree of graphitization of the original samples is found [1]. The same connection between structural perfection and the amount of defects produced by neutron irradiation is found for samples of carbon black processed at various temperatures [2]. The utilization of magnetoresistive effects during the study of radiation defects in graphites allowed one to observe a change in layer defects [3], since the latter cause essential changes in the concentration and the mobility of charge carriers. In this paper, the effect of the degree of graphitization on the change in magnetoresistive effects for a GMZ brand structural material before and after irradiation by a $2.4 \cdot 10^{20}$ cm^{-2} ($E \geq 0.18$ MeV) integrated neutron flux at a temperature of 150°C is investigated.

The degree of graphitization for the material being studied was varied by the processing of the semifinished GMZ product in the 1500-3000°C temperature range and was evaluated relative to the intensity of the (112) and (110) diffraction maxima [4]. The Hall coefficient R_x, the magnetoresistance R_M, the specific electrical resistance ρ, and the crystal lattice parameters (the interlayer spacing d_{002}, diameter, and height of the crystals L_a, L_c) were measured for the samples before and after irradiation.

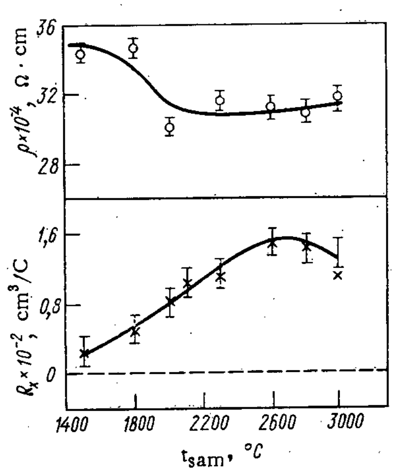

Fig. 1. Dependence of the Hall coefficient and the electrical conductivity for irradiated samples on the temperature of the preliminary processing.

Translated from Atomnaya Énergiya, Vol. 35, No. 3, pp. 207-208, September, 1973. Original article submitted September 11, 1972.

Declassified and Approved For Release 2013/01/22 : CIA-RDP10-02196R000400020003-6

TABLE 1. Structural and Magnetoresistive Characteristics of Samples of Semifinished GMZ before Irradiation

t_{sam}, °C	Degree of graphitization	L_a, Å	L_c, Å	$\rho\times10^{-4}$, Ω·cm	R_M, %	$R_x\times10^{-2}$, cm_3/C
1500	0	90	75	35,6	0	0
1800	0	130	80	36,0	0	10,4
2000	0,05	280	120	31,4	0	14,7
2300	0,21	660	190	13,8	3,2	−2,6
2600	0,36	1000	215	12,0	4,8	−4,6
2800	0,40	> 1000	215	9,4	6,1	−4,5
3000	0,54	> 1000	240	8,4	10,0	−5,2

The x-ray structural characteristics were determined in a URS-50 Institute of Metals diffractometer using copper radiation. During the calculation of the lattice parameters, experimental corrections conforming to a standard-graphite from a Taiga deposit were introduced.

Magnetoresistive effects and electrical resistance were measured by a potentiometric technique in constant electric and magnetic fields (H = 18 kOe) at temperatures of 300 and 77°K.

Consistent with the increase in the dimensions of the crystallites and the change in the zone structure, the degree of graphitization of the original samples varied from 0 to 0.54. Improvement in the structure of a carbon material is accompanied by an increase in mobility, a decrease in the concentration of charge carriers, and an increase in the electron component in the charge transport process [5]. The characteristics of the original samples, presented in Table 1, show that, with an increase in the degree of graphitization, the magnetoresistance increases, the sign of the Hall coefficient changes from positive to negative, and the electrical resistance decreases.

During the process of irradiation, the structure of the samples was subjected to considerable amorphism: the dimensions of the crystals decreased and the interlayer spacing increased (the relative change in the interlayer spacing for all samples was found to be approximately the same: 6-7%). The electrical characteristics also changed, these changes proving to be different for samples with a different initial degree of graphitization. Thus, if the electrical conductivity of the original samples differed by a factor of ~4, after irradiation it became approximately the same. At the same time, the electrical conductivity for highly graphitized samples increased sharply, but for those of low-perfection it decreased somewhat compared with the original value.

The magnetoresistance of the irradiated samples dropped to zero, but the Hall coefficient became positive. The dependence of R_x and ρ for the irradiated samples on the temperature of the preliminary processing is shown in Fig. 1.

Measurements at 300 and 77°K showed that the R_x for the irradiated samples does not depend on the temperature of the measurement, i.e., the free charge carriers are found in a degenerated state. In this case, one can easily calculate the concentration of the "hole" charge carriers. It was found to be ~100 times greater than the concentration of the normal charge carriers in the original samples.

The extraordinary drop in the electrical conductivity after irradiation of poorly graphitized samples is connected with this increase in the concentration of the charge carriers, but the changes in the rest of the characteristics determining ρ (the material's density and the charge carriers' mobility) for poorly graphitized samples were found to be less important.

The calculations also showed that the number of extra "holes" created by the irradiation decreases with an increase in the degree of structural perfection of the original samples. Thus, in a sample processed at 1500°C, the concentration of "holes" after irradiation is $12.7\cdot10^{20}$ cm^{-3}, but at 3000°C it is $4.4\cdot10^{20}$ cm^{-3}. Layer defects (vacancies and their aggregates), having developed during irradiation, are also found in the same proportion [3]. Under prescribed irradiation conditions when intermediate atoms and their aggregates are primarily mobile [6], annealing occurs due to migration to sinks (crystal boundaries) and annihilation by vacancies. In this case, the large mobility of intermediate atoms in samples with a large degree of perfection of crystalline structure contributes to the "healing" of a large number of vacancies that correspondingly reduces the concentration of extra "holes" [2]. However, the entire situation and the final result can be essentially changed, if one irradiates at higher temperatures when the vacancies become mobile.

LITERATURE CITED

1. B. Kelly and J. Brocklehurst, Tenth Biennial Conference on Carbon, RD-123 (1973), p. 195.
2. G. Arnold and S. Mrozowski, Carbon, 6, 243 (1968).
3. A. S. Kotosonov, Dissertation [in Russian], Moscow (1971).

4. V. I. Kasatochkin, Izv. AN SSSR Otd. Tekhn. Nauk., 9, 204 (1951).
5. S. Mrozowski, Carbon, 9, 97 (1971).
6. W. Reynolds and P. Thrower, in: Radiation Damage in Reactor Materials, IAEA, Vienna (1963), p. 553.

ON A FORMULA FOR THE COMPUTATION OF THE CROSS SECTION FOR THE PRODUCTION OF A PAIR OF γ-QUANTA IN THE STATISTICAL MODELLING OF TRANSPORT PROCESSES

O. S. Marenkov

UDC 539.121.72/75

In the statistical modelling (by the Monte Carlo method) of the transport in matter of γ-quanta of medium and high energy, two elementary interaction processes are usually considered – incoherent scat-

TABLE 1. The Coefficients $\varkappa_i$ for the Computation of the Macroscopic Cross Section (cm^2/g) for Pair Production and the Error δ in the Approximation

Element	$\varkappa_0$	$-\varkappa_1$	$\varkappa_2$	$-\varkappa_3$	δ, %
Hydrogen	0,002442	0,002849	0,0009310	0,00005349	4,4
Helium	0,001951	0,002399	0,0008369	0,00005718	1,1
Lithium	0,002220	0,002814	0,001012	0,00007295	1,2
Beryllium	0,002872	0,003695	0,001349	0,0001001	1,3
Boron	0,003546	0,004624	0,001709	0,0001288	1,9
Carbon	0,004476	0,005882	0,002191	0,0001677	2
Nitrogen	0,005106	0,006752	0,002530	0,0001954	2,3
Oxygen	0,005728	0,007617	0,002869	0,0002233	2,5
Fluorine	0,006058	0,008067	0,003043	0,0002376	2,6
Neon	0,006954	0,009299	0,003521	0,0002768	2,6
Sodium	0,007244	0,009740	0,003705	0,0002926	2,8
Magnesium	0,008010	0,01082	0,004130	0,0003271	2,8
Aluminum	0,008448	0,01142	0,004369	0,0003475	2,9
Silicon	0,109440	0,01276	0,004885	0,0003904	2,8
Phosphorus	0,009618	0,01307	0,005019	0,0004011	2,9
Sulfur	0,01045	0,01424	0,005482	0,0004389	3
Chlorine	0,01059	0,01448	0,005584	0,0004481	3,1
Argon	0,01048	0,01435	0,005546	0,0004466	3
Potassium	0,01187	0,01628	0,006301	0,0005086	3,2
Calcium	0,01259	0,01736	0,006740	0,0005440	3,2
Scandium	0,01226	0,01698	0,006621	0,0005367	3,4
Titanium	0,01242	0,01727	0,006743	0,0005459	3,3
Vanadium	0,01263	0,01760	0,006887	0,0005580	3,4
Chromium	0,01337	0,01868	0,007326	0,0005948	3,5
Manganese	0,01348	0,01891	0,007433	0,0006020	3,3
Iron	0,01442	0,02018	0,007920	0,0006423	3,1
Cobalt	0,01448	0,02038	0,008031	0,0006517	3,3
Nickel	0,01539	0,02177	0,008604	0,0006989	3,4
Copper	0,01537	0,02166	0,008548	0,0006953	3,4
Zinc	0,01564	0,02221	0,008802	0,0007161	3,3
Germanium	0,01564	0,02233	0,008884	0,0007225	3,3
Molybdenum	0,01770	0,02632	0,01075	0,0008780	3,1
Silver	0,01775	0,02727	0,01135	0,0009263	3,1
Cadmium	0,01685	0,02636	0,01107	0,0009024	3,4
Tin	0,01736	0,02712	0,01139	0,0009306	3,1
Antimony	0,01695	0,02678	0,01131	0,0009204	3
Iodine	0,01730	0,02753	0,01169	0,0009571	3
Barium	0,01615	0,02667	0,01155	0,0009464	3,2
Tungsten	0,01031	0,02354	0,01162	0,0009433	2,9
Platinum	0,007286	0,02104	0,01108	0,0008950	2,8
Gold	0,006205	0,02015	0,01088	0,0008750	2,9
Mercury	0,005470	0,01943	0,01068	0,0008545	2,9
Lead	0,005390	0,01954	0,01079	0,0008690	2,8
Bismuth	0,003814	0,01822	0,01049	0,0008410	2,9
Radium	—0,0006037	0,01411	0,009386	0,0007354	3,2
Thorium	—0,002451	0,01237	0,008909	0,0006891	3,3
Uranium	—0,003333	0,01170	0,008805	0,0006829	3,1
Plutonium	—0,007237	0,008101	0,007825	0,0005862	3

Translated from Atomnaya Énergiya, Vol. 35, No. 3, pp. 209–210, September, 1973. Original article submitted October 18, 1972.

tering and electron–positron pair production. For all elements, incoherent scattering can be treated as Compton scattering from a free electron, for energies greater than 1 MeV. The energy dependence of the integral cross section for the Compton interaction of γ-quanta is given, up to a constant multiplier, by the expression

$$\sigma(\beta)=\left(\frac{2}{\beta}-\frac{8}{\beta^2}-\frac{16}{\beta^3}\right)\ln(1+\beta)+\frac{16}{\beta^2}+(1+\beta)^{-1}+(1+\beta)^{-2},$$

where β is twice the energy of the quantum in units of the electron rest mass energy. In a wide range of energies there does not exist an accurate theoretical or empirical formula for the computation of the integral cross section for the production of a pair of photons. The cross sections for pair production, calculated on the basis of approximate theories, and applied to various energy ranges and atomic numbers, are usually tabulated.

Reference [1], which characterizes the state of the theoretical studies on the cross sections for the interaction of gamma quanta up to the year 1970, presents a systematic summary table of the total and partial cross sections for 100 elements in the energy range from 0.001 to 100 MeV. The cross section for pair production in the field of a nucleus is given for the energy interval 1.5 to 100 MeV; the cross section for pair production in the Coulomb field of the electrons is given for the energy interval 3 to 100 MeV. The errors in the numerical values of the pair production cross sections does not exceed 5%.

The tabulated form of the pair production cross section is a definite inconvenience in the numerical modelling of γ-transport. It is therefore of practical importance to express the integrated cross section of pair production (in the field of the nucleus and in the field of the electrons) in the form of a formula. A study of theoretical and experimental work on the cross section for the production of a pair of γ-quanta shows that, from the physical point of view, the functional dependence of $\varkappa = \varkappa(\beta)$ can be well approximated by a polynomial in $\ln \beta$. Such an approximation was found to be valid for 100 elements in the energy interval 1.5 to 100 MeV; the maximum error was 3.3%. However, the use of such an approximation and of Eq. (1), in the computation of $\varkappa$ and σ for statistical modelling, is uneconomical from the point of view of machine time cost. Two calls to the subroutine which calculates the logarithmic function must occur for each value of β, since there is no simple (from the computational point of view) functional relationship between $\ln \beta$ and $\ln(1 + \beta)$. Therefore the functional dependence $\varkappa = \varkappa(\beta)$ was approximated by a polynomial in $\ln(1 + \beta)$,

$$\varkappa=\sum_{i=0}^{3}\varkappa_i\,[\ln(1+\beta)]^i. \tag{2}$$

The coefficients $\varkappa_i$ were computed from the tabulated data of [1] by the method of least squares using weight functions of the power type [2]. Results for the 48 elements most often encountered in problems of applied and technical physics are presented in Table 1. The energy interval is 1.5 to 100 MeV. The maximum error of the approximation is 3.5%, except for hydrogen.

LITERATURE CITED

1. E. Storm and H. Israel, Nuclear Data Tables, Section A, 7, No. 6, 565 (1970).
2. O. S. Marenkov and R. S. Derzhimanov, Atomnaya Énergiya, 18, No. 5, 520 (1965).

DOSIMETRY OF IONIZING RADIATIONS USING GLASS COLORANT DETECTORS

V. V. Tkachenko, B. A. Briskman, L. M. Kovalenko, Ya. I. Lavrentovich, and N. F. Orlov

UDC 539.1.074

Colorant aluminophosphate glasses doped with manganese have been used successfully in the dosimetry of accelerated charged particles, and also in measurements of doses of γ-radiation in mixed γ–neutron fields. (Such data are virtually nonexistent in the literature.) It was found that the shape of the absorption spectrum in the visible region due to the formation of Mn^{3+} ions in response to irradiation of glasses by different modes of ionizing radiations corresponds to the absorption spectrum obtained when glasses are bombarded by Co^{60}-emitted γ-radiation [1]. The degree of coloration of the glasses was measured at the absorption maximum at wavelength $\lambda = 5600\mu$, in order to obtain quantitative data.

Figure 1 shows how the optical density S (in cm^{-1}) of irradiated glasses varies with the absorbed dose D (in Mrad) of protons, deuterons, and α-particles accelerated in a cyclotron. The counterpart for γ-radiation emitted by Co^{60} is also plotted, to afford a useful comparison.

The γ-radiation dose absorbed in the glasses was calculated on the basis of readings from a ferrous sulfate–cupric sulfate dosimeter [2], and the dose of heavy charged particles was calculated on the basis of data on streams of particles and energy losses and range losses in those glasses, using a procedure described in [3]. Path lengths and mean LET values of heavy charged particles in the glasses are tabulated, as calculated on the basis of stopping power formulas involving Bragg's rule.

TABLE 1. Path Lengths and Mean LET Values of Heavy Charged Particles in Aluminophosphate Glasses

Type of radiation	Energy, MeV	Mean LET, keV/μ	Path length, mg/cm^2
Protons	7	13,1	82,3
Deuterons	14	13,1	164,6
α-Particles	28	52,4	82,3

It is clear from Fig. 1 that heavy charged particles are less effective in processes involving the formation of color centers than Co^{60} γ-radiation (LET $\approx$ 0.2 keV/μ). Given the relatively slight difference between the various LET values of the heavy charged particles (compared to the LET value of the γ-radiation), no essential difference was observed in the effect of protons, deuterons, and α-particles on the glass.

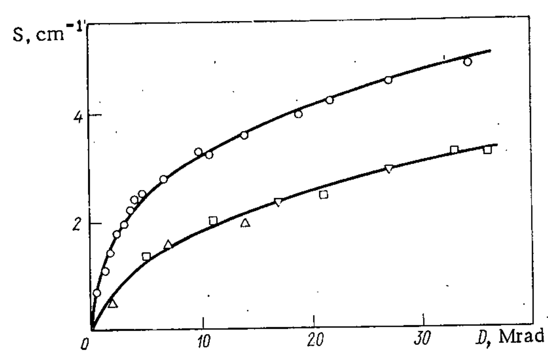

Fig. 1. Dependence of optical density of glass detectors on absorbed dose at wavelength $\lambda = 5600\mu$: ○) Co^{60}-emitted γ-radiation; ▽) protons, E = 7 MeV; △) deuterons, E = 14 MeV; □) α-particles, E = 28 MeV.

Translated from Atomnaya Énergiya, Vol. 35, No. 3, pp. 210-211, September, 1973. Original article submitted October 31, 1972.

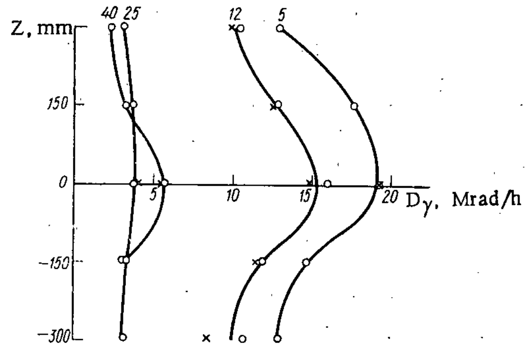

Fig. 2. Distribution of γ-radiation dose rate over height of VVR-Ts reactor core, as measured with calorimeters (×) and glass detectors (○). Numerals correspond to numbers assigned to experimental channels in reactor.

When the glasses are irradiated by 7 MeV electrons, the LET of which is close to that of γ-radiation, the dependence of the optical density on absorbed dose is found to be in excellent agreement with a similar dependence for Co^{60}-emitted γ-radiation. We should take note of the incorrect calculations of absorbed electron dose based on [4], in view of the commensurability of the electron path lengths and the thickness of the glasses,* and the nonuniform distribution of absorbed dose with respect to thickness, which means that the nonlinearity in the calibration dependence in turn makes it more difficult to reduce the optical density to unit thickness of the glass.

An investigation of the possible use of glass colorant detectors to measure doses of γ-radiation in mixed γ–neutron fields was performed in the experimental channels of the VVR-Ts reactor. As the calculations show, the real relationship of the γ-radiation dose and neutron dose, for the absolute majority of in-pile measurements, is such that the kerma of the neutrons in the glasses amounts to unity and a fraction of the percentage of total absorbed dose. Taking the loss of effectiveness in the formation of color centers in the glasses with rising LET of the particular mode of radiation into account, we can safely neglect the effect of neutrons on the readings of glass detectors. That is confirmed by results of experiments depicted in Fig. 2. The agreement (~10%) between dose rates of γ-radiation in the channels of a 10 MW reactor, as measured with adiabatic calorimeters [5] and glass colorant detectors calibrated for Co^{60} emission, is clearly in evidence.

Consequently, investigations indicate the possibility, in principle, of using colorant aluminophosphate glasses actived by manganese not only to measure doses of γ-radiation from isotope sources, but also for dosimetry of accelerated charged particles and measurements of doses of γ-radiation in mixed γ–neutron fields.

The authors are indebted to A. N. Belyakov for helpful discussions of the work.

LITERATURE CITED

1. V. M. Trofimov, N. F. Orlov, and N. Z. Andreeva, At. Énerg., 29, No. 2, 155 (1969).
2. E. Hart and P. Walsh, Rad. Res., 1, 342 (1954).
3. Ya. I. Lavrentovich et al., Khimiya Vysokikh Énergii, 30, 147 (1969).
4. Yu. S. Ryabukhin, A. G. Vasil'ev, and A. N. Belyakov, At. Énerg., 19, No. 6, 535 (1965). Also "Correction" in: At. Énerg., 25, No. 2, 173 (1968).
5. B. A. Briskman, Yu. V. Matveev, and A. G. Vasil'ev, At. Énerg., 27, No. 4, 342 (1969).

*Aluminophosphate glasses sized 10 × 10 × 2 mm were employed in this work.

YIELDS OF FRAGMENTS FOR PHOTOFISSION OF Np^{237}

M. Ya. Kondrat'ko, V. N. Korinets,
K. A. Petrzhak, and O. A. Teodorovich

UDC 539.173.3:546.799.3

By a radiochemical method we measure the yields of fragments for the fission of Np^{237} by betatron bremsstrahlung for a change in the maximum energy in the range 10-24 MeV.

For the irradiation we use a device [1] that allows us to distribute the samples to be irradiated in the region of maximum intensity of the bremsstrahlung without breaking down the airtightness of the vacuum chamber of the betatron. The fissionable material, in the form of NpO_2 is applied in a thin (200 $\mu g/cm^2$) uniform layer onto a metallic substrate. The target is an assembly of 35-40 neptunium samples, with interposed aluminum absorbers. The thickness of the substrate and the absorber is chosen to be sufficient for the complete absorption of the fragments (about 6 mg/cm^2).

Radiochemical analysis was applied only to fragments retained by the absorbers. After irradiation the target is removed and analyzed. The absorbers are dissolved in acid or in alkali in the presence of a

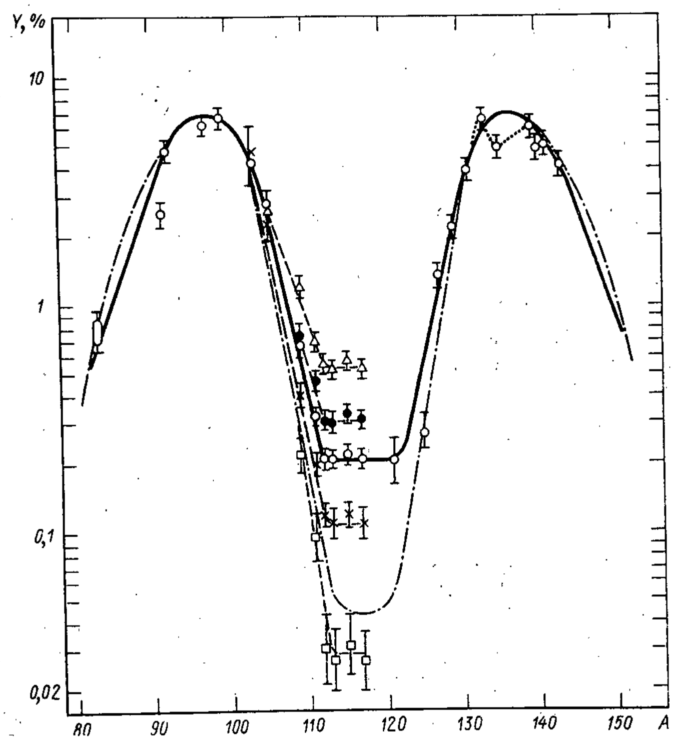

Fig. 1. Curves of the distribution of yields of fission fragments. Data of the present study for Np^{237} (γ, f): (– □ –) 10 MeV; (– × –) 12 MeV; (– ○ –) 14 MeV; (– ● –) 16 MeV; (– Δ –) 24 MeV; (–·–·–) data of (12) for Np^{237} (n, f).

Translated from Atomnaya Énergiya, Vol. 35, No. 3, pp. 211-213, September, 1973. Original article submitted November 30, 1972.

TABLE 1. Yields of Fragments for Photofission of Np^{237} (%)

Isotope	Maximum bremsstrahlung energy $E_{\gamma 0}$, MeV					
	24	20	16	14	12	10
Br^{83}	—	—	—	{0,76±0,05; 0,86±0,06}	—	—
Sr^{91}	—	—	—	2,55±0,18	—	—
Sr^{92}	—	—	—	4,76±0,48	—	—
Zr^{97}	—	—	—	6,23±0,66	—	—
Mo^{99}	—	—	—	6,84±0,49	—	—
Ru^{103}	4,47±0,35	4,88±0,87	—	4,25±0,43	4,72±0,84	—
Ru^{105}	2,65±0,18	2,87±0,18	—	2,86±0,22	2,34±0,34	—
Pd^{109}	1,20±0,11	0,88±0,09	0,73±0,06	0,63±0,04	0,40±0,07	0,22±0,03
Ag^{111}	0,70±0,06	0,53±0,04	0,47±0,03	0,32±0,03	0,20±0,02	0,095±0,010
Pd^{112}	0,55±0,05	0,47±0,04	0,31±0,03	0,21±0,02	0,13±0,02	0,031±0,008
Ag^{113}	0,51±0,04	0,40±0,03	0,31±0,03	0,21±0,02	0,11±0,02	0,027±0,005
Cd^{115}	0,56±0,04	0,43±0,03	0,33±0,03	0,22±0,02	0,12±0,02	0,032±0,008
Cd^{117}	0,53±0,04	0,40±0,03	0,32±0,03	0,21±0,02	0,11±0,02	0,027±0,007
Sn^{121}	—	—	—	0,21±0,05	—	—
Sn^{125}	—	—	—	0,32±0,03	—	—
Sb^{127}	—	—	—	1,36±0,08	—	—
Sb^{129}	—	—	—	2,18±0,21	—	—
I^{131}	—	—	—	3,90±0,27	—	—
I^{133}	—	—	—	6,54±0,40	—	—
I^{135}	—	—	—	4,91±0,33	—	—
Ba^{139}	5,49±0,32	6,02±0,35	5,64±0,33	6,08±0,36	5,44±0,32	6,37±0,33
Ba^{140}	4,82±0,24	4,83±0,24	4,96±0,23	4,90±0,20	4,94±0,25	4,98±0,26
Ce^{141}	—	—	—	4,99±0,31	—	—
Ce^{143}	—	—	—	4,06±0,42	—	—

known amount of nonactive isotopic carriers. Measures are taken to guarantee the complete exchange between carriers and the radioactive isotopes that are being investigated. In the solution, chemical operations are carried out, based on a fault in the aluminum. The separation and purification of the fission products being investigated are carried out with the use of standard precipitation, distillation, or extraction methods [2, 3]. The final precipitates in gravimetric form are applied with a uniform thin layer (1-4 mg $/cm^2$) to metallic substrates of thickness 1.35 mg/cm^2, dried, and weighed. The β activity is measured in 4π-counters.

Corrections for self-absorption and absorption in the substrate were determined experimentally for certain isotopes with a simple β-decay scheme [4]. The obtained calibration dependencies enabled us to estimate with accuracy 2-3% the absolute efficiency of recording of every β-active isotope with known decay scheme. For recording of the conversion electrons we corrected the calculation errors.

The curves of the radioactive decay were processed by the method of least squares with the introduction of known decay constants. Components which could be attributed to radioactive impurities were not observed.

The absolute activities, adjusted for chemical yield, reduced to values of activity of saturation. The factors of accumulation of the fragment isotopes were calculated taking account of the accumulation and the decay of their precursors along the β chain. The necessary values of the independent fractional yields of the separate precursors were estimated, based on the hypothesis of equal displacement of charge. It was assumed that the semiempirical parameters of the charge distribution, proposed by Wahl [5], have a universal character and can be extended to the photofission of neptunium.

The fragment yields were determined with respect to the Ba^{140} yield as the ratio of the absolute saturation activities, and the total yields of isobaric chains with given mass number were recalculated in value. For mass 117 the ratio of the decay branches of Ag^{117} ($T_{1/2}$ = 1.1 min), leading to the formation of Cd^{117m} (3 h) and Cd^{117} (50 min), was taken equal to 0.82 : 0.18 [6, 7]. In decay schemes of nuclei having masses 121 and 125 we do not know the ratios of the decay branches leading to the formation of isomers of tin. Therefore the experimental values of the yields for Sn^{121} (27.5 h) and Sn^{125} (9.7 days) were not recalculated to the ends of the decay chains, and are cumulative yields of the isomers.

For the normal isotope Ba^{140} a series of absolute measurements of the yield were carried out for six values of maximum energy of the braking spectrum. The number of Ba^{140} nuclei produced were determined from the absolute β activity of the radiochemical samples. The total number of fission events were recorded using mica detectors [8]. In order to do this, in a composite target, we introduced, in addition, thin layers of NpO_2 (1-2$\mu g/cm^2$), adjacent to plates of natural muscovite. After irradiation, tracks of the radiation destructions in mica appeared in fluoric acid and were counted under a microscope. The effect of the inhomogeneity of the radiation beam was negligibly small for the same dimensions and form of control and "radiochemical" samples of neptunium. For assembly of the target the relative position of the samples were reproduced with accuracy 0.1-0.2 mm. Five control samples enabled us to take into account the decrease in intensity with target depth. The relative content of neptunium in the control and "radiochemical" layers were determined from the α activity.

The measured values for the yields for 24 mass numbers are presented in Table 1. The error in the direct determinations of the Ba^{140} yields was about 5%; in the remaining cases, the error is greater, since it includes errors of the relative measurements. The systematic error, caused by the presence of Pu^{239} ($< 0.4\%$) in the target, is negligible. The differences in efficiency of collection of light and heavy fragments did not exceed 1%. The values for the yields, given in the table, are averaged over 2-4 independent measurements.

Figure 1 shows a mass distribution curve for the fission products of Np^{237} by bremsstrahlung with maximum energy $E_{\gamma 0} = 14$ MeV. In this figure, values are presented for the yields in the region of symmetric fission for other energies of bremsstrahlung. The curve has the usual double-humped character with "peak-to-valley" ratio of about 20. The most probable yields correspond to the mass numbers 98.4 and 137. The width of the group maxima at the midheight is approximately equal to 15.2 mass units. The distribution is symmetric with respect to the mass number 117, which corresponds to the emission of an average of three prompt neutrons per fission event. This value agrees with the estimated quantity $\nu \approx 3.15$, obtained for the photofission of Np^{237} on the basis of the systematization of the mean number of fission neutrons [9, 10].

Normalization of the mass-distribution integral to 200% gave a value for the Ba^{140} yield equal to 4.87 $\pm$ 0.10. The result agrees with the value 4.90 $\pm$ 0.20, measured directly.

The yield of the Sn^{125} isomer lies considerably below the mass-distribution curve. If we assume that the point corresponding to the yield of mass 125 is located on the smooth curve, we can estimate the fraction of Sn^{125} (9.7 days) in the total yield of the chain of magnitude of the order of 0.39 $\pm$ 0.07. Within the limits of the error this value agrees with the results of [7, 11].

The uncertainty in the yield of mass 83 is caused by the insufficiently exact information about the decay scheme of the precursor of Br^{83} – the short-lived As^{83}. The total yield for A = 83 was calculated for two limiting assumptions: As^{83} completely converted into Se^{83} (69 sec) and As^{83} completely converted into Se^{83} (25 min) [sic] with the latter decaying into Br^{83} (2.4 h).

In the group of heavy fragments we note a certain understating in the yield for A = 135 in comparison with neighboring masses, which can be considered as an effect of the "fine structure." A similar deviation for mass 135 is observed for the fission of Np^{237} by epicadmium neutrons [12].

The "peak-to-valley" ratio for Np^{237} photofission for $E_{\gamma 0} = 14$ MeV is considerably less than for the fission of this nucleus by epicadmium neutrons.

LITERATURE CITED

1. O. P. Nikotin, B. T. Plachenov, and V. P. Sergeev, Proceedings of Lensovet Leningrad Technological Institute [in Russian], Vol. 55 (1961), p. 28.
2. Radiochemical Studies. The Fission Products. National Nucl. Energy Series. Plutonium Project Record, Div. IV, Vol. 9, N. Y. (1951).
3. Radiochemical Analysis of Fission Products [in Russian], Yu. M. Tolmachev (editor), Izd. Akad. Nauk SSSR, Moscow (1960).
4. M. Ya. Kondrat'ko, O. P. Nikotin, and K. A. Petrzhak, Pribory i Tekh. Éksperim., No. 3, 47 (1964).
5. A. Norris and A. Wahl, Phys. Rev., 146, 926 (1966).
6. T. Kivikas and B. Forkman, Nucl. Phys., 64, 420 (1965).
7. M. Ya. Kondrat'ko and K. A. Petrzhak, At. Énerg., 23, 559 (1967).
8. M. Ya. Kondrat'ko, O. P. Nikotin, and K. A. Petrzhak, At. Énerg., 27, 544 (1969).
9. Yu. S. Zamyatnin, in: Physics of Fission of Atomic Nuclei [in Russian], Gosatomizdat, Moscow (1962), p. 98.

10. I. I. Bondarenko et al., Second Geneva Conference (1958), Vol. 1, Atomizdat, Moscow (1959), p. 438.
11. N. I. Borisova, B. V. Kurchatov, et al., in: Physics of Fission of Atomic Nuclei [in Russian], Gosatomizdat, Moscow (1962), p. 48.
12. R. Stella et al., J. Inorg. Nucl. Chem., 31, 3739 (1969).

DISTRIBUTION OF MASSES OF FRAGMENTS IN THE REGION OF THE SYMMETRIC PHOTOFISSION OF U^{235} AND Np^{237}

M. Ya. Kondrat'ko, V. N. Korinets, and K. A. Petrzhak

UDC 539.173.3

In a study devoted to the yields of fragments of the photofission of Np^{237} [1] it was shown that the distribution curve for the fragments with respect to mass has a double-humped character. In the region of mass numbers 111-121 the measured values of the yields are almost the same, and the "valley" of the mass curve has a horizontal plateau without any noticeable structure. With variation of the maximum energy of bremsstrahlung $E_{\gamma 0}$ from 10 to 24 MeV the yields of the symmetric fission increase, but the form of the mass curve in the symmetric region remains unchanged.

It is known that for the fission of a number of heavy nuclei, the mass distributions, besides the two peaks of the asymmetric fission, contain a more-or-less expressed third peak – the central peak of the symmetric fission. For the fission of Ra^{226} by protons [2] and by photons [3] the central peak is comparable in amplitude and in width with the peaks of light and heavy fragments. The local maxima of the yields in the symmetric region of mass numbers were observed for the fission of Ac^{227} by reactor neutrons [4] and isotopes of thorium by reactor neutrons [5, 6], by neutrons with energy 14 MeV [7] and by bremsstrahlung [8]. For the photofission of U^{235} [9] we observe a stable excess of yields of the most symmetric fission (A = 115 and 117) over the yields of neighboring fragments in the symmetric region. The central maximum is less distinguishable, the greater the atomic number and mass of the fissionable nucleus. In the fission of U^{238} and heavier nuclei, a central peak was not observed.

TABLE 1. Yields of Fragments for Photofission of U^{235} ($E_{\gamma 0}$ = 14 MeV)

Mass number	Isotope	Present study	Data from [9]
109	Pd^{109}	0,292±0,030	—
111	Ag^{111}	0,189±0,020	0,165±0,020
112	Pd^{112}	0,142±0,013	—
113	Ag^{113}	0,170±0,020	0,166±0,015
115	Cd^{115}	0,224±0,020	0,214±0,020
117	Cd^{117}	0,218±0,021	0,208±0,020 *
121	Sn^{121}	—	0,169±0,020
127	Sb^{127}	—	0,84±0,08

* Value reduced to total yield of chain.

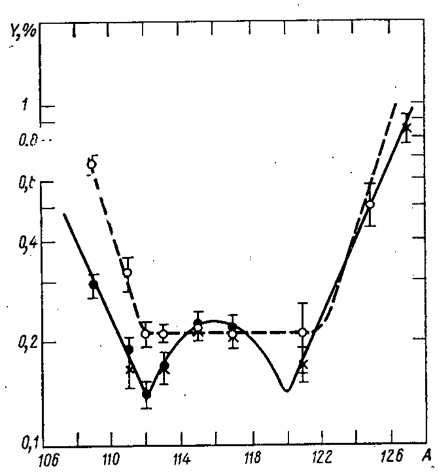

Fig. 1. Distribution of masses of fragments in the region of symmetric photofission; —●—) data of the present study; —×—) data of [9] for U^{235}; —○—) data of [1] for Np^{237}.

Translated from Atomnaya Énergiya, Vol. 35, No. 3, pp. 214-215, September, 1973. Original article submitted December 11, 1972.

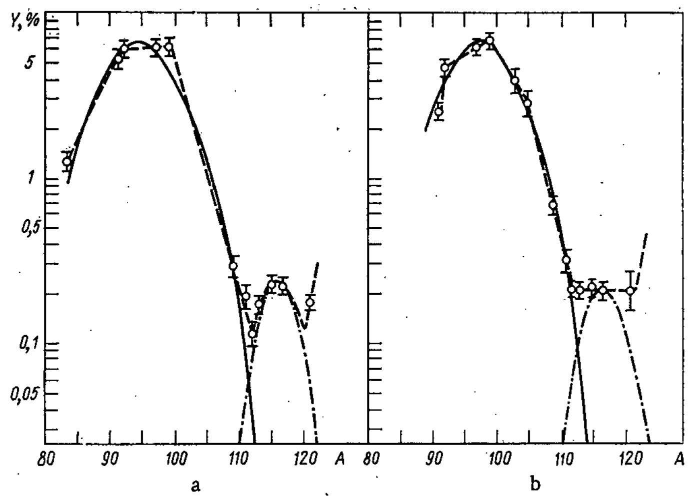

Fig. 2. Distribution curves for the yields of photofission fragments: a) U^{235} (the present study, [9]); b) Np^{237} [1].

To refine the shape of the mass-distribution curve we measured the yields of six products of the symmetric and almost symmetric fission of U^{235} by bremsstrahlung photons with maximum energy 14 MeV. A radiochemical method was used to analyze the recoil fragments emitted from the thin target and absorbed in the collector layers. The experimental conditions (method of irradiation and analysis, measuring apparatus, treatment of results) completely agreed with those used in experiments on the photofission of Np^{237} [1].

Table 1 gives results of measurements, converted to the value of the total yields and in good agreement with earlier measurements [9].

For the photofission of $U^{235}(E_{\gamma 0} = 14$ MeV) in the mass curve there is clearly observed a group of fragments of the symmetric fission with a maximum for mass number 116 (Fig. 1). According to the results of [9] it is precisely this mass number that corresponds to the completely symmetric fission U^{235}. The "valley" in the region of mass numbers 111-113 with minimum at A = 112 has a reproducible character, falls outside the limits of statistical errors, and, evidently, is not related to the systematic error of the experiment or the processing, since the yields of the Np^{237} photofissions that were measured under completely identical conditions do not have similar irregularities.

It is known that with increasing mass of the fissionable nucleus the position of the group of heavy fragments remains practically constant (right up to the spontaneous fission of Cm^{242}), and the group of light fragments moves in the direction of larger mass numbers. This regularity is observed also with comparison of the yields of the photofission of U^{235} and Np^{237}. For Np^{237} the yields of the masses 109-113 are considerably greater compared with U^{235}, whereas the yields of the masses 127-131 are rather close in value.

We can assume that the presence or absence of structure in the experimental mass spectra in the symmetric-fission region is related principally to the position of the group of light fragments relative to the mass distribution in the symmetric region. Thus, in Fig. 2, the peaks of the light fragments are approximated by normal-distribution curves. Although, as is known, the peaks of the principal groups of fragments are not symmetric with respect to the mean mass, and have characteristic deviations from the probability function (related to, e.g., the fine structure of the fission), the selected shape of the curve describes quite well the experimental mass spectra in the region of internal slopes. The selection of a Gaussian was carried out based on the optimum agreement with experimental values for the yields in the region of the maximum and the right slope of the group of light fragments. In the region of masses greater than 109, the normal-distribution curves were extrapolated, and were calculated from the experimental mass curves. For both comparable nuclei this led to an effect of groups of symmetric fission, which was also well described by a normal-distribution function.

The groups of the fragments of the symmetric photofission of U^{235} and Np^{237} have the same width (about 7 mass units at the middle of the maximum) and are shifted relative to each other by one mass unit.

Groups of the light fragments have a large relative shift (approximately two mass units). For Np^{237} the symmetric-fission group proves to be too close to the intense peak of the light fragments, so that masses in the form of an allowed peak develop in the experimental spectra.

For the photofission of Th^{232} ($E_{\gamma 0}$ = 25 MeV) [8], the symmetric-fission yields are a minimum for A = 103-105 and a maximum for A = 112-115. In comparison with the U^{235} photofission, the light-fragment group shifts by approximately three mass units to the left and the central maximum appears more clearly.

These results confirm the existence of a separate group of final fission products in the symmetric region. Evidently, for excitation energy ~10 MeV the mass number 236 is a critical value of mass of a fissionable nucleus from the point of view of the resolution of this group in the experimental mass-distribution curves.

LITERATURE CITED

1. M. Ya. Kondrat'ko et al., this issue, p. 862.
2. R. Jensen and A. Fairhall, Phys. Rev., 109, 942 (1958).
3. R. Duffield et al., Proc. of the Second Intern. Conf. on the Peaceful Uses of Atomic Energy, Geneva, UN, Vol. 15 (1958), p. 678.
4. R. Iyer et al., Phys. and Chem. of Fission, Proc. of Symp., Salzburg, IAEA, Vienna, Vol. 1 (1965), p. 439.
5. N. I. Borisova, R. A. Zenkova, B. V. Kurchatov, et al., Yadernaya Fizika, 8, 695 (1968).
6. R. Iyer, C. Matthews, et al., J. Inorg. Nucl. Chem., 25, 465 (1963).
7. L. Gevaert and R. Jervis, Canad. J. Chem., 48, 641 (1970).
8. L. Gevaert, and R. Jervis, and S. Subarrao, ibid., p. 652.
9. M. Ya. Kondrat'ko and K. A. Petrzhak, At. Énerg., 23, No. 6, 559 (1967).

PERMANENT ELECTRIC POWER COMMISSION

The eleventh session of section 5 (nuclear power stations) of the COMECON Permanent Commission on Electric Power was held May 21-26 of this year at the I. V. Kurchatov nuclear power station facilities in Belyi Yar. Delegations from Bulgaria, Hungary, the German Democratic Republic, Poland, Rumania, the Soviet Union, Czechoslovakia, and Yugoslavia took part in the deliberations of the session (which was chaired by the head of the Soviet part of section 5, A. N. Grigor'yants, head of the Glavatoménergo body of the USSR Ministry of Power and Electrification). Major topics in nuclear power development affecting COMECON member-nations came under discussion, as well as topics involving nuclear power station safety at all phases, in design, construction, and operation. Agreement was reached on a draft report dealing with organization and realization of inspection work on the state of the metal and welded joints in piping and equipment while the nuclear power station is generating power, and a program of research work geared to preventing environmental pollution was discussed. The Polish delegation acquainted the participants of this session with a draft report it had worked out on the standard contents of engineering safety measures in the construction and operation of nuclear power stations. Suggestions on formulating specifications and requirements for concretes and concrete structures to be used as shielding against ionizing radiations were discussed, as well as agreed-upon techniques for calculating probabilities of radiation accidents at nuclear power stations, nuclear power station biological shielding calculations where type VVÉR reactors are installed, and propagation of radioactive products into the terrain and environment surrounding nuclear power stations.

The Soviet delegation presented for the section's consideration a fully worked out program rendering an account of experience in the startup and operation of the third power-generating unit at the Novaya Voronezh' nuclear power station, as the leader in a series of such power generating units to be built in COMECON member-nations. Agreement was reached on similar reports to be formulated by GDR and Czechoslovak delegations in the 1972-1975 period dealing with startup and operating experience referable to the first power generating units of the Nord nuclear power station and the A-1 nuclear power station.

Some important decisions were taken on improving forms of collaboration between member-nations of COMECON in the field of nuclear power. Visits to nuclear power stations now under construction or already generating power are to be arranged on a broad scale as an effective means of expanding exchanges of experience in the design, construction technology, installation and rigging, and startup and adjustment phases of work on nuclear power stations, and periodic joint conferences are to be scheduled with specialists of the workteam on reactor science and engineering of the SÉV PKIAÉ [Permanent Commission on Nuclear Power of the COMECON] as well as with specialists of the COMECON Permanent Commission on the machinery industry.

The conference participants heard information from the COMECON secretariat on the needs of COMECON member-nations in power equipment and fuels in the development of hydraulic electric power stations, power stations burning fossil fuels, and nuclear power stations, and also on planning work in the field of nuclear power, and specialized production of equipment for nuclear power stations.

A motion-picture film on the Belyi Yar nuclear power station was viewed with great interest.

After a thoroughgoing report by the Belyi Yar power station chief engineer G. A. Shasharin on operating experience with the two Belyi Yar reactors, the participants were familiarized with the power station's first echelon and with the progress of construction work on the third power generating unit, which will incorporate a 600 MW(e) fast reactor.

The next, twelfth, session of the nuclear power station section will be held at Balaton (Hungary) in September of this year.

Translated from Atomnaya Énergiya, Vol. 35, No. 3, p. 216, September, 1973.

AN EFFECTIVE FORM OF COLLABORATION BETWEEN COMECON MEMBER-NATIONS

V. P. Averkiev

With the object of deepening and expanding scientific and technical ties between the socialist countries, COMECON has put into practice a form of collaboration such as scientific and technical councils on coordination of work involving the solution of the most important and most promising developmental problems for the economies of the COMECON member-nations. One of the first such councils to be organized, in 1971, was the Coordination Scientific-Technical Council on Radiation Techniques and Technology, known as KNTS-RT, a working organ of the PKIAÉ SÉV [Permanent Commission on Atomic Energy of the COMECON].

In summarizing the first two and a half years of its existence and experience, at the fifth session held in the GDR in April 1973, the KNTS-RT took note of the successful completion of the program of collaboration adopted at its first session in 1971, and of the large amount of work done during the period elapsed since that time in laying down the scientific-technical, economic, and organizational prerequisites for speeding up the development and effective incorporation into the national economies of the interested COMECON member-nations of radiation processes and radiation facilities on an industrial scale.

The council went about its work in the following manner. To begin with, basic developmental trends in radiation equipment, techniques, and technology were reviewed and discussed, and a decision was made to concentrate efforts on incorporating into the national economy of the interested nations those promising processes such as radiation grafting and radiation-induced vulcanization of polymers, radiation modification of wood, radiation processing of foodstuffs and agricultural products, radiation sterilization of medical materials and wares.

In each of these areas, KNTS-RT members made reports which included a profound analysis of the worldwide level of work attained in each specific field, and on suggestions for organizing acceptance of those radiation processes in the national economies of the interested nations. A detailed discussion of the reports then enabled the council to work out specific measures, including measures designed to promote work on stimulating the interest of the various nations in the production of, and stimulating their demands for, each of the forms of radiation-processed products referred to, on optimizing designs of radiation facilities, and on arriving at unified techniques for monitoring and inspecting irradiated products, etc.

One vital stage in the work of the KNTS-RT was to work out unified regulatory documents for all of the COMECON member-nations in the field of radiation equipment, techniques, technology, and costs. At the present time, the council has discussed and agreed upon such regulatory documents as the "Basic terms in radiation practice, technology, and economics," "Current engineering specifications for research, multipurpose, and specialized facilities in radiation processing," and "A procedure for determining radiation process engineering costs." Work is now in progress on the documents "Unified procedures in dosimetric monitoring of radiation engineering processes" and "Unified public health rules regarding the design and operation of high-level radiation facilities."

A large volume of work has been done by specialists of the COMECON member-nations on working out regulatory documents covering radiation sterilization of medical materials and wares, in line with the PKIAÉ SÉV research coordination master plan. Starting with the second half of 1973, these plans are to be carried to fruition within the framework of KNTS-RT activities, and must eventuate in the confirmation of all unified procedures regulating the technology of radiation sterilization of medical materials and wares and inspection of the irradiated products.

Translated from Atomnaya Énergiya, Vol. 35, No. 3, pp. 216-217, September, 1973.

In addition to the preparation of regulatory documents in these areas, the council is also planning on unitization of radiation processor modules, and has decided to proceed ahead to formulation of a scientific forecast of the developmental outlook in basic trends of radiation practice and technology.

The council is paying serious attention to improvements in and expansion of exchanges of experience and scientific-technical information between COMECON member-nations in the field of radiation techniques, equipment, and technology. A prominent role has been played in this area by the conference of COMECON member-nation specialists on acceptance of high-level radiation facilities and radiation technology held in Budapest, October 1972, under the sponsorship of the council. This conference attracted over 80 specialists from Bulgaria, Hungary, the German Democratic Republic, Poland, Rumania, the Soviet Union, and Czechoslovakia. A scientific symposium on radiation processing of foodstuffs and agricultural products is being held in Bulgaria in October 1973, and symposiums on graft polymerization of monomers and on radiation sterilization of medical wares are being proposed for the coming years.

The coordination councils, as a new form of collaboration between COMECON member-nations, have fully justified themselves, and are contributing to the further deepening and improvement of collaboration and socialist economic integration of the COMECON member-nations.

COLLABORATION DAYBOOK

A conference of specialists from the German Democratic Republic, Poland, Rumania, the Soviet Union, and Czechoslovakia, on spent fuel reprocessing, was held April 9-11, 1973, in Prague.

The status of work in this area and proposals for refining some of the tasks dealing with aqueous techniques of reprocessing spent reactor fuels as envisaged in the program of collaboration between COMECON member-nations in the area "Research on reprocessing of fuels from nuclear power stations" were discussed.

Research aimed at optimizing spent fuel reprocessing flowsheets with uranium, plutonium, and neptunium as recovery outputs is being pursued in Poland, the Soviet Union, and Czechoslovakia. Some promise is seen in technological processes involving the use of centrifugal automatically controlled extractors, and integrated processing of fuels to yield valuable elements and concentrates of valuable elements.

Close attention is being given to the study of conditions and methods in the preparation of process solutions for solvent extraction, in research on redox reactions involving neptunium, ruthenium, plutonium, uranium, on the behavior of niobium and zirconium in aqueous and organic solutions, solvent extraction technology, choice of selective complexants for zirconium and niobium with the object of improving purification techniques in solvent extraction.

Proposals from GDR and Czechoslovak delegations on collaboration in the study of engineering costs topics pertinent to reprocessing of spent nuclear fuels were heard.

The third session of the KNTS Coordination Scientific-Technical Council on reprocessing of spent thermal reactor fuels was held April 12-14, 1973, in Prague.

Participating were delegations from Bulgaria, the German Democratic Republic, Poland, Rumania, the Soviet Union, and Czechoslovakia.

The council heard information on results of the session of the fast reactors KNTS on radiochemical processing of spent fuel from fast reactors, and deemed it convenient to include those topics in the agenda of the program of collaboration on "Research on reprocessing of fuels from nuclear power stations."

Results of conferences of specialists on fluoride methods of fuel reprocessing and development of techniques for process control and monitoring (September 1972, Leningrad), on transport of spent nuclear fuel (March 1973, Berlin), on aqueous methods of reprocessing spent fuel elements, engineering costs in reprocessing spent fuel elements, and safety techniques in this area (April 1973, Prague), were heard at this session.

A report from the KNTS secretariat on an annotated reference report for 1972, and on the completion of research stipulated in the collaboration program, was heard and discussed.

The council was informed of the possibility of publishing a compendium of expanded annotations on those aspects of the research that have already been completed, in the form of appendices to the periodical Jaderná Energie published in Czechoslovakia.

PKIAÉ SÉV has scheduled for April 1974 the third symposium on reprocessing of spent nuclear fuel, to be held in Czechoslovakia. The agenda of the symposium was drafted and agreed upon.

Engineering specifications and requirements for design work on equipment were discussed in detail.

Engineering specifications proposed by GDR specialists were found suitable as a basis for developmental work on procedures and equipment useful in determining the degree of burnup of fuel assemblies and fuel elements.

Translated from Atomnaya Énergiya, Vol. 35, No. 9, pp. 217-218, September, 1973.

The fourth session of the KNTS on radioactive wastes and deactivation was held April 24-27, 1973, in Moscow, in accordance with the guidelines set down in the PKIAÉ SÉV work plan.

The session heard reports from Bulgarian, Hungarian, East German, Polish, Rumanian, Soviet, and Czechoslovak delegations on the results of scientific research work and experimental design work during 1972, carried out by those countries within the framework of the program of collaboration in the area of deactivation of radioactive wastes and deactivation of contaminated surfaces of equipment and rooms. It was reported that the bulk of this work is being completed on a high scientific and technical level of sophistication and is keeping up with deadlines set.

The 1972 annual resumé and progress report on radioactive pollution of the Danube was discussed. The research findings in this case show the present stage characterized by a decline in the level of global radioactive contamination by nuclear fallout, while the level of radioactive contamination of the Danube water system during that period presents no radiation hazard, and is two to three orders of magnitude below yearly-average tolerance concentrations.

The specialists discussed the criteria for selecting methods of solidifying radioactive wastes worked out within the framework of the program of collaboration, in relation to the properties of the wastes and natural burial disposal conditions, and recommended that those criteria be used to advantage in solving the problem of safe burial of radioactive wastes.

A summary was also made of the 1972 activities of the coordination council, and of scientific and technical conferences held on deactivation of wastes; several other topics also came under discussion.

The 16th session of the PKIAÉ SÉV work team on reactor science and engineering and nuclear power was held in Moscow, May 15-18, 1973. Participating in this session were specialists from Bulgaria, Hungary, East Germany, Poland, Rumania, the USSR, and Czechoslovakia, as well as staff members of the COMECON Secretariat.

Organization of collaborative efforts in the field of dissociating gases as coolants for fast reactor facilities, in the field of nuclear reactor and power station monitoring and control, was discussed at the session, as well as reactor shielding physics, and collaborative efforts on speeding up the design and construction of nuclear power generating stations incorporating VVÉR type reactors.

Agreement was reached on instituting a commission with responsibilities in all of the areas discussed.

THE ALL-UNION SEMINAR ON THE METROLOGY OF IONIZING RADIATION

I. A. Yaritsyna

The All-Union Seminar on the Metrology of Ionizing Radiation was held on April 10-12, 1973, at the D. I. Mendeleev All-Union Scientific Research Institute of Metrology (VNIIM) in Leningrad.

Participants in the Seminar included 220 representatives from 55 different institutions and organizations in the Soviet Union. Forty-two reports were delivered. The plenary meeting dealt with fundamental questions of the development of the metrology of ionizing radiation.

At the present time the VNIIM has worked out the primary state standards for the unit of activity of radionuclides, exposure dose, absorbed dose of beta rays and neutrons, neutron flux, and neutron flux density, as well as the special state standard of the unit mass of radium. It has been shown that in order to extend the limits of measurement and achieve substantial increases of accuracy, we must have not only improvements in existing standards but also the development of new standards for the metrological servicing of new fields of measurement.

In the next few years the VNIIM will develop standards for the units of equivalent dose, absorbed dose of photon radiation in the 20-60 keV range and the 5-50 MeV range, units of intensity of electron and photon radiation in the 5-50 MeV range, and units of energy flux of photon and electron radiation.

The All-Union Scientific Research Institute of Physicotechnical and Radio-Engineering Measurements (VNIIFTRI) is currently developing a special state standard for the unit of activity of radionuclides in gases and a special state standard of the unit of concentration of radioactive aerosols. It was reported that a primary state standard of the unit of absorbed dose rate of photon radiation in the 0.1-1 rad/sec range had been developed and confirmed at the end of 1972 (Yu. I. Bregadze, A. V. Tultaev et al.).

S. A. Shestopalova commented on the need for developing at the VNIIM a standard unit of gamma-ray energy; it has been proposed that the energy of certain nuclear transitions be used as such a standard.

At the Neutron Measurements section, a report by O. L. Andreev et al. told of a method for transmitting the dimension of a unit of the flux density of thermal neutrons from the isotropic field of a standard to devices with directional flux. In another report, O. L. Andreev and E. P. Kucheryavenko told of calculations used for determining neutron temperatures on the basis of cadmium ratios for gold and manganese and the Wescott parameter r. Both of these investigations were carried out at the VNIIM.

A report by R. D. Vasil'ev et al. dealt with a thermal-neutron source developed at the VNIIFTRI, based on a neutron generator, in which the $T(D,n)He^4$ reaction is used. Two targets of this generator are placed in a graphite prism; a small air cavity is situated in the middle of the prism, symmetrically with respect to the targets. A controlled and regulated field of thermal neutrons is established in this cavity.

A report by V. G. Zolotukhin et al. dealt with forecasting the albedo background for different kinds of neutron measurements (Moscow Engineering Physics Institute – MIFI).

Of special interest was a report by S. P. Makarov (I. V. Kurchatov Institute of Atomic Energy) on an all-wave neutron counter. Its geometric dimensions are much smaller than those of the widely known counters of this type. A proposal was made for a detector in the form of a combination of slow-neutron and fast-neutron detectors and resonance-absorber detectors. The efficiency of the counter varies by 17% as the neutron energy varies from 0.05 to 1.5 MeV. The authors used a boron–hydrogen scintillator. A

Translated from Atomnaya Énergiya, Vol. 35, No. 3, pp. 219-220, September, 1973.

resonance absorber consisting of a set of metal plates (cadmium, indium, thulium, and silver) was placed between a cylindrical polyethylene moderator and the scintillator.

A report of unquestionable practical interest was the report by D. A. Kuznetsov et al. (I. V. Kurchatov Institute of Atomic Energy) on n-γ discrimination on the basis of the shape of a signal pulse from a stilbene scintillation detector.

Reports delivered at the Activity Measurement section included important innovations in the measurement methods previously used. E. A. Khol'nova et al. (VNIIM) reported on a new high-sensitivity alpha calorimeter based on three differential-dual calorimeters of the static type. This calorimeter can be used for measuring the alpha activity of radionuclides in the 10^7-$3 \cdot 10^{12}$ dis/sec range with an error of 0.3-0.5% and a confidence coefficient of 99%. A second report by E. A. Khol'nova et al. dealt with the standardization of H^3 and C^{14} specimens.

F. M. Karavaev et al. reported on a rapid method for measuring tritium and carbon activity. They had conducted relative measurements of the activity of aqueous solutions of tritium and carbon by introducing specific portions of them into a liquid scintillator whose activity was then compared with the known activity of a specimen.

A report by V. I. Albul and V. G. Baranov (VNIIFTRI) dealt with measurements of the activity of liquid specimens of tritium converted to vapor, using ionization chambers.

A. A. Konstantinov et al. (VNIIM) reported on the characteristics of measurements on the activity of certain electron-capture radionuclides. Thus, the activity of Fe^{55}, which emits only x-rays and Auger electrons when it disintegrates, is measured by means of a proportional counter. This counter operates with different gas mixtures at different pressures. The activity of electron-capture radioisotopes whose disintegration is accompanied by the emission of gamma rays as well is measured by the method of coincidences of x-rays and gamma quanta. Radionuclides of this type include Mn^{54}, Co^{57}, Zn^{65}, Sr^{85}, Y^{88}, and Ce^{139}. The counter of a gamma-ray detector – an NaI(Tl) crystal – is used as an x-ray detector.

V. Ya. Alekseev (VNIIM) reported on the measurement of the alpha activity of radioisotopes in the 10^4-10^8 dis/sec range. The total error was 0.2-0.5%, with a confidence coefficient of 95%. Comparison of these results with the results obtained by the calorimetric method showed that the two agreed within 0.15%.

A report by K. N. Shalotenko, A. E. Kochin, and N. M. Anikeev, presented by the VNIIM and the State Institute of Applied Chemistry (GIPKh), told of the measurement of a specimen radioactive solution of thymine tagged with C^{14}. The measurements were made with a 4π β-counter. The sources, mounted on thin organic films, were found to be fairly stable and yielded results which were reproducible to within 3%.

A. F. Drichko (VNIIM) showed that the current in cylindrical 4π ionization chambers used for checking Co^{60} and Cs^{137} gamma sources is proportional not to the dimensions of the chamber but to the distance between the electrodes, averaged over a solid angle with vertex at the center of the gamma source. This relation makes it possible to determine the sensitivity of a chamber for given dimensions of its elements or to select the dimensions of chamber elements for a given sensitivity.

In the Measurement of Doses of Ionizing Radiation section Yu. V. Lysanov, G. P. Ostromukhova, and I. A. Uryaev (VNIIM) analyzed the existing types of testing apparatus using a diffuse field, directed beams of radiation, and plane sources. They noted a tendency toward the development of devices with a diffuse field of gamma radiation. Studies have been conducted on the scattering of radiation in air for beams with various kinds of geometry. It was proposed that the similarity method be used for checking dosimetric apparatus with an upper limit ranging to 300-500 R/h. A report by N. D. Willebald and I. A. Uryaev (VNIIM) discussed the measurement of the parameters of pulse x-rays. To determine the transfer of the radiation energy, the authors used a scintillation detector based on TF-1 glass, and to measure the transfer of photons, they used a reticulated filter on the cathode of the photomultiplier. G. V. Abramov et al. (VNIIM) reported on the standard of a unit of absorbed dose in the photon energy range of 5-50 MeV, developed by using the VNIIM betatron. The absorbed dose will be measured by the calorimetric method in the 100-1,000 rad range.

A. P. Balashov discussed a relatively simple method for measuring the energy of beams extracted from electron accelerators by partial absorption of the beam in a metal plate of known thickness.

V. N. Tuchin and M. F. Yudin reported that they had used a spectrometric method for precise measurements of low dose rates (less than $3 \cdot 10^{-6}$ R/sec) in the gamma-ray energy range of 0.1-2 MeV.

Z. P. Balon et al. discussed the advantages of using the filtration of radiation in checking dosimeters on a standard UPGD tester, as well as a number of methodological refinements that can be used for improving the accuracy of tests of dosimetric instruments.

Yu. P. Vagin, Yu. A. Medvedev, and B. M. Stepanov (All-Union Scientific Research Institute of Optical-Physical Measurements – VNIIOFI) presented a new method for measuring the absorbed dose rate from single pulses of ionizing radiation, based on measuring the spectral intensity of gas fluorescence in the optical range. A photodetector and a fluorescence chamber are used to ensure linearity of local measurements of instantaneous dose rates from pulsed beams of electrons and gamma quanta in the 10^3-10^7 rad/sec range at energies of 0.1-10 MeV, with an error of approximately 10%. The Radiation Detectors and Applied Spectrometry section was also active.

Some reports were of a general nature. Among these was a report by E. A. Kuz'min on the problems involved in the measurement of nuclear constants for thermonuclear reactors; the report explained the reasons that a number of constants must be determined with higher accuracy.

S. A. Baranov reported on the present state of precise energy measurements on the most intensive groups of alpha particles of some transuranium elements.

A resolution adopted by the Seminar stated that questions discussed were of great current interest and that similar seminars should be held periodically.

Declassified and Approved For Release 2013/01/22 : CIA-RDP10-02196R000400020003-6

INTERNATIONAL CONFERENCE ON HIGH-ENERGY PHYSICS RESEARCH EQUIPMENT

V. A. Vasil'ev

The regularly scheduled international conference on research equipment for high-energy physics studies was held May 8-12 in Italy. This conference was organized by the National Laboratory and National Nuclear Physics Institute at Frascati, with the support of the International Union of Pure and Applied Physics (IUPAP) and the Italian National Nuclear Power Committee (CNEN). About 250 specialists representing all of the leading scientific research centers in the world were in attendance. Most representative were the delegations from CERN, the USA, Italy, France, West Germany, Britain, and the JINR. The Soviet Union was represented at the conference by scientists from the Institute of High-Energy Physics [IFVÉ], the Institute of Theoretical and Experimental Physics [ITÉF], and the Moscow Engineering Physics Institute [MIFI].

The conference deliberations proceeded as follows: plenary sessions at which the agenda included specially invited papers and tutorial review papers, alternating with panel sessions at which papers on more narrowly specialized topics were delivered, so that everyone could have practical opportunities to report on details of some particular line of development of research. A compendium of annotations of the reports and papers to be presented at the conference was published on the eve of the conference, so that the delegates were able to find their way around the conference and were able to arrange meaningful contacts between specialists hailing from different scientific research centers while the conference was in progress.

The conference agenda covered problems and achievements in the field of detectors of high-energy particles, systems for shaping beams of particles from accelerators with optimum parameters for up-to-date experiments, and also some topics concerning processing experimental data. Many of the reports and floor discussions dwelt upon possibilities of effective utilization of equipment and the latest methods for detecting high-energy particles in applied research (solid state physics, microbiology, medicine, etc.).

In recent years, experimental arrangements and equipment useful for effective work on high-intensity beams of particles have been undergoing intensive development. The development of accelerators designed for energies of hundreds of billions of electron-volts has been prompting searches for methods of recording particles of superhigh energies which would make it possible to record the characteristics of those particles, and the processes by which they interact, with sufficient accuracy, at low cost, and with a high degree of reliability.

One of the new methods which can be used in the design of detectors of superhigh-energy particles was first proposed and developed in the Soviet Union (G. M. Garibyan et al., Erevan Physics Institute). A detailed review of the research work done on transient radiation was presented by L. Juan (USA). Recent work by Soviet and American scientists has demonstrated satisfactory agreement between the characteristics of transient radiation, in particular the energy dependence of the radiation intensity in the optical and x-ray regions of the spectrum, and theoretical prediction based on calculations. It is assumed that the best detectors for recording transient radiation are proportional chambers with xenon and krypton added.

General-purpose particle detectors which have found favor in recent years are multi-wire proportional chambers with their excellent time resolution (less than 100 nsec) and space resolution (less than 1 mm). G. Sharpak (CERN) has reported, specifically, the building of new large experimental facilities in

Translated from Atomnaya Énergiya, Vol. 35, No. 3, pp. 220-222, September, 1973.

which proportional chambers with tens of thousands of wires are in use. Facilities of this type feature high aperture ratio or transmission and fast response. Naturally, fairly large computers have to be used in the acquisition and processing of experimental data at such facilities.

Many of the conference participants took note of the great promise offered by drift chambers, which even outperform proportional chambers in some of their characteristics (high spatial resolution, less expensive auxiliary electronic instrumentation). At the present time, the technology of fabrication and the design features of drift chambers have been studied attentively, and some laboratories in France and the USA are busy building large-volume track-delineating detectors on the basis of drift chambers.

The further development of streamer type track chambers is proceeding along the path of introducing the target into the chamber volume, as well as measuring the relative increase in ionization along the track. The high speed of response, the relative ease of processing the experimental data, and several other advantages, favor using magnetic spark spectrometers with streamer chambers in combination with liquid-hydrogen targets in the same areas of physics experimentation where bubble track chambers used to brook no competition. New outlooks for the further development of this procedure are now opening up with the burgeoning opportunities for utilization of holographic information pickup from streamer type chambers. A report on this development was presented by the JINR Nuclear Problems Laboratory and by the Leningrad Institute of Nuclear Physics of the USSR Academy of Sciences. The bubble chambers remain convenient and in fact unreplaceable, given new engineering improvements in the design of many bubble chambers. The principal improvements in the techniques associated with liquid-hydrogen bubble chambers involve successful attempts to introduce a heavy liquid (e.g., liquid neon) into the effective chamber volume for the purpose of enhancing the effectiveness with which neutral particles and γ-photons are recorded. The thermodynamical conditions selected in the interior of the chamber are such that the liquid neon, separated by a thin film or by Plexiglas from the liquid hydrogen, is sensitive to the track. That expands the range of application of bubble chambers in physics experimentation, and without adding to the cost of bubble chambers. Fast cyclic bubble chambers capable of operating at frequencies up to 100 Hz are now being built at some laboratories in the Soviet Union, USA, and West Germany.

Equipment for automatic processing of film data from track chambers is being improved. Cathode-ray tubes of high resolution are being employed, as well as systems incorporating mechanical means of scanning the light beam. Desk-top control computers and specialized data processors are also being employed more widely in combination with this type of equipment. The most suitable auxiliary equipment for television pickup of data from large spark chambers and streamer type chambers are plumbicons, whose sensitivity to light is ten times greater than the sensitivity of other tubes. Additional light amplifiers can be brought into play when even that level of sensitivity is inadequate to the experiment.

High-speed electronic equipment and experimental data processing systems operating in real time have been undergoing impressive development. The count speed of flipflops in modern high-speed electronic logic circuits is 350 MHz, the delay of a signal passing through a gate is 1 nsec (MECL-III series gate circuits). Further improvements in performance are expected in coming years. Wide use is being made of videomagnetic tapes to record blocks of information in large bulk, since that makes it possible to record data at rates up to 8 Mbit/sec. The feasibility of recording experimental information is decided upon through rapid preliminary processing with the aid of special fixed-program data processors. Final processing of the recorded data is best handled by means of large modern computers with bilateral hookups to small computers directly participating in the specific experiments. When these hookups are properly organized, a large computer can be used to service several experiments at the same time.

Several review papers and personal communications were devoted to recent achievements in the development of such traditional procedures as those used with Cerenkov counters and scintillation counters. Designs of Cerenkov counters have been largely stabilized, and the resolution $\Delta\beta/\beta$ attained at the present time is $4 \cdot 10^{-6}$ to $6 \cdot 10^{-6}$ in the case of threshold gas counters and differential gas counters. Further improvements are associated with a severe cost penalty, in view of the complexity of the optical system and the increased size resulting. Total-absorption counters with NaI crystals that have been designed at Stanford (these counters are known as SLACK) are dimensioned $40 \times 40 \times 40$ inches. Resolution for 15 GeV electrons is 0.7%.

The design of a filament type crystal particle counter utilizing solid (frozen) argon was been noted as a significant achievement in the development of basically new particle detector types. The possibility of designing such a detector was first demonstrated in experiments carried out at the JINR Nuclear Problems Laboratory, and subsequently confirmed at Berkeley (USA). Many specialists have affirmed that the use of filament type crystal counters can play an essential role in the development of x-ray structural research in biology and in medicine, since they will make it possible to increase the sensitivity and resolving power of the method while simultaneously lowering the dosage of radiation exposure for the rest objects by a considerable amount.

In conclusion, we should point out that Soviet scientists and specialists have made a significant contribution to the development of new techniques for detecting high energy particles. Leading specialists throughout the world, upon taking the floor at the conference to review basic trends in specific areas of science and engineering, noted the importance of the findings reported by Soviet scientists and engineers in their work on transient radiation, on the design of filament solid argon counters, on the development of techniques for using spark chambers and streamer type chambers, on the design of high-speed electronic circuitry, and on holographic acquisition of data from track-delinating instruments. The participation of Soviet specialists in the conference made it possible to obtain the latest information on the achievements and experiences of our foreign colleagues. Utilization of this experience, and the further development of international collaboration on a broad front in this area, will undoubtedly provide new and important scientific information on the physics of the atomic nucleus and on high-energy particles.

The conference proceedings are to be published in the coming months.

S. M. Gorodinskii

PERSONNEL PROTECTION EQUIPMENT FOR WORK WITH RADIOACTIVE MATERIALS*

Reviewed by E. D. Chistov

The book under review constitutes a monograph dealing with the present scientific level of theoretical and experimental research and practical utilization of personnel protection equipment for work with radioactive materials. It contains an introduction, a general (first) chapter and a special section [second to ninth chapers (inclusive)], plus bibliography, two appendices, and a subject index.

The introduction to the first chapter brings the reader up to date with research and development work on personnel protection equipment, particularly in cases where radioactive materials may gain access to the human organism; basic paths of such access are considered, and the designations and classifications of personnel monitoring and protection equipment are indicated.

The most important problem concerning the development of personnel protection equipment is the investigation of materials to be used in the design of such equipment; that is the subject matter of the second chapter. Methods for investigating rubber-base polymeric film materials are presented. The presentation in the third chapter is grounded on methods of physiological and public health evaluation of personnel protection equipment, since it is only such research that can provide the solution to whether particular personnel protection equipment will prove useful in practice.

The fourth chapter offers extensive theoretical and experimental material backing up research findings pertaining to quantitative estimates of protection performance, and shows that personnel protection equipment can be reliable and effective.

The fifth to ninth chapters (inclusive) deal with research and development work on insulating coveralls for maintenance and repair work in areas of radioactive contamination, protection equipment for respiratory organs in work with radioactive materials, special protective clothing for everyday wear on the job, protective gloves and footwear, and supplementary film type special protective clothing. The materials for this portion of the book provide a complete illustration of the research preceding the acceptance of personnel protection equipment in the nuclear industry. It is shown that the personnel protection equipment developed in the USSR on the basis of performance and protection properties matches the best available anywhere in the world, and in some points is superior to all rivals.

The last chapter describes methods for deactivating personnel protection equipment made of various materials (cotton, lavsan type dacrons, film polymeric materials, rubber). Practical recommendations on deactivation procedures are included.

The great merit of this second edition of the book is the exhaustive bibliography (426 sources) and the consistent presentation of the original material. The book is published in a professional manner of text presentation, factual material is lucidly illustrated (86 diagrams and 47 tables of data). This is without question a valuable practical science manual for workers dealing with radioactive materials, and for the needs of radiation safety and public health stations.

*Second Edition, Atomizdat, Moscow, 1973.

Translated from Atomnaya Énergiya, Vol. 35, No. 3, p. 222, September, 1973.

E. Storm and H. Israel

INTERACTION CROSS SECTIONS OF GAMMA-RADIATION (ENERGIES 0.001-100 MeV AND ELEMENTS FROM 1 THROUGH 100)*

Reviewed by O. S. Marenkov

This text by E. Storm and H. Israel, in which partial and total cross sections are tabulated for interaction of γ-photons and the first hundred elements over an energy range covering five orders of magnitude, is a highly useful and necessary reference manual intended for a broad range of specialists in the field of atomic and nuclear physics and numerous technical applications associated with the use of different types of γ-emission sources. Since the Soviet scientific literature does not boast of any similar reference publication on the interaction cross sections of γ-photons, the publication of this Russian translation should go a long way toward filling that gap. Unfortunately, the translation and editing of this work by E. Storm and H. Israel under Atomizdat auspices falls short of that promise, since the translation published here is not the latest edition of tables of cross sections (E. Storm and H. Israel, "Photon cross sections from 1 keV to 100 MeV for elements Z-1 to Z-100," Nuclear Data Tables, section A, 1970, vol. 7, No. 6, pp. 565-680), but instead an earlier edition (E. Storm and H. Israel, "Photon cross sections from 0.001 to 100 MeV for elements 1 through 100." La-3753. Los Alamos Scientific Laboratory, New Mexico, 1967). The 1970 edition contains revisions and refinements of the partial interaction cross sections based on theoretical papers published in the 1967-1969 period. New data on incoherent scattering functions, and form factors of coherent scattering, were used; calculations of photosections are provided for different models of the screened potential. Only tables of pair production cross sections underwent virtually no changes. Consequently, all of the partial cross sections are theoretical predictions, and the accuracy of the numerical data is higher than in the 1967 edition; that applies particularly to the photoabsorption process. The list of literature surveyed runs to 112 titles.

Several comments on the abridged Russian edition of the 1967 tables of cross sections are also in order. The incoherent scattering cross sections should have been grouped in a separate column in the tabular material. There was no point in duplicating the incoherent scattering cross sections data for energies at which the binding effect of electrons is insubstantial. The reference material on fluorescent emission left out in the translation would have been of interest to a fairly broad range of specialists. Errors that can be ascribed to misprints crop up in the foreword by the translators and in the explanatory text accompanying the tables of data.

*A handbook, Atomizdat, Moscow, 1973.

Translated from Atomnaya Énergiya, Vol. 35, No. 3, p. 223, September, 1973.

Declassified and Approved For Release 2013/01/22 : CIA-RDP10-02196R000400020003-6